UNIVERSITY
OF MICHIGAN
JUL 13 1951
ENGINEERING
LIBRARY

JOURNAL OF THE AERONAUTICAL SCIENCES

VOLUME 18 JULY, 1951 NUMBER 7

CONTENTS

The Effect of Changes in Altitude on the Controlled Behavior of a Gas-Turbine Engine.....SEYMOUR C. HIMMEL AND RICHARD P. KREBS 433

On Turbulent Fluid Motion.....MAX M. MUNK 442

Simplified Design Comparisons of Axial Compressors.....FRANK L. WATTENDORF 447

The Turbulent Boundary Layer in a Compressible Fluid with Positive Pressure Gradient.....CARLO FERRARI 460

Tables of the Theodorsen Circulation Function for Generalized Motion.....YUDELL L. LUKE AND MAX A. DENGLER 478

Three-Dimensional Shock-Wave Reflections.....E. MIGOTSKY AND M. V. MORKOVIN 484

The Laminar-Turbulent Transition in a Boundary Layer—Part I.....H. W. EMMONS 490

Readers' Forum: "A Possible Relation Between Cellular Flame Structure and Quenching," by Raymond Friedman; "The Combined Supersonic-Hypersonic Similarity Rule," by Milton D. Van Dyke; "On the Velocity of Sound in Fluids," by C. Truesdell; "The Analogy Between Irrotational Gas Flow and Minimal Surfaces," by C. Truesdell; "On Broszko's Theory of Turbulent Flow," by William Squire; "Equivalence of the Spanwise Lift Distribution to the Spanwise Lift-Influence Function for Slender Wings and Wing Bodies," by G. K. Morikawa and A. E. Puckett.....499–504

Published by the

INSTITUTE OF THE AERONAUTICAL SCIENCES, INC.

JOURNAL OF THE AERONAUTICAL SCIENCES

Editor: HUGH L. DRYDEN, *Director, N.A.C.A.*

Associate Editor: ROBERT R. DEXTER *Managing Editor:* BERNEICE H. JARCK

Editorial Committee

Aerodynamics

Francis Clauser
Howard Emmons
R. Paul Harrington
R. T. Jones
Carl Kaplan
W. B. Klemperer
John G. Lee
H. W. Liepmann
C. C. Lin
H. F. Ludloff
John R. Markham
Clark B. Millikan
Shatswell Ober
W. Bailey Oswald
Allen E. Puckett
Elliott G. Reid
H. J. F. Reid
Russell Robinson
G. B. Schubauer
W. R. Sears
John Stack
Theodore von Kármán
Richard von Mises

Flight Testing

W. K. Ebel
R. R. Gilruth
Melvin N. Gough
Robert Stanley
E. G. Stout

Meteorology

C. F. Brooks
D. M. Little
E. J. Minser
F. W. Reichelderfer
H. C. Willett

Structures and Materials

W. B. Bleakney
E. W. Conlon
J. P. Den Hartog
L. H. Donnell
E. C. Hartmann
N. J. Hoff
E. E. Lundquist
C. F. Nagel, Jr.
J. S. Newell
Alfred S. Niles
W. Ramberg
E. Reissner
F. R. Shanley
H. W. Sibert
C. R. Strang
S. Timoshenko
H. S. Tsien
Chi-Teh Wang

Rotating Wing Aircraft

Robert Coleman
K. H. Hohenemser
Bartram Kelley
Ralph McClarren
R. H. Miller
R. H. Prewitt
Igor I. Sikorsky

Physiologic Problems

H. G. Armstrong
Louis H. Bauer
Eugene Du Bois
W. Randolph Lovelace, II
Ross A. MacFarland
A. D. Tuttle

Flight Propulsion

George W. Brady
Frank W. Caldwell
L. S. Hobbs
E. E. Johnson
Joseph Keenan
R. P. Kroon
Arthur Nutt
Hans Reissner
Abe Silverstein
C. Fayette Taylor
E. S. Taylor
P. Taylor
E. S. Thompson
H. S. Tsien

Aircraft Design

W. E. Beall
W. K. Ebel
Hall L. Hibbard
Richard Hutton
C. L. Johnson
I. M. Laddon
C. J. McCarthy
Fred E. Weick
Robert J. Woods

Air Transport

Charles Froesch
J. A. Herlihy
R. D. Kelly
Otto E. Kirchner
Jerome Lederer
John C. Leslie
R. Dixon Speas

Instruments

Allan G. Binnie
W. G. Brombacher
Charles H. Colvin
B. M. Craig
C. S. Draper
S. G. Eskin
O. E. Esval
W. L. Howland
George H. Purcell
C. F. Savage
O. Hugo Schuck
L. N. Schwien
C. L. Seward, Jr.
L. D. Statham
R. C. Sylvander
D. K. Warner
P. F. Weber
Elmer P. Wheaton

Vibration and Flutter

Lee Arnold
M. A. Biot
William Bollay
Chieh-Chien Chang
Martin Goland
J. P. Den Hartog

Fuels and Oils

D. P. Barnard
J. H. Doolittle
Graham Edgar
R. T. Goodwin
S. D. Heron
A. M. Rothrock

SUBSCRIPTION RATES

JOURNAL OF THE AERONAUTICAL SCIENCES, Published Monthly.—United States and Possessions: 1 Year, $12.00; Single Copies, $1.50. Foreign Countries Including Canada (American Currency Rate): 1 Year, $13.00; Single Copies, $1.50.

AERONAUTICAL ENGINEERING REVIEW, Published Monthly.—United States and Possessions: 1 Year, $3.00; Single Copies, $0.50. Foreign Countries Including Canada (American Currency Rates): 1 Year, $3.50; Single Copies, $0.50.

Notices of change of address should be sent to the Institute at least 30 days prior to actual change of address.

Manuscripts for publication, proofs, and all correspondence should be addressed to the Editorial Office of the JOURNAL.

Correspondence regarding subscriptions may be addressed to Publication Office, 20th and Northampton Sts., Easton, Pa., or to the Editorial Office of the JOURNAL OF THE AERONAUTICAL SCIENCES, 2 East 64th Street, New York 21, New York.

Copyright, 1951, by the Institute of the Aeronautical Sciences, Inc.

Entered as Second Class Matter at the Post Office, Easton, Pa., May 1, 1937. Acceptance for mailing at a special rate of Postage provided for in the Act of August 24, 1912. Authorized April 29, 1937.

JOURNAL OF THE AERONAUTICAL SCIENCES

VOLUME 18 JULY, 1951 NUMBER 7

The Effect of Changes in Altitude on the Controlled Behavior of a Gas-Turbine Engine

SEYMOUR C. HIMMEL* AND RICHARD P. KREBS†

Lewis Flight Propulsion Laboratory, N.A.C.A.

SUMMARY

For the various phases of flight operation of an aircraft powered by a gas-turbine engine, a considerable range of power output is required of the engine. Not only are different power levels required, but changes from one power level to another must be accomplished in a short period of time. It is the function of the control to conduct the engine quickly and safely from one operating level to another without encountering excessive values of speed, torque, and temperature. The design of a control system for a gas-turbine engine is further complicated by the fact that the reaction of the engine to a given change in one of the independent variables changes with the initial control setting and with altitude. As a result, the control is expected to regulate what amounts to a variety of power plants.

This paper presents a theory of the change in engine response with altitude which has been derived independently by several analysts, together with some experimental data corroborating these analyses. The data show that the response of the engine at any altitude may be computed from measurements made at sea level.

The sea-level and altitude transient behavior of an engine operating under a proposed control are studied with the aid of an electronic analog computer to illustrate the effect of the changes in engine dynamics with altitude. From these studies, it appears necessary to use compensation to vary the gain and time variant parameters of the control loops with altitude if satisfactory performance is to be obtained.

ANALYSIS

FROM THE ANALYSIS OF THE EQUATION describing the dynamic behavior of a turbine-propeller engine, we will develop the variation of engine dynamic performance with changes in altitude. The analysis is based on the following assumptions: For small excursions from a point of equilibrium, engine torque is a function of fuel flow and engine speed

$$Q_e = Q_e(W_f, N) \tag{1}$$

and propeller torque is a function of blade angle and engine speed

$$Q_p = Q_p(\beta, N) \tag{2}$$

The only energy storage units are the engine and propeller inertias. The engine operates dynamically in a quasi-static state.

The relation between engine speed and fuel flow with constant propeller blade angle, based on the foregoing assumptions, can be expressed by the following:

$$(I_e + I_p)\frac{d\,\Delta N}{dt} + \left[\left(\frac{\partial Q_e}{\partial N}\right)_{W_f} + \left(\frac{\partial Q_p}{\partial N}\right)_{\beta}\right]\Delta N = \left(\frac{\partial Q_e}{\partial W_f}\right)_N \Delta W_f \tag{3}$$

This equation relates the time derivative of speed change, and the speed change itself, with the change in fuel flow, and I_e is the moment of inertia of the engine alone and I_p is the moment of inertia of the propeller alone. The term multiplying the change in speed is made up of the sum of two partial derivatives—the changes of torque with speed at constant fuel flow and at constant blade angle. The term modifying the change in fuel flow is the partial of torque with respect to fuel flow at constant speed. From this differential equation the so-called "response" of engine speed to fuel flow at constant blade angle can be written in operational notation as given in Eq. (4).

$$\left(\frac{\Delta N}{\Delta W_f}\right)_{\beta} = \frac{(\partial Q_e/\partial W_f)_N}{\left[\left(\frac{\partial Q_e}{\partial N}\right)_{W_f} + \left(\frac{\partial Q_p}{\partial N}\right)_{\beta}\right]} \times \frac{1}{\left[1 + \dfrac{I_e + I_p}{(\partial Q_e/\partial N)_{W_f} + (\partial Q_p/\partial N)_{\beta}}\,p\right]} \tag{4}$$

where the ΔN and ΔW_f are, respectively, the change

Presented at the Flight Propulsion Session, Nineteenth Annual Meeting, I.A.S., New York, January 29–February 1, 1951.

* Aeronautical Research Scientist, Controls Branch, Engine Research Division.

† Aeronautical Research Scientist, Engine Research Division.

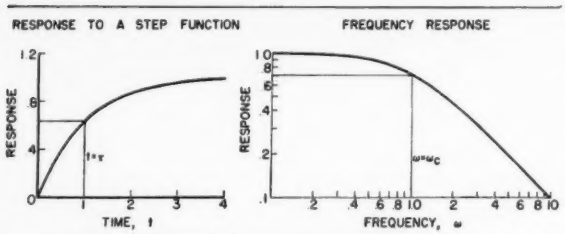

FIG. 1. Theoretical response of speed to fuel flow.

in speed and the change in fuel flow. The symbol p is a differential operator.

The right-hand side of this equation can be considered as the product of two factors—a gain or sensitivity factor

$$\frac{(\partial Q_e/\partial W_f)_N}{[(\partial Q_e/\partial N)_{W_f} + (\partial Q_p/\partial N)_\beta]}$$

and a time variant factor

$$\frac{1}{1 + \dfrac{(I_e + I_p)}{[(\partial Q_e/\partial N)_{W_f} + (\partial Q_p/\partial N)_\beta]}\, p}$$

The gain factor tells how large a change in speed results from a given change in fuel flow; the time dependent factor tells in what manner and how fast this change is effected. This equation gives the response of engine speed to fuel flow and is independent of the nature of the change in fuel flow.

The dynamic response of a system can be determined in a number of ways. One method is to apply a step change to the independent variable of the response (in this example fuel flow) and to study the time history of the dependent variable (in this case speed). Were this to be done, the response of speed to a step change in fuel flow would be as shown in the left-hand portion of Fig. 1. In this figure we have plotted only the time variant or "how fast" portion of the response. This is equivalent to dividing the response by the gain factor or "normalizing" the response. It is seen that the response is zero at zero time and approaches its final value of unity exponentially. A second method of determining dynamic response is to apply a constant amplitude sinusoidal oscillation over a series of frequencies to the independent variable (fuel flow) and to measure the speed oscillations. The normalized response as determined from such an experimental procedure is shown on the right-hand side of Fig. 1. When the frequency of the applied sinusoidal fuel flow is low, the speed follows the change in fuel flow yielding a normalized response close to unity, but as the frequency increases, the speed change is reduced in amplitude, for a constant magnitude of fuel flow change, and the response decays.

A system that yields responses such as those shown is quantitatively described by a single entity known as the time constant. This time constant is the time for the speed to reach 63.3 per cent of its final value in the case of a step change in fuel flow or, in the case of the sinusoidal input, the reciprocal of the frequency at which the amplitude of the response falls to 70.7 per cent of its zero frequency value, the so-called break frequency. In the particular system under consideration, the time constant is given by

$$\tau_c = \frac{I_e + I_p}{(\partial Q_e/\partial N)_{W_f} + (\partial Q_p/\partial N)_\beta} \tag{5}$$

The foregoing time constant is descriptive of the response of the combination of engine and propeller and is therefore referred to as the time constant of the combination, τ_c.

Thus, the dynamics of the system can be determined by subjecting the engine to either a step change in fuel flow or a series of sinusoidal varying fuel flows. Other responses within the engine, such as speed to torque or temperature to propeller blade angle, can be obtained by proper choice of the dependent and independent variables. Some of the responses—for example, that of speed to torque at constant blade angle—are equivalent to cutting the shaft between the engine and propeller and considering either of these components separately according to laws of rigid body dynamics.

From the response of speed to torque at constant fuel flow and at constant blade angle, two new time constants are defined—namely, the time constant of the engine alone and that of the propeller alone. Any other response, whether between a dependent and an independent variable or between two dependent variables, is defined by a gain factor and a combination of the three time constants. Therefore, knowledge of the three time constants is essential to the complete description of the power-plant dynamics and to the design of a control system.

When the flight altitude is increased, the relation between increments of the engine variables is changed. For example, the change of torque for a given change of engine speed at constant blade angle is decreased because of the decreased air density at high altitude. The inertia of the components, however, is independent of altitude. Hence, a change in component dynamics is to be expected with changes in flight altitude. These changes in dynamics are twofold. There is a change in the speed of response and a change in the sensitivity of response. Quantitatively, the change in the speed of response can be evaluated by a consideration of the change in time constant. The time constant involves the relation between torque and speed, as is shown in Eq. (5), and, hence, the time constant will vary as the $\sqrt{\theta}/\delta$, where θ is the ratio of ambient static temperature to sea-level temperature and δ is the ratio of ambient static pressure to sea-level static pressure. In other words, if the time constant is multiplied by a generalization factor $\delta/\sqrt{\theta}$, the product is invariant with altitude. This product is referred to as

generalized time constant. This variation of time constant with altitude is perfectly general and is applicable to all time constants involved in the responses.

Consideration of the quantities involved in any given response will make it possible to determine the generalization factor for a particular response sensitivity. No single generalization factor is applicable to all response sensitivities, but each can be considered individually. For example, the gain factor for the response of speed to fuel flow has the dimensions of speed over fuel flow. Because speed is generalized by the $\sqrt{\theta}$ and fuel flow is generalized by $\delta\sqrt{\theta}$, the generalization factor for the gain term in the speed-fuel flow response is δ. Because it is possible to generalize both the sensitivity and the time constant individually, it should be possible to generalize the complete dynamic response.

Thus far, no physical significance has been attached to the partial derivatives appearing in the response equations. These partial derivatives have the value of the slopes of their respective steady-state performance curves. Thus, it should be possible to determine dynamic response from the steady-state performance curves of the engine and the moments of inertia of its components.

The foregoing is an analytical approach to the determination of the dynamics of the engine. The direct method for determining the dynamic response and its variation with flight altitude is to subject the engine to controlled changes in the independent variables and to record the time history of the dependent variables. Such an investigation has been conducted in the Altitude Wind Tunnel of the N.A.C.A. Lewis Flight Propulsion Laboratory.

Experimental Program

The Lewis Altitude Wind Tunnel is of the return type with a 20-ft. diameter test section and is so designed as to permit the simulation of altitude conditions. A turbine-propeller engine was mounted on an airfoil that spanned the test section of the tunnel. For the dynamic response investigations the frequency-response technique was used, because, with the application of a sinusoidal oscillation to either fuel flow or propeller blade angle, all of the other engine variables execute sinusoidal fluctuations permitting a simple determination of the response of any one variable to another. Application of a sinusoidal change to either fuel flow or blade angle is experimentally feasible. Therefore, a separate fuel system was designed to impress sinusoidal fuel flows of variable frequency and amplitude on the engine.

Dynamic response tests were run at pressure altitudes of 10,000, 20,000, and 30,000 ft. at a fixed tunnel air temperature. For the dynamic response runs, the engine variables were measured by highly sensitive fast-acting instruments and were recorded on a galvanometric oscillograph or strip chart recorders. These instruments had sufficiently fast response so that no correction of the data for instrument dynamics was necessary except for the temperature data.

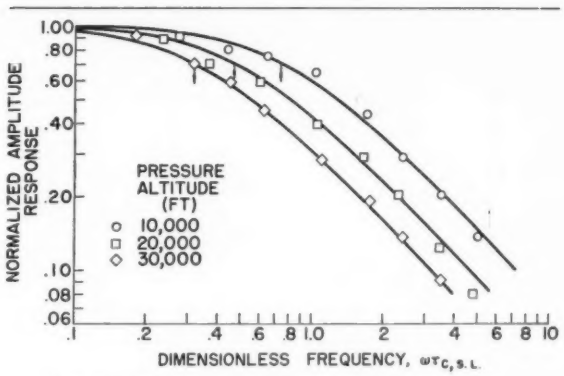

FIG. 2. Experimental response of speed to fuel flow.

Results

Some of the results of the dynamic response investigation are shown in the succeeding figures, wherein the amplitude response is plotted against the frequency of the applied sinusoidal fuel flow. In these figures the amplitude responses have been normalized and the frequency nondimensionalized. Normalization consisted of dividing the amplitude of the response by the gain or sensitivity factor for the response. The nondimensional frequency consists of the product of the frequency of the applied oscillations, ω, and the sea-level time constant of the engine-propeller combination, τ_{cSL}.

The amplitude response of engine speed to sinusoidally varying fuel flows with the propeller blade angle held constant is shown in Fig. 2. Responses are shown for three different altitudes. The general shape of the response curve is similar to that of a first-order dynamic system of the type shown in Fig. 1. It can be seen that the break frequencies for the three curves decrease with increasing altitude, indicating a slower response as the flight altitude increases. The time constant of the engine-propeller combination at 10,000 ft. is approximately one and four-tenths times the value at sea level, while for 30,000 ft. the time constant is approximately three and one-tenth times that at sea level.

In a similar manner, the speed response of the propeller alone and its associated time constant can be determined by a consideration of the speed-shaft torque relationship at constant propeller blade angle. The nature of this response is similar to that of the response of the engine-propeller combination—that is, a first-order lag system—and the response is affected in the same manner by changes in altitude.

The dynamics of the engine alone and its associated

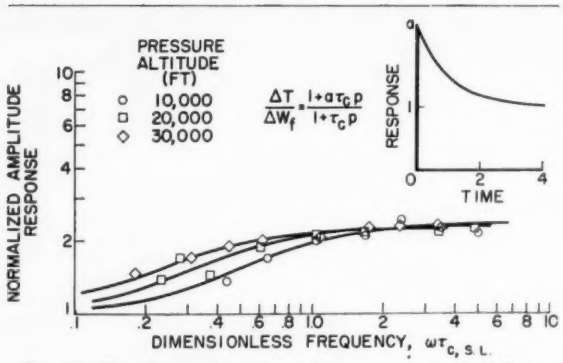

FIG. 3. Experimental response of temperature to fuel flow.

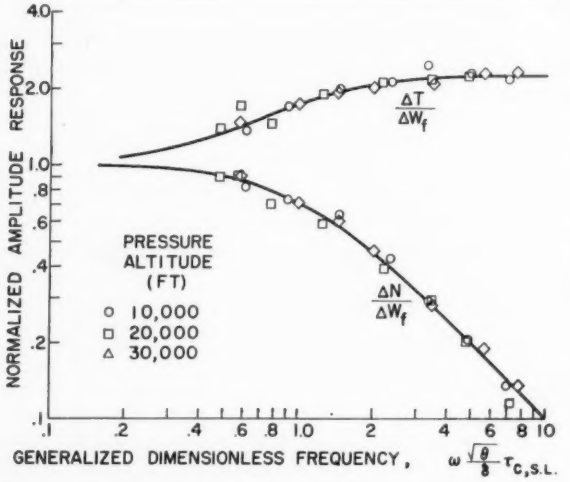

FIG. 4. Generalized experimental responses of temperature and speed to fuel flow.

time constant may be determined by a mathematical synthesis of the two aforementioned responses or by the application of the frequency-response technique using a fixed fuel flow and variable blade angle and considering the speed-shaft torque relationship under these conditions. The engine alone is also found to have a response similar to that of the engine-propeller combination.

The foregoing responses have all dealt with speed as the dependent variable. Another dependent variable of considerable interest from the standpoint of engine longevity and control application is the turbine-outlet temperature. A nondimensional amplitude response of turbine-outlet temperature to sinusoidally varying fuel flows at fixed blade angle is shown in Fig. 3. These data have had the thermocouple lag removed. A frequency response of this nature can be described by a system whose response equation is shown in the left-hand inset. Such a system arises from the combination of a lead network with a lag network, where the time constant of the lag is that of the engine-propeller combination and the time constant of the lead is some multiple a times this time constant. For the case shown, the value of a is greater than unity and is equal to the amplitude of the normalized frequency response at infinite frequency. The response of such a system to a step input is shown in the right-hand inset, and it can be seen that the dependent variable overshoots its final value. It can be shown that the ratio of the peak value to the final value is the constant a in the response equation.

As in the case of the speed-fuel flow response, the progression of the temperature response toward the decreasing frequencies with increasing altitude indicates increased response times at altitude. The high frequency value of the response is approximately the same for all altitudes. This indicates that the percentage temperature overshoot for a step change in fuel flow is independent of altitude.

The data of the preceding responses for all three altitudes have been replotted in Fig. 4 against a nondimensional abscissa generalized for altitude in the manner discussed in the "Analysis" section. Shown in Fig. 4 are both the temperature and speed responses to fuel flow. It is seen that the application of the generalization factor has rendered the responses invariant with altitude as predicted by theory. The dynamic response at any altitude can be predicted from the dynamic response at sea level.

It is of interest to compare the values of the time constants involved in the preceding responses as determined from the experimental dynamic response investigations with those that may be computed from the moments of inertia and the slopes of the steady-state engine performance curves. The comparison is shown in Fig. 5. Here, the data on the left-hand side for the time constants of both the engine-propeller combination and the propeller alone and the overshoot ratio for the temperature-fuel flow response were determined directly from the frequency response investigations. The time constant for the engine alone was determined by synthesis. It is interesting to note the relative values of the three time constants. The time constant of the

	PRESSURE ALTITUDE (FT)	TIME CONSTANT RATIOS DYNAMIC-RESPONSE $\frac{\tau}{\tau_{c,S.L.}}$	DYNAMIC-RESPONSE $\frac{\tau\delta/\theta}{\tau_{c,S.L.}}$	STEADY-STATE $\frac{\tau\delta/\theta}{\tau_{c,S.L.}}$
ENGINE-PROPELLER COMBINATION	10,000 20,000 30,000	1.4 2.1 3.1	1.00 1.00 0.97	0.99
PROPELLER	10,000 20,000 30,000	0.57 0.71 1.11	0.41 0.35 0.35	0.36
ENGINE	10,000 20,000 30,000	3.1 5.4 7.4	2.2 2.6 2.3	2.4

PRESSURE ALTITUDE (FT)	TEMPERATURE OVERSHOOT RATIO DYNAMIC-RESPONSE	STEADY-STATE
10,000 20,000 30,000	2.35 2.30 2.25	2.28

FIG. 5. Comparison of results.

combination falls between that of the propeller alone and that of the engine alone. The propeller time constant is approximately one-third that of the combination, and the engine time constant is about two and one-half times that of the combination.

From the appropriate slopes of the generalized steady-state performance curves and the moments of inertia of the components, the generalized time constants on the right-hand side were computed. An examination of the two sets of values show that they agree within 10 per cent of one another. The values for the combination are extremely close, while the greatest discrepancy appears in the determination of the generalized time constant for the propeller alone from the data taken at 10,000 ft. As a result of this good agreement over the range of altitudes investigated, it is concluded that the steady-state performance data afford a reliable means of determining the dynamic performance of the engine.

Controlled Behavior

The significance of the changes of engine dynamics with changes in altitude can be illustrated by considering engine behavior when acted upon by a linear control system. A linear control system was chosen so that effects of changes in engine dynamics would not be masked by control nonlinearities. In order to study these effects, we have computed the behavior of a complete controlled system at two different altitudes using an electronic analog computer. For this purpose we have chosen a control wherein the change in fuel flow is regulated in proportion to the sum of the speed error and its time integral and the change in propeller blade angle is regulated in proportion to the sum of the shaft torque error and its time integral. Such a control is referred to as a double-loop proportional-plus-integral control. The complete control system is shown diagrammatically in Fig. 6.

The engine is represented diagrammatically by the large block. It has inputs of fuel flow and propeller blade angle and outputs of speed, torque, and temperature. The speed is fed back and compared to the speed setting, and the difference or speed error energizes that portion of the control which regulates the fuel flow. Included in the operational representation of the control is the time delay of the fuel system, represented by a first-order lag of time constant $\tau_{L,1}$. In a similar manner, the torque error controls the blade angle. A time lag in the propeller has been included in this loop, represented by a first-order lag of time constant $\tau_{L,2}$.

Such a controlled system possesses what is known as interaction—that is, because each of the dependent variables is influenced by both of the independent variables, a change in the setting of one of the control loops will cause the independent variable in the other loop to change. Interaction can be studied by representing

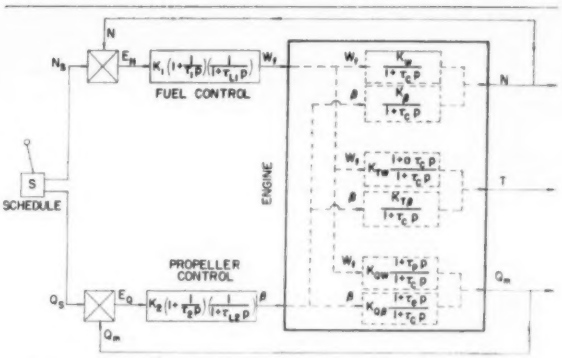

Fig. 6. Schematic diagram of engine-control combination.

the engine by a combination of transfer functions representing the response of a dependent variable to one of the independent variables, as was done in the diagram. Included in the diagram is a representation of the turbine-outlet temperature as a function of the two independent variables—fuel flow and propeller blade angle.

In the interest of simplicity of engine operation, we have made the control "single lever" operated by scheduling the speed and torque setting to ensure steady-state operation of the engine along a predetermined operating line and have incorporated some form of barometric compensation in the scheduling to keep the engine on the operating line as the altitude is changed.

The engine gains or sensitivities have been chosen as those determined from the experimental investigation of the turbine-propeller engine. The time constant of the engine-propeller combination has been arbitrarily selected to be 1 sec. at sea level. The other time constants were chosen in the same proportion to the combination time constant as those determined in the experimental investigation.

The control has four adjustable parameters. They are: the two control gains, K_1 and K_2, and two integral time constants, τ_1 and τ_2. The magnitudes of these parameters were chosen to give a good response at sea level—that is, fast response in the speed and torque and tolerable temperature and fuel flow overshoots. A sea-level response that was considered to be desirable is shown in Fig. 7. On this and succeeding figures the variables shown are speed, torque, temperature, fuel flow, and blade angle. The abscissa for all figures represents a 20-sec. time interval, and the final value of all variables represents the steady-state value corresponding to the final value of the power setting. At sea level the change in power setting consisted of a 100-r.p.m. change in speed and a 215-lb.-ft. change in torque. It can be seen that the speed and torque quickly come up to their final values. The first speed-pip is reached in 0.5 sec., whereas the torque hits its peak value in 0.2 sec. and is practically constant after $1^1/_4$ sec. There is a temperature overshoot of 86 per cent which lasts for 0.7 sec. This temperature over-

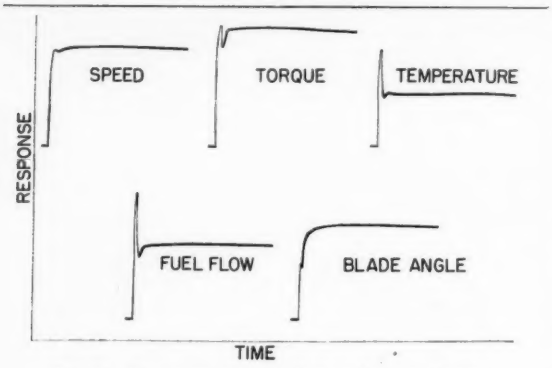

FIG. 7. Response of controlled engine; sea level.

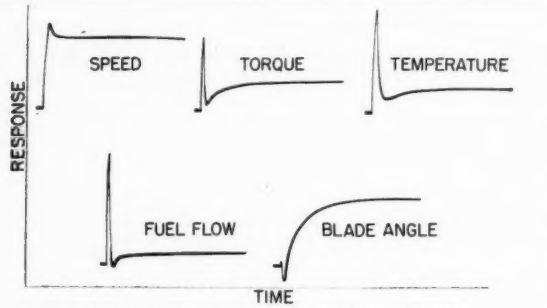

FIG. 8. Response of controlled engine; 40,000 ft.

shoot amounts to approximately 45°R. above the final value. Such a fast speed response requires a 68 per cent overshoot in fuel flow. This overshoot is not considered of sufficient magnitude and duration to precipitate burner blowout. The change of blade angle is small, only about 1.7°, and the fastest response demanded by the control is approximately 5° per sec., a figure easily met by today's propellers.

Let us now take our engine and control up to 40,000 ft. (Fig. 8) and observe the response to an equivalent change in control lever setting. The change of speed is still 100 r.p.m., but, because of the barometric compensation in the scheduling device, the change in torque is reduced to 40 lb. ft. to keep the engine on the steady-state operating line. There is still a fast response of speed—that is, the speed crosses its final value in 0.3 sec. with a slight overshoot. There are, however, intolerable overshoots in torque, temperature, and fuel flow. The severe torque overshoot endangers the reduction gearing. The temperature overshoot stresses the turbine blading, and the fuel flow overshoot might very well blow out the combustors. Such excesses are not to be tolerated because they represent conditions severely endangering the engine. This poor response is the result of mismatch between the engine and assumed control, because the dynamics of the engine have changed with the change in altitude while the control has retained its sea-level characteristics.

The foregoing results have shown the need for some compensation of the control to match the change in engine performance with a change in altitude. It has been previously stated that the change in the engine response consists of a change in engine sensitivity and a change in time of response. Likewise, the control has a sensitivity parameter and a time response parameter. It is the change in engine sensitivity which is primarily responsible for the large overshoots in Fig. 8. This change in engine sensitivities has long been recognized by control designers, and this recognition has resulted in compensation being built into the gains of the controller.

The purpose of the control-gain compensation is to keep the loop gain of the system constant at all altitudes. This loop gain is the product of the engine and the control sensitivities within the loop. When the gains of both loops are kept constant by means of a barometric compensation on K_1 and K_2, the response of the controlled engine at a flight altitude of 40,000 ft. is as shown in Fig. 9.

The gain compensation has succeeded in greatly reducing the torque, temperature, and fuel flow overshoots. The fuel flow and temperature overshoots have now regained values comparable to those at sea level, but the compensation has rendered the responses of all the variables oscillatory. The damping in both loops is of approximately the same magnitude. Two cycles of oscillation are observed in all variables, and about 9 sec. are required before the variables retain their final values.

The application of barometric compensation to the gains of the control produced an oscillatory system.

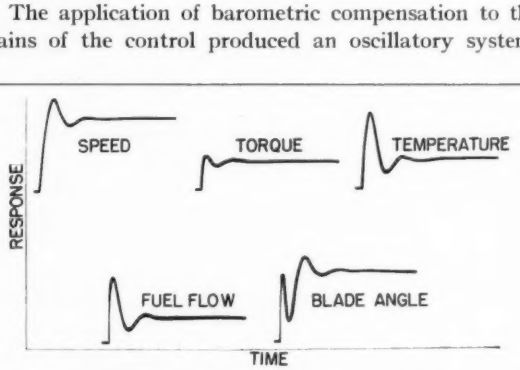

FIG. 9. Response of controlled engine; 40,000 ft., gain compensation.

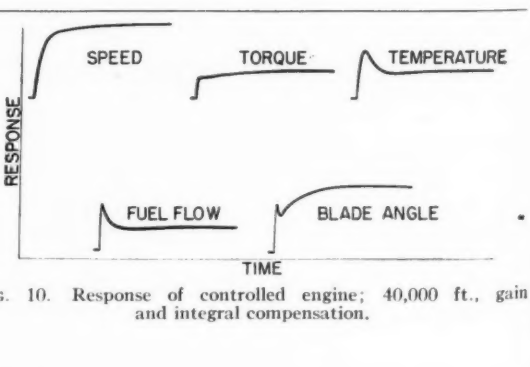

FIG. 10. Response of controlled engine; 40,000 ft., gain and integral compensation.

This response is the result of applying compensation to only one of the two sets of control parameters. The application of barometric compensation to the integral time constants, as well as the gains of the control, produces a much more to be desired engine behavior at this altitude, as is shown in Fig. 10. All oscillations in speed and torque have been removed, and the temperature and fuel flow overshoots are even smaller than those encountered at sea level. The speed of response has been considerably reduced below that of the controlled response at sea level. The torque reaches 80 per cent of its final value in 0.4 sec. but requires almost the full 20 sec. to attain its final value. The speed reaches 94 per cent of its final value in 5.3 sec. Therefore, with a completely barometrically compensated control, we have an oscillation-free system in which the speed of response is three times as fast and the temperature overshoot one-third as large as for the uncontrolled engine at this altitude.

It may be expected that the results shown in Fig. 10 should be similar to those shown for sea level (Fig. 7) with the exception that the time response should be approximately $\sqrt{\theta}/\delta$ or four and six-tenths times as long. However, compensation has not rendered the two systems exactly proportional. One reason for the lack of similarity is that barometric compensation does not compensate for the change in temperature with altitude. Secondly, reference to Fig. 6 shows that, when the gains of the individual loops are maintained constant, the contributions of the interaction do not retain their same proportional magnitude in the system.

Let us look at the effect of compensating K_1 barometrically. K_1 acts on those portions of the engine whose sensitivity is designated by K_W and K_{QW}. K_W is the sensitivity of the speed-fuel flow response, and K_{QW} is the sensitivity of the torque-fuel flow response. While K_1 has been decreased by the factor δ to compensate for the change in the factor K_W, which increased by the factor $1/\delta$ due to the change in altitude, the factor K_{QW} increased by only $1/\sqrt{\theta}$. Therefore, barometric compensation of K_1 does not properly compensate for the change in K_{QW}. Thus, even though barometric compensation does not preserve absolute similarity of response at all altitudes, the resultant engine behavior is satisfactory.

Summary

We have arrived at a number of facts concerning the dynamic behavior of the engine. Specifically, we have shown that the dynamic behavior of the engine varies both as to sensitivity and time of response with changes in altitude. The variation of response with flight altitude is predictable, in that it was possible to generalize the experimental responses in a manner similar to that used to generalize the steady-state performance of the engine. Further, it has been shown that it is possible to analytically determine the dynamic responses of the engine, within a reasonable margin of error, from the steady-state performance curves of the engine and the moments of inertia of its components.

Applying this information, we have demonstrated the effect of the change in flight altitude on the controlled behavior of the engine, indicating the serious mismatch of engine and control which can arise from the changed engine dynamics at altitude, and the need for compensating the control to accommodate the changes.

Gain compensation of the control, while removing some of the undesirable features of the uncompensated control action, gave rise to another objectionable feature—an oscillatory system. This situation was alleviated by barometric compensation of the integral time constants to account for the changed engine response times. This compensation removed the oscillations from the system at the expense of the speed or response. The slower response is, however, more rapid than that of the uncontrolled engine and is acceptable.

The preceding discussion has been limited to the turbine-propeller engine. However, the basic results and the method of approach indicated are equally applicable to any gas-turbine engine.

Appendix (A)

Symbols

a = temperature overshoot ratio
I = polar moment of inertia (referred to engine speed)
K_W = gain of speed-fuel flow response at constant blade angle
K_β = gain of speed-blade angle response at constant fuel flow
$K_{Q.\beta}$ = gain of torque-blade angle response at constant fuel flow
$K_{Q.W}$ = gain of torque-fuel flow response at constant blade angle
$K_{T.W}$ = gain of temperature-fuel flow response at constant blade angle
$K_{T.\beta}$ = gain of temperature-blade angle response at constant fuel flow
N = engine speed
p = differential operator d/dt
Q = torque (referred to engine speed)
t = time
T = temperature
W_f = fuel flow
β = blade angle
Δ = incremental change from steady-state
δ = pressure correction factor = ambient static pressure/N.A.C.A. standard sea-level pressure
θ = temperature correction factor = ambient static temperature/N.A.C.A. standard sea-level temperature
τ = time constant
ω = frequency

Subscripts

c = engine-propeller combination
e = engine
L = lag
m = measured
p = propeller

s = setting
SL = sea level
1 = fuel control loop
2 = propeller control loop

Appendix (B)—Derivation of Dynamic-Response Equations and Time Constants

The dynamic responses and the time constants are developed from the following assumptions:

The engine torque is assumed to be a function of fuel flow and speed; propeller torque is assumed to be a function of propeller blade angle and speed.

$$Q_e = Q_e(W_f, N) \tag{B1}$$
$$Q_p = Q_p(\beta, N) \tag{B2}$$

Similarly, any engine variable may be expressed as a function of two other variables.

More explicitly, Eqs. (B1) and (B2), when linearized for incremental excursions about a steady-state point, can be written as

$$\Delta Q_e = (\partial Q_e/\partial W_f)_N \, \Delta W_f - (\partial Q_e/\partial N)_{W_f} \Delta N \tag{B3}$$
$$\Delta Q_p = (\partial Q_p/\partial \beta)_N \Delta\beta + (\partial Q_p/\partial N)_\beta \Delta N \tag{B4}$$

where the subscripts on the partial derivatives indicate the constant factor and where the signs are determined by the physical nature of the partial derivative.

The difference between engine torque and propeller torque accelerates the engine; therefore, referring all terms to engine speed by multiplication by the appropriate function of the gear ratio,

$$Q_e - Q_p = (I_p + I_e)\,(dN/dt) \tag{B5}$$

If only incremental changes in the torques are considered, Eq. (B5) may be written as

$$\Delta Q_e - \Delta Q_p = (I_p + I_e)\,(d\Delta N/dt) \tag{B6}$$

Substitution of Eqs. (B1) and (B2) in Eq. (B6) yields

$$\left(\frac{\partial Q_e}{\partial W_f}\right)_N \Delta W_f - \left(\frac{\partial Q_p}{\partial \beta}\right)_N \Delta\beta - \left[\left(\frac{\partial Q_p}{\partial N}\right)_\beta + \left(\frac{\partial Q_e}{\partial N}\right)_{W_f}\right] \Delta N = (I_p + I_e)\frac{d\Delta N}{dt} \tag{B7}$$

At constant propeller blade angle, substituting p for d/dt in Eq. (B7) and rearranging terms yields the response of speed to fuel flow

$$\left(\frac{\Delta N}{\Delta W_f}\right)_\beta = \frac{(\partial Q_e/\partial W_f)_N}{[(\partial Q_p/\partial N)_\beta + (\partial Q_e/\partial N)_{W_f}]} \times \left(\frac{1}{1 + \tau_e p}\right) = K_W \left(\frac{1}{1 + \tau_e p}\right) \tag{B8}$$

where the time constant, τ_e, is given by

$$\tau_e = \frac{I_p + I_e}{[(\partial Q_p/\partial N)_\beta + (\partial Q_e/\partial N)_{W_f}]} \tag{B9}$$

This time constant is descriptive of the dynamics of the engine-propeller combination and is therefore referred to as the time constant of the combination.

In a similar manner, at constant fuel flow, the response of speed to blade angle is

$$\left(\frac{\Delta N}{\Delta\beta}\right)_{W_f} = \frac{-(\partial Q_p/\partial\beta)_N}{[(\partial Q_p/\partial N)_\beta + (\partial Q_e/\partial N)_{W_f}]} \times \left(\frac{1}{1 + \tau_e p}\right) = K_\beta \left(\frac{1}{1 + \tau_e p}\right) \tag{B10}$$

It is to be noted that the time constants in Eqs. (B8) and (B10) are the same, the difference in the responses being the gain or sensitivity term.

The dynamics of the engine alone and of the propeller alone may be determined by introducing a new variable, shaft or measured torque, Q_m, and considering the response of speed to the variable. This is equivalent to cutting the shaft between the engine and propeller and considering either of these components separately according to the laws of rigid body dynamics.

The difference between engine torque and shaft torque accelerates the engine; thus,

$$Q_e - Q_m = I_e(dN/dt) \tag{B11}$$

Considering only incremental changes in engine and shaft torque, Eq. (B11) may be written

$$\Delta Q_e - \Delta Q_m = I_e(d\Delta N/dt) \tag{B12}$$

Substitution of Eq. (B3) in Eq. (B12) yields

$$\Delta Q_m = \left(\frac{\partial Q_e}{\partial W_f}\right)_N \Delta W_f - \left(\frac{\partial Q_e}{\partial N}\right)_{W_f} \Delta N - I_e\left(\frac{d\Delta N}{dt}\right) \tag{B13}$$

At constant fuel flow, substituting p for d/dt and rearranging terms yields the response of speed to measured torque.

$$\left(\frac{\Delta N}{\Delta Q_m}\right)_{W_f} = -\frac{1}{(\partial Q_e/\partial N)_{W_f}}\left(\frac{1}{1 + \tau_e p}\right) \tag{B14}$$

where the time constant involved is given by

$$\tau_e = I_e/(\partial Q_e/\partial N)_{W_f} \tag{B15}$$

Eqs. (B14) and (B15) describe the dynamics of the engine alone.

The difference between shaft torque and propeller torque accelerates the propeller. Considering incremental changes, this difference can be written as

$$\Delta Q_m - \Delta Q_p = I_p(d\Delta N/dt) \tag{B16}$$

Substituting Eq. (B4) yields

$$\Delta Q_m = \left(\frac{\partial Q_p}{\partial \beta}\right)_N \Delta\beta + \left(\frac{\partial Q_p}{\partial N}\right)_\beta \Delta N + I_p\left(\frac{d\Delta N}{dt}\right) \tag{B17}$$

At constant blade angle, this expression can be reduced and rearranged to yield the response of speed to measured torque:

$$\left(\frac{\Delta N}{\Delta Q_m}\right)_\beta = \frac{1}{(\partial Q_p/\partial N)_\beta}\left(\frac{1}{1 + \tau_p p}\right) \tag{B18}$$

where the time constant, τ_p, is given by

$$\tau_p = I_p/(\partial Q_p/\partial N)_\beta \tag{B19}$$

Eqs. (B18) and (B19) describe the dynamics of the propeller alone.

A variable of importance in the control of an engine is some characteristic temperature downstream of the combustion chamber. The responses of that temperature to the independent variables of the engine may be derived as follows.

Temperature is assumed to be a function of fuel flow and speed.

$$T = T(W_f, N) \tag{B20}$$

Considering only incremental changes of the variables, Eq. (B20) can be written as

$$\Delta T = (\partial T/\partial W_f)_N \Delta W_f - (\partial T/\partial N)_{W_f} \Delta N \tag{B21}$$

At constant propeller-blade angle, the relation between speed and fuel flow is given by Eq. (B8). Substitution of Eq. (B8) in Eq. (B21) yields the response of temperature to fuel flow at constant blade angle.

$$\left(\frac{\Delta T}{\Delta W_f}\right)_\beta = \left(\frac{\partial T}{\partial W_f}\right)_N - \left\{\frac{\left(\frac{\partial T}{\partial N}\right)_{W_f}\left(\frac{\partial Q_e}{\partial W_f}\right)_N}{\left[\left(\frac{\partial Q_p}{\partial N}\right)_\beta + \left(\frac{\partial Q_e}{\partial N}\right)_{W_f}\right]}\right\} \frac{1}{(1 + \tau_e p)} \tag{B22}$$

Eq. (B22) can be written in the form

$$\left(\frac{\Delta T}{\Delta W_f}\right)_\beta = K_{T,W}\left(\frac{1 + a\tau_e p}{1 + \tau_e p}\right) \tag{B23}$$

where

$$K_{T,W} = \left(\frac{\partial T}{\partial W_f}\right)_N - \frac{\left(\frac{\partial T}{\partial N}\right)_{W_f}\left(\frac{\partial Q_e}{\partial W_f}\right)_N}{\left[\left(\frac{\partial Q_p}{\partial N}\right)_\beta + \left(\frac{\partial Q_e}{\partial N}\right)_{W_f}\right]} \tag{B24}$$

and

$$a = (\partial T/\partial W_f)_N / K_{T,W} \tag{B25}$$

At constant fuel flow, the relation between speed and blade angle is given by Eq. (B10). Substitution of Eq. (B10) in Eq. (B21) yields the response of temperature to blade angle.

$$\left[\frac{\Delta T}{\Delta \beta}\right]_{W_f} = \frac{\left(\frac{\partial T}{\partial N}\right)_{W_f}\left(\frac{\partial Q_p}{\partial \beta}\right)_N}{\left[\left(\frac{\partial Q_p}{\partial N}\right)_\beta + \left(\frac{\partial Q_e}{\partial N}\right)_{W_f}\right]} \times \left[\frac{1}{(1 + \tau_e p)}\right] = K_{T,\beta}\left(\frac{1}{1 + \tau_e p}\right) \tag{B26}$$

For the analysis of the controlled system, it is necessary to know the response of the measured or shaft torque to the independent variables. This may be done in the following manner:

The response of measured torque to fuel flow at constant blade angle may be obtained by eliminating the ΔN between Eqs. (B8) and (B18) in this manner:

$$[\Delta Q_m/\Delta W_f]_\beta = [\Delta Q_m/\Delta N]_\beta [\Delta N/\Delta W_f]_\beta \tag{B27}$$

Substituting the responses of Eqs. (B8) and (B18) in Eq. (B27) yields

$$\left[\frac{\Delta Q_m}{\Delta W_f}\right]_\beta = \frac{\left(\frac{\partial Q_p}{\partial N}\right)_\beta \left(\frac{\partial Q_e}{\partial W_f}\right)_N}{\left[\left(\frac{\partial Q_p}{\partial N}\right)_\beta + \left(\frac{\partial Q_e}{\partial N}\right)_{W_f}\right]} \times \left[\frac{(1 + \tau_p p)}{(1 + \tau_e p)}\right] = K_{Q,W}\left(\frac{1 + \tau_p p}{1 + \tau_e p}\right) \tag{B28}$$

Similarly, the response of measured torque to propeller blade angle may be obtained by eliminating the ΔN between Eqs. (B10) and (B14); thus,

$$[\Delta Q_m/\Delta \beta]_{W_f} = [\Delta Q_m/\Delta N]_{W_f} [\Delta N/\Delta \beta]_{W_f} \tag{B29}$$

Substitution of the appropriate responses yields

$$\left[\frac{\Delta Q_m}{\Delta \beta}\right]_{W_f} = \frac{\left(\frac{\partial Q_e}{\partial N}\right)_{W_f}\left(\frac{\partial Q_p}{\partial \beta}\right)_N}{\left[\left(\frac{\partial Q_p}{\partial N}\right)_\beta + \left(\frac{\partial Q_e}{\partial N}\right)_{W_f}\right]} \times \left(\frac{1 + \tau_e p}{1 + \tau_e p}\right) = K_{Q,\beta}\left(\frac{1 + \tau_e p}{1 + \tau_e p}\right) \tag{B30}$$

The foregoing responses and time constants may all be presented in a generalized or "corrected" form. For example, the response of speed to fuel flow may be written in generalized form as

$$\left[\frac{\Delta N/\sqrt{\theta}}{\Delta W_f/\delta\sqrt{\theta}}\right]_\beta = \frac{\left(\frac{\partial Q_e/\delta}{\partial W_f/\delta\sqrt{\theta}}\right)_{N/\sqrt{\theta}}}{\left[\left(\frac{\partial Q_p/\delta}{\partial N/\sqrt{\theta}}\right)_\beta + \left(\frac{\partial Q_e/\delta}{\partial N/\sqrt{\theta}}\right)_{W_f/\delta\sqrt{\theta}}\right]}\left[\frac{1}{\left(1 + \tau_e \frac{\delta}{\sqrt{\theta}} p\right)}\right] \tag{B31}$$

where the generalized time constant, $\tau_e(\delta/\sqrt{\theta})$, is given by

$$\tau_e \frac{\delta}{\sqrt{\theta}} = \frac{I_e + I_p}{\left(\frac{\partial Q_p/\delta}{\partial N/\sqrt{\theta}}\right)_\beta + \left(\frac{\partial Q_e/\delta}{\partial N/\sqrt{\theta}}\right)_{W_f/\delta\sqrt{\theta}}} \tag{B32}$$

On Turbulent Fluid Motion

MAX M. MUNK

Naval Ordnance Laboratory

Abstract

Turbulent fluid motion is a daily and common experience, and still it comes as a surprise to the inquisitive student of hydrodynamics. It came to him as a surprise even in the early period of boundary-layer study at a time when the possibility of turbulence had already been well recognized. By now we are resigned to the frequent occurrence of turbulence but have still to suppress the feeling of slight mental frustration or incongruence whenever we give serious thought to it. In spite of half a century of intense mathematical effort, the frequent instability of laminar flow is not clearly understood, and turbulence has not been laid bare as a simple consequence of the kinematics and dynamics involved. It has so far been denied to our inquisitive minds to see turbulence clearly, distinctly, and intuitively as a direct consequence of the underlying laws of motion.

There are presented in this paper some broad thoughts toward clarification of the turbulence problem. There are thoughts that may perhaps suggest to one or the other reader a more precise and perhaps more heuristic inquiry. These thoughts do not fully satisfy. They carry the inquiry forward without bringing it to full conclusion. Still they set the mind a little bit at ease and blunt the edge of consternation and frustration.

The arguments will be chiefly directed to the straight channel flows of the incompressible fluid, which are the plane Couette flow and the Poiseuille flow. These are the simplest cases, but the territory of inquiry is much broader and the thoughts presented are indeed fairly general. Also, in the following, it will not be necessary to give much attention to the three-dimensional aspect of the flow; the present issue is basically two-dimensional. Actual turbulence is, of course, always three-dimensional.

The following is directed to readers reasonably prepared for the discussion. It seems therefore unnecessary to define commonly used terms; nor does it seem necessary to describe the phenomenon in question.

Energy Considerations

The two-plane channel flows just referred to satisfy a minimum condition with respect to their work dissipation. The laminar channel flows do not involve the active manifestation of mass forces. The viscosity forces are in equilibrium with the pressure distribution. It has been shown by Lamb in *Hydrodynamics* that, in consequence of this, the laminar undisturbed channel flows have less work dissipation than any other flow consistent with the boundary conditions.

A straight plane laminar flow not having the Couette or Poiseuille velocity profile is not in equilibrium. Aside from this, it does not have absolute minimum dissipation; this would contradict the proposition just made. It has, however, a relative minimum of dissipation. As long as the boundary conditions are complied with and the time average of the flow is maintained (whereby the "basic" flow or velocity profile is maintained), the dissipation is increased by the superposition of any "disturbance" flow periodic in the flow direction such that its space average is zero. This follows directly from the fact that the rate of dissipation per unit volume is proportional to the sum of the squares of certain space derivatives of the velocity distribution and because, in this case, the total rate of dissipation is proportional to the space integral of the vorticity square.

The kinetic energy of the channel flow is clearly not a minimum, but the flow of the same flux having minimum kinetic energy has constant velocity.

The work supplied to the flow can conveniently be figured out by using a reference system such that the total channel flux is zero. The channel walls move then in their own direction, and the work supplied per unit time is equal to the product of the wall velocity times the surface friction force. The latter is linear in terms of the vorticity at the wall. It follows that the total energy supply is not changed by a purely space periodic disturbance, but it remains unchanged as long as the flow itself does not change.

From energy considerations it follows, therefore, that no disturbance can grow on an unchangeable laminar basic flow initially at equilibrium. That is to say, any instability of the steady laminar channel flow must involve more than a sole increase of the magnitude of the disturbance. It must involve a change of the basic flow itself or, in other words, a change of the basic velocity profile. Any increase of a space periodic disturbance is to be interpreted as being associated with a proper velocity profile change. This is already necessary during the first millionth of a second, otherwise the disturbance could not increase for want of energy supply. The basic flow must change to one supplying more energy. It is immaterial that the work deficiency involved is at first small, being of second order. The lack of even this small amount of energy would prove fatal and would invalidate the result.

The linearized theory does not consider the energy balance or the velocity profile change. This hampers the clarification process and, furthermore, raises doubts as to the significance of the results. As to the clarification, the linearized theory leaves a gap just where the greatest fullness is required. We look first and almost exclusively to the energy balance to settle the question of stability or instability. If an initial tapping of an available energy source has to be carefully avoided lest the energy stream opened cannot be stopped again, we recognize instability without too

Received September 25, 1950.

much curiosity concerning the kinematics of the problem. The kinematic aspect is not likely to satisfy us and becomes problematical if it is arrived at without regard to, or even in defiance of, the energy balance.

We can easily see how the basic flow must change in case of instability for increased energy supply. There must be vorticity increase at the wall and, hence, a vorticity decrease at some region spaced from the wall, since the total vorticity is invariant. We are at this moment discussing the space average—that is, a definite basic velocity profile into which the initial undisturbed laminar velocity profile has been changed.

Concentrating the vorticity near the wall tends to even out the velocity profile and is thus not inconsistent with a diminished kinetic energy of the flow. Thus, a certain amount of energy that may provide for increased dissipation becomes available. This effect is, however, not significant, and it is not important for explaining the occurrence of turbulence. This kinetic energy is finite and is available one time only, whereas continued turbulence requires a continuous supply of excess work to be continuously dissipated by excess dissipation. The kinetic energy is a secondary source of energy and cannot explain or support continuous excess dissipation.

Vorticity Discrimination

We have arrived at a basic flow, not necessarily in equilibrium by itself, associated with a whirl or disturbance distribution. The total sum of the disturbance vortices is zero. These whirls or disturbance vortices deteriorate by viscosity, and new ones spring up from the basic flow and from the instability of the disturbance flow itself, so that with developed turbulence the disturbances remain statistically constant. Likewise, through viscosity effects, the basic flow tends to approach the laminar basic flow. A mechanism is therefore needed to keep the turbulent basic flow different from the laminar basic flow. The disturbance itself must have such an effect; there is nothing else that may. The cardinal point of inquiry, or at least an important one, is, accordingly, a search for a mechanism that brings that about. On either side of the channel there is an equal number of disturbance vortices of both directions. The vortices corotational with the vorticity of the basic flow last longer near the walls and are shorter lived near the channel center than the counterrotational vortices, whereby the laminar basic flow is changed in profile and whereby said changed basic profile is conserved. We want to understand how and why that happens, for, if we do, we see a reason for turbulence.

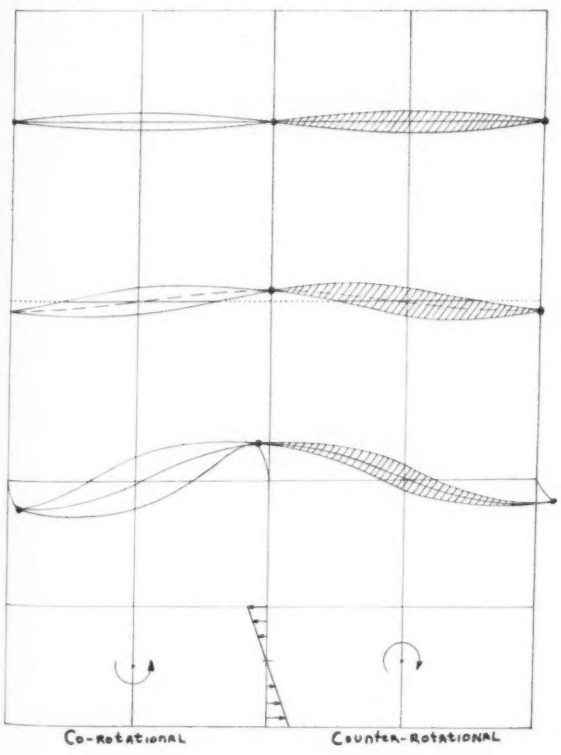

Fig. 1. Vortex discrimination.

It is immediately apparent that the linear terms of the equations of motion cannot have such a discriminative effect. The clarification has to lean on the quadratic terms. In view of the fact that the solution of the linearized equation took a lifetime, it seems to be an almost hopeless undertaking to try to solve the complete or correct equation. We shall, therefore, content ourselves with qualitative discussions of some kind as the only alternative at this time to giving up the problem altogether.

It will be important to find out whether any vortex discrimination operates diffusively or with local concentration. If the discrimination leads merely to a change of the velocity profile without maintaining or bringing about a pronounced disturbance motion, it would not support turbulence. The increased energy supply would then be promptly dissipated in an orderly fashion by way of the changed velocity profile reverting to the initial laminar velocity profile. If, however, concentration of certain vorticity whirls takes place, a case is made for instability of the laminar flow and for the creation or maintenance of the turbulent flow. For whatever the flow may be, the sum total of its vorticity is invariant. Turbulence is characterized by local vorticity concentrations as contradistinguished from a mere velocity profile change. Local vorticity concentration is itself turbulence.

The Streamwise Vortex Row

The quadratic character of the equations of motion precludes superposition of individual solutions. The different aspects of the ensuing motion are not represented by particular solutions, and yet we must spe-

cialize. We shall, therefore, study a special flow that we believe to be typical.

Any disturbance vorticity concentrated within a small area will be associated with some opposite disturbance vorticity at another point. The channel flows we are considering are basically shear flows. They will stretch out any compact region of disturbance vorticity in a streamwise direction. The combination of the basic flow and disturbance vorticity periodic in streamwise direction and approximately concentrated along one undisturbed stream line appears accordingly as a typical combination flow. Most of the disturbance is approximately nonrotational and can, therefore, be represented by a potential. The disturbance flow can be approximated by two different potential flows—one on either side of the vortex line—of the type $\cosh y \sin x$. In addition, a boundary-layer flow will occur at each wall to eliminate slipping. The vorticity at the inner vorticity line per unit length is equal to the velocity jump of the two flows at their common boundary. It is supposed that the inner vorticity has already spread out by reason of viscosity and that it keeps on doing so similar to a boundary layer.

So far, there is symmetry with respect to the two rotational directions. We try to concentrate our attention on possible vortex discrimination. The viscosity effect is basically a linear diffusion effect. Within an unlimited region, the square of the radius of gyration of anything diffusing increases at a constant rate proportional, in the present case, solely to the kinematic viscosity having the proper physical dimension—area divided by time. If the region available for spreading out is bounded, naturally the square of the radius of gyration cannot continue to increase, and the rate of increase must be smaller. These are all details; the essential effect is that increase of said square takes place until positive and negative vortices merge, whereby they annihilate each other. Above all, diffusion is linear and does not discriminate between the two vorticity directions.

The square of the radius of gyration of the disturbance vortex concentration would not remain equal even in absence of viscosity. Convection by the basic flow and self-convection by the disturbance takes place and changes said square. Here is a possible key to turbulence. The self-convection of our special disturbance flow exposes the disturbance vortices to convection by the basic flow whereby they spread out or move together ("cumulate"), depending on whether the vortices are corotational or counterrotational with the basic flow vorticity. Here, we clearly have vortex discrimination, and this is a sufficient reason for subsequent change of energy supply. The inner vortex line is bent by self-convection into a wave, and the nodal points of the wave coincide with the points of maximum vorticity. Let the vortex line initially coincide with the stream line of zero velocity of a Couette flow. After the waving has taken place, the vortices of corotational direction become flowwise compressed or telescoped (or cumulated), and the vortices of counterrotational direction become spread out in flow direction by the convection of the basic flow, whereby the points of zero disturbance vorticity become pairwise and alternately more spaced and less spaced. Thereby, the diffusion effect of viscosity is aided by, or added to, with the counterrotational vortices, but it is counteracted with the corotational vortices. All disturbance vortices travel toward the channel walls, but the counterrotational vortices become spread out thinner than the corotational vortices. The counterrotational vortices will slow down and acquire relatively more area near the vortex line, and the corotational vortices will speed up and penetrate farther away from the vortex line and will acquire relatively more area near the walls.

This takes place everywhere and, again, secondarily locally in smaller scale as an incident of a sufficiently large disturbance itself. The result can only be statistically understood. The vortex discrimination does not cancel out statistically, being essentially a quadratic effect and having everywhere the same sign. It leads ultimately to increase of work supplied by the wall friction and thus favors instability of the laminar flow or statistical equilibrium of the turbulent flow, provided the cumulation is large enough to exceed the effect of viscosity diffusion. It is *a priori* clear that the Reynolds Number of the flow determines whether cumulation is relatively large or not. Viscosity is dominating at extremely small Reynolds Numbers. This calls for stability of the laminar flow. At extremely large Reynolds Numbers the pressure modifications caused by viscosity are comparatively small. A much smaller scale of whirling is necessary to make the influence of viscosity on the pressure distribution comparable to the mass effect influence on the pressure distribution. Conditions are unfavorable for larger whirls. The smaller ones have more tendency to cancel out statistically because secondary cumulation becomes more dominant. This is again more favorable to stability of the laminar flow. Viscosity effects and mass effects in balanced combination are most favorable to cumulation at the right scale. At extremely large Reynolds Numbers there is, finally, not enough viscosity effect left with the Poiseuille flow for breaking up the line of fluid particles of maximum vorticity along the wall.

There must be a limit to cumulation by vortex discrimination. After a certain intensity of turbulence has been established, a statistical equilibrium is reached and turbulence no longer increases. Cumulation reaches saturation because it is not linear. Vorticity in shear flow gives rise to less cumulation if the vorticity is concentrated along a narrow channel strip than if it is evenly spread out through the entire channel. Most of the turbulent channel flow has only small shear, and the flow region of large shear becomes

narrow. The increasing cumulation required becomes, finally, equal to the decreasing cumulation taking place.

Diffusive Spreading Out

The following vector analytical equations are written with the use of the positive and negative signs as originally proposed by Hamilton. The equation of diffusion of a scalar quantity F appears then as

$$F_T = \nu\nabla \cdot \nabla F \tag{1}$$

∇F denotes the antigradient—that is, a vector equal and opposite to the vector conventionally designated as the gradient. $\nabla \cdot \nabla F$ designates the Laplacian with the conventional sign, so that an ordinary three-dimensional maximum has a negative Laplacian. Eq. (1) indicates, therefore, a smoothing out or leveling out.

The space integral,

$$\int dS \quad r \cdot rF \tag{2}$$

represents the negative moment of inertia of the distribution F. We assume that the space integral

$$\int dS\, F \tag{3}$$

is finite and that the space in which diffusion occurs is uninterrupted and unlimited. We examine the time change of the negative moment of inertia of F with respect to the origin of the reference system chosen. Applying Green's theorem two times in succession—that is, applying two times Gauss' theorem by way of integration by parts—gives

$$\frac{d}{dT}\int dS\, r\cdot r\, F = \nu \quad \int do\, r\cdot r\, \nabla F - 2\int do\cdot rF + 6\int dS\, F\Big) \tag{4}$$

The space integral (3) is constant provided the surface integral $\int do\cdot\nabla F$ approaches zero with increasing space inclosed by the surface o. Hence, if all surface integrals occurring vanish as the smallest distance of the surface from the origin approaches infinity, there results

$$d/dT\,(\int dS\, r\cdot rF/\int dS\, F) = -6\nu \tag{5}$$

That is to say, the square of the radius of gyration of the quantity F increases uniformly at the rate 6ν. In the two-dimensional space, the equivalent rate of increase is only 4ν, and in the one-dimensional space, it is only 2ν.

If the space available for the diffusion is finite, there is naturally an upper limit to the square of the radius of gyration. The rate 6ν is then the upper bound of the rate of increase.

Quantitative Estimate

We proceed to a rough quantitative estimate of the intensity of the cumulation effect to compare it with the diffusion. We assume a vortex row periodic in the stream direction X situated parallel to the wall of a Couette flow at a distance therefrom equal to 2.5 length units. The channel width may be 10 length units. The disturbance flow potentials Φ_1 and Φ_2 may be

$$\left.\begin{aligned}\Phi_1 &= \sin x \cosh (5 - y)\\ \Phi_2 &= \sin x \cosh (5 + y)\,\frac{\sinh 2.5}{\sinh 7.5}\end{aligned}\right\} \tag{6}$$

The cross velocity component $\partial\Phi/\partial y$ of the two potential flows agrees at the vortex line and is equal to

$$V = \sin x \sinh 2.5 \tag{7}$$

The streamwise components do not agree at the vortex line, so that the combined flow is associated with the vorticity per unit length of the vortex line of intensity equal to the difference of that velocity component.

$$Q = \cos x \cosh 2.5 \left(1 + \frac{\cosh 7.5}{\sinh 7.5}\sinh 2.5\right) \approx 2\cos x \cosh 2.5 \tag{8}$$

Furthermore, the shear at the channel walls will give rise to suitable additional boundary layers, whereby slipping is eliminated. The vorticity [Eq. (8)] will also spread out in cross-stream direction so that they will soon occupy an interface layer of finite thickness similar to a boundary layer.

The general features of such vortex row have already been described above. We direct our attention to the cumulation only. The distance from the initial vortex line attained by the vortices is proportional to the time, and the streamwise distance X traveled is proportional both to the cross distance that determines the streamwise velocity and to the time. In all, therefore, it is proportional to the square of the time. Cumulation is not a linear effect, but it is a quadratic effect relative to time.

We proceed to compute the increase of the square of the radius of gyration of the corotational vortices caused by cumulation during a certain time interval T. The integral

$$\int_\alpha^{\alpha + 2\pi} x \sin x\, dx = 2\pi \tag{9}$$

α designating any arbitrary constant, will occur in the computation.

The vortex of strength [Eq. (8)] traveling with the velocity [Eq. (7)] has been displaced through the distance

$$\int_0^t V\, dt$$

and has thereby acquired a streamwise velocity

$$\omega\int_0^t V\, dt$$

The streamwise displacement X is therefore equal to

$$X = \int\int (1/2)\omega \sin x \sinh 5\, dt\, dx \qquad (10)$$

The square of the radius of gyration has been decreased by

$$\int_{-\pi/2}^{\pi/2} \omega \sin x \cos x\, dx \int_0^t \int_0^t \sinh 2.5 \cosh 2.5\, dt^2 \qquad (11)$$

The first integral in Eq. (11) has the value $\pi\omega$. The length of the row occupied by each group of corotational vortices is π. The chosen width, 10, of the channel is reasonably commensurate with the length π. The difference of the two wall velocities is 10ω, ω designating the angular velocity of the cross fluid lines. The Reynolds Number of the Couette flow using the width and said velocity difference is, accordingly, 100ω. The maximum velocity V given by Eq. (7) is then sinh $2.5 = 6$. An acceptable average velocity may, perhaps, be 4. An average travel distance for the vortices may be one-fifth of the width—that is, 2. This gives a time interval of travel equal to $^1/_2$, during which cumulation acts. The total corotational vorticity considered is 2 cosh $2.5 = 12$. All this leads to a decrease of the square of the radius of gyration equal to

$$\pi\omega(1/2)^2\, 36/(1/2) = 18\pi\omega \qquad (12)$$

The viscous diffusive increase of the same square is perhaps

$$3t\nu = (3/2)\nu \qquad (13)$$

Setting Eqs. (12) and (13) equal to each other leads to a Reynolds Number indicative of the critical one where stability has its limit. This gives $18\pi\omega/(3/2)\nu = 1$, $\omega/\nu \sim 1$. Hence, $R = 100$.

Considering the side portion of a turbulent Poiseuille flow as similar to a Couette flow, the Reynolds Number defined by the width of the Poiseuille flow is perhaps 5 to 10 times as large as the number previously found—that is, $R = 500 - 1{,}000$.

The result of this rough estimate depends greatly on the choice of the cumulation distance and of the cumulation time. All that can be said is that a reasonable choice of both is conceivably consistent with the correct Reynolds Number.

The Poiseuille flow has variable vorticity, and the disturbance flow would disarrange that vorticity. This disarranging plays an important part in the linearized theory. It may, by itself, contribute to instability, but only if it is supported by cumulation. This disarranging would constitute a detail of the destabilizing effect of cumulation.

The Linearized Theory

The ultimate cumulation-diffusion ratio appears independent of the initial strength of the disturbance. The linear kinematic effects are indeed dominant during the initial time elements, but even then they are vitally dependent on the velocity profile changes. In the final result, diffusion and cumulation are side-by-side with equal order of magnitude, their relative importance not being dependent on the initial magnitude of the disturbance. This raises serious doubts about the significance of the results yielded by the pure linearized theory disregarding cumulation. The Reynolds Number computed as critical is not necessarily critical. Linearized instability does not appear to be demonstrated to be either a necessary or a sufficient condition for actual instability.

The linearization seems to have been resorted to by a routine striking out of all quadratic terms. These terms may, however, be of significance and may not even be small. Since the absence of a solution of the exact equation makes it impractical to examine the justification of linearization by mathematical procedure, such examination may be performed by the intuitive faculty. Linearization is open to great doubt when resorted to without any examination.

The importance of cumulation is even greater in connection with the question of statistical equilibrium of the velocity profile of the turbulent flow. Linearized theory has never been applied to this question, although it may be if completely and broadly applicable. There is little doubt that this statistical equilibrium is closely allied with cumulation and vortex discrimination.

Conclusion

It is of significance that the instability of the laminar flow has been traced back to shear and not to vorticity. The distance between properly selected pairs of fluid particles must diminish. A fluid body rotating like a solid has rotation but no shear. Such motion is stable and cannot give rise to turbulence because it cannot have dissipation. The couple that would supply the energy to be dissipated would not be associated with an increase of the moment of momentum, in contradiction to Newton's laws of dynamics. The mechanism described accordingly not only makes us expect turbulence of shear flows under suitable conditions but also meets the test of not predicting turbulence of the pure rotational flow.

We have reached the end of the inquiry. We started out without seeing a mechanism that produces turbulence, and now we see such a mechanism reasonably clearly. We see the counterrotational disturbance vortices slowed down in their race with the corotational vortices on their way toward the walls, because positive cumulation is reserved for the corotational vortices. This vortex discrimination leads to increased wall rotation and wall friction and, hence, to increased energy supply. Nothing indicates that the excess energy supplied is dissipated so uniformly as to exclude the formation of new disturbances. Thus, a foundation for continual turbulence is laid. The increasing velocity profile steepness near the wall finally leads to saturation of the vorticity and to statistical equilibrium.

Simplified Design Comparisons of Axial Compressors*

FRANK L. WATTENDORF†

Air Engineering Development Division, U.S.A.F.

ABSTRACT

This paper reports a continuation of studies initiated in 1944 regarding potential improvements of turbojet propulsion systems for supersonic flight as suggested originally by Dr. Theodore von Kármán, Chairman of the U.S.A.F. Scientific Advisory Board and Chief Scientific Advisor to the Air Engineering Development Division.

Simplified design comparisons of axial compressors with particular emphasis on the attainment of a high rate of mass flow per unit frontal area are discussed. This feature is important not only in the application of turbojets to the propulsion of supersonic aircraft but also in the study of future potential requirements for jet engine component testing and for application to the design of more compact compressor systems for wind tunnels such as those at the Arnold Engineering Development Center.

A comparison is made of some aspects of axial compressor design for accommodating a high rate of mass flow. In particular, the influence of hub ratio and axial Mach Number on the stage-pressure ratio based on assumed limitations of all relative and absolute Mach Numbers is given for compressor types designed according to various principles such as free vortex flow, rigid body prerotation, and arbitrary distribution of rotor work.

The important relationship between maximum temperature rise and mass-flow ratio is derived for several compressor types so that a general qualitative picture is given of the influence of compressor type on the relationship between temperature rise and mass-flow ratio. This study represents a qualitative method of comparing compressor types and refers to the inlet stage alone, which is usually critical for mass flow.

NOTATION

a	=	ratio of hub diameter to tip diameter
A	=	area
c	=	velocity of sound
c_p	=	specific heat at constant pressure
C	=	absolute velocity
C_L	=	blade lift coefficient
C_T	=	temperature rise coefficient
g	=	gravitational constant
J	=	mechanical equivalent of heat
M	=	limiting intake Mach Number
M.F.R.	=	mass-flow ratio
P	=	absolute pressure
R	=	radius at tip
T	=	absolute temperature
ΔT	=	stage temperature rise
U	=	circumferential speed of blade element
U_F	=	tangential component of whirl induced by rotor
V	=	axial velocity
W	=	relative velocity

Subscripts

aR	=	conditions at rotor hub
ax	=	axial component
cr	=	conditions at local sonic velocity
m	=	mean velocity of intake and exit velocities
0	=	stagnation conditions before rotor
r	=	conditions at any radius
R	=	conditions at rotor tip
u	=	tangential component
1	=	intake conditions of cascade
2	=	exit conditions of cascade

Presented at the General Aerodynamics Session, Nineteenth Annual Meeting, I.A.S., New York, January 29–February 1, 1951.

* Grateful acknowledgment of the helpful assistance and contributions of Dr. H. von Ohain and M. Lawson, of the Air Engineering Development Division, is made.

† Deputy Chief Scientific Advisor.

INTRODUCTION

DURING RECENT YEARS, the art of axial compressor design has become increasingly more complex. In particular, there has been a steadily growing requirement for moving larger masses of air at higher pressure ratios.

With the large amount of excellent research and development work being conducted in the field of axial compressors by the N.A.C.A., the industry, the Military Services, and the universities, it becomes increasingly more difficult for research planners to obtain an overall picture of the field. With this in mind and from the point of view of the research planner, the present paper deals with a simplified qualitative comparison of axial compressor types, with special emphasis on the relationship between mass flow and the stage-pressure ratio.

It should be emphasized that, although many effects are neglected in the interest of obtaining rapid generalized comparison, continued and accelerated research on these effects is strongly urged.

The present paper contributes to two projects in particular.

(1) Potential improvements of gas-turbine-propulsion systems (project of the U.S.A.F. Scientific Advisory Board under Dr. Theodore von Kármán). By increasing the mass flow through the compressor and the remaining internal system of a turbojet for the same frontal area the following improvements in the performance of an aircraft or missile are made possible: (a) increase of maximum flight Mach Number and (b) increase of range at high Mach Number.

(2) Potential improvements of flow generating systems for test facilities (project of the Air Engineering Development Division under Major Gen. F. O. Car-

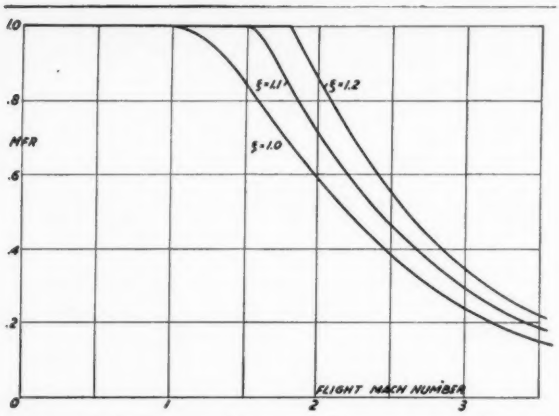

FIG. 1. Maximum possible mass-flow ratio versus flight Mach Number for a turbojet engine suspended in the free air stream. Isentropic flow in the intake diffusor is assumed. ξ equals the ratio of maximum nacelle diameter to inner diameter of the compressor housing.

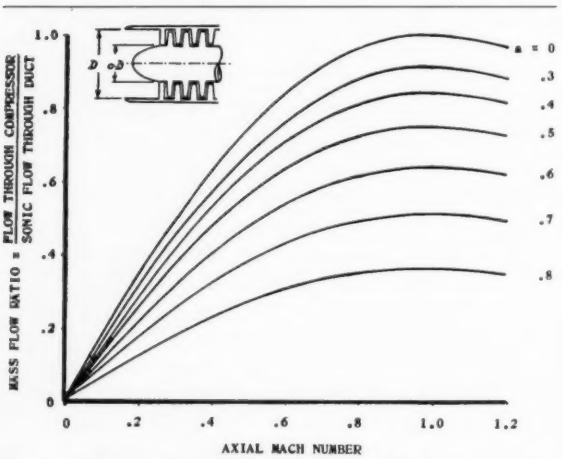

FIG. 2. Influence of axial Mach Number and hub ratio on the mass-flow ratio of an axial compressor.

roll). For test facilities of the magnitude and type of those under construction for the Arnold Engineering Development Center, the compressor or flow generating system is usually the largest single item of expense and complexity. Increasing the mass flow for the compressor system with no increase in external dimensions leads to the following advantages: (a) saving of expense due to smaller size; (b) greater compactness (savings in ducts, building, and auxiliaries); and (c) utilization of higher speeds of rotation for electric motors.

To explain these potential design improvements, the following comparative analysis of the relationship between stage temperature rise and mass-flow ratio is developed for different compressor types, with simplifying assumptions. This is to facilitate the presenting of an overa'l physical picture of the problem and to spotlight areas worthy of further detailed study and exploitation.

HISTORICAL BACKGROUND

Since the thrust of a turbojet is a function of the mass flow through the unit and the jet velocity, studies of potential improvements of a turbojet naturally involve study of possibilities of increasing the mass flow through the system and increasing the jet velocity—i.e., by utilizing higher operating temperatures. Studies of this nature were initiated in 1944 and 1945 by the A.A.F. Scientific Advisory Group.[1, 2] A further study of this series was carried out in 1946 by Morton Alperin, who showed the potentialities of the turbojet for supersonic flight for increased values of thrust per unit frontal area.

Over a period of years, the N.A.C.A. has been conducting extensive studies of potential turbojet improvements. For instance, a report of Hensley, Sanders, and Kress[3] shows the importance of the mass-flow factor in improving turbojet performance, and Wood[4] shows potentialities of the turbojet for supersonic flight.

To the best of the author's knowledge, the first design of a turbojet with special emphasis on the attainment of high values of mass flow per unit frontal area was proposed in 1947 to the Air Materiel Command by Northrop Aircraft, Inc. In particular, Eugene Hunsaker presented original ideas on axial compressor design for unusually high mass flow. Discussions between the author and Mr. Hunsaker were essential contributions to the present paper.

DEFINITION OF MASS-FLOW RATIO

The factor used in this paper to represent mass-flow characteristics of axial-flow compressors is the ratio of the actual mass flow moved by the compressor to the maximum mass flow that could be passed at local sonic speed through the hollow compressor housing under unchanged isentropic stagnation conditions. This ratio is identical with the ratio of the critical area of the passing mass flow to the cross-sectional area of the hollow compressor housing.

The relationship between maximum possible mass-flow ratio and flight Mach Number is shown in Fig. 1. The diagram is based on the assumption that in the supersonic speed range the highest possible mass flow per second for an engine suspended in the free air stream cannot exceed the amount of air which would be passed with flight velocity through an area equal to the frontal area of the engine.

The relationship between mass-flow ratio, axial Mach Number, and hub ratio is shown in Fig. 2. By definition, the combination of zero hub diameter and axial Mach Number of 1 corresponds to a mass-flow ratio of 1. The importance of having a high inlet axial Mach Number and a small hub diameter for obtaining high mass-flow ratios is shown by the curves. Two facts are especially significant—namely, (a) increasing the inlet Mach Number pays good dividends up to a value of about 0.7 to 0.8, above which the returns are diminishing, and (b) decreasing the hub ratio is advantageous

down to 0.3 and 0.4, below which returns are diminishing.

It should be pointed out that the mass-flow ratio peaks at Mach Number 1, above which it decreases again. This shows that the utilization of supersonic axial velocities would have no advantage from a mass-flow basis, since it would decrease rather than increase the mass flow. Most axial compressors as used for many years in stationary gas turbine practices have hub ratios above 0.7 and axial flow below $0.5M$. In recent years, aircraft and wind-tunnel applications have brought an ever increasing need to increase the mass flow to a considerable extent. It, therefore, becomes important to study potential limits of increasing the mass flow. Referring again to Fig. 2, the question is: How near a mass flow ratio of unity is it feasible to approach? This naturally leads to the question of the limitations on inlet Mach Number and hub ratio in terms of the compressor blading design and the stage-pressure ratio or temperature rise.

A series of blading design methods will be considered in this paper based on the limitations of high subsonic flow with several simplifying assumptions.

Temperature Rise of a Blade Element

The approach of this paper will be, in general, to study the relationships between stage-pressure ratio and mass flow for a number of different assumptions in order to give an overall physical picture of potential compressor performance, especially from the mass-flow point of view.

Before starting this more general study, it is helpful to isolate one blade element and examine the influence of axial velocity, which is characteristic for mass flow and stage temperature rise. Fig. 3 shows a simplified velocity diagram for the maximum temperature rise for a blade element, assuming subsonic flow.[5]

As shown in reference 5, the maximum temperature rise of a blade element is obtained when the relative velocities of the air entering the rotor and the downstream stator have the highest permissible values under the Mach Number limitations. With both of these relative velocities limited by the approach to the speed of sound, a symmetrical velocity diagram is obtained. The temperature rise is proportional to the product of rotor speed and flow deflection through the rotor. Since the base of the velocity triangle is equal to the sum of rotor speed and flow deflection, the maximum value of the product is obtained when both legs are equal.

The following simplifying assumptions are made: (a) constant axial velocity through the stage at the location of the element; (b) constant value of the velocity of sound through the stage, which appears justified since the stage temperature rise in a subsonic compressor is small relative to the inlet temperature; and (c) limiting Mach Number equal for rotor and stator.

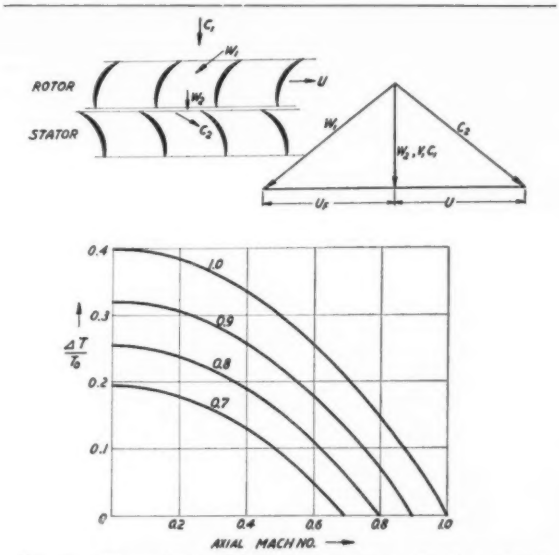

Fig. 3. Theoretical maximum temperature rise for a blade element as a function of relative intake Mach Number and axial Mach Number.

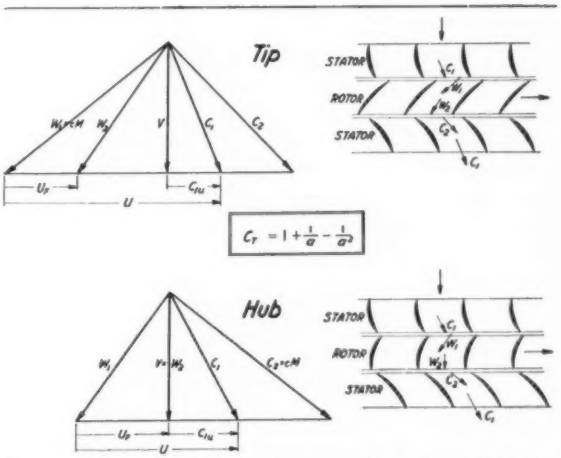

Fig. 4. Free vortex with positive prerotation and axial relative discharge velocity at hub.

Fig. 3 shows a typical plot of the relationship between axial Mach Number and blade element temperature rise for several assumed values of the limiting relative Mach Number. It is seen that the temperature rise goes in the opposite direction to the inlet axial Mach Number and decreases rapidly at high Mach Numbers; therefore, it is important for any specific design to determine the best compromise between these two factors.

With this introductory view of the behavior of a blade element, the rotor as a whole will now be considered, rather than one element. This results in an additional variable—namely, the hub ratio a.

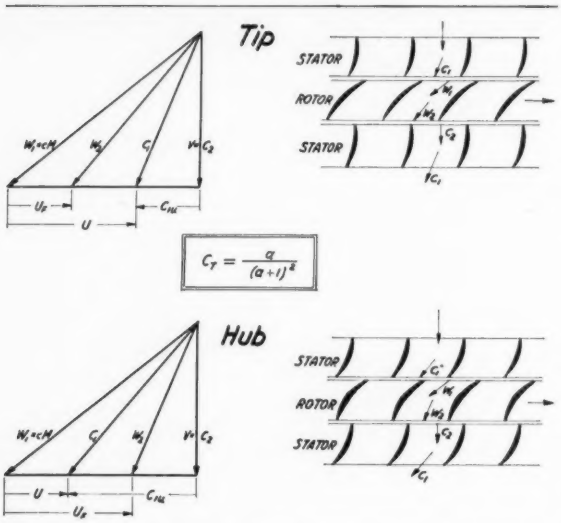

FIG. 5. Free vortex with negative prerotation and axial absolute discharge velocity over blade length.

INVESTIGATION OF COMPRESSOR TYPES

(1) *Free-Vortex Flow Principle*

The so-called free-vortex method of design has been well known for many years. It is called free vortex because the tangential component of absolute velocity varies inversely as the radius, as it does in a free vortex. This is the easiest type to work with theoretically, since it involves a constant value of work or temperature rise over the whole area, constant axial velocity, balanced pressure, and no radial flow. For this reason it has been widely used in practice for many years. It came into use in the 1920's when such scientists as von Kármán, Prandtl, Betz, Ackeret, and Troller made popular the application of airfoil theory to rotating-blade systems.

(*a*) *Positive Prerotation, Axial Relative Exit Velocity.*—Fig. 4 shows typical velocity diagrams for free-vortex flow with positive prerotation. The tangential component developed by the rotor varies inversely as the radius. Study of the velocity diagrams shows that at the tip the relative intake velocity is critical for limiting Mach Number and that at the hub the absolute discharge velocity is limiting. Now, since in the present study increasing the mass flow is an important objective, low values of the hub ratio are of particular interest. As the hub ratio decreases, the relative exit velocity approaches the axial direction at the hub and can even exceed it. However, for the first investigation, the simplifying assumption of axial relative exit velocity at the hub will be introduced. This assumption simplifies the calculations and is in approximate agreement with many existing compressors of this type. With the above assumption and the Mach Number limitation, the following formula can be derived (as shown in the Appendix):

$$Jgc_p\Delta T = U_F U_R = [1 + (1/a) - (1/a^2)]c^2(M^2 - M_{ax}^2)$$

giving the relationship between temperature rise, hub ratio, and relative and axial Mach Numbers. In order to isolate further the hub ratio effect, a temperature coefficient (C_T) is introduced by dividing the temperature rise by the difference in the squares of the relative and axial Mach Numbers—i.e.,

$$C_T = \frac{Jgc_p\Delta T}{c^2(M^2 - M_{ax}^2)} = 1 + \frac{1}{a} - \frac{1}{a^2}$$

This formula immediately shows the inherent disadvantage of this type of compressor for high mass flow, since the temperature coefficient drops to zero for a hub ratio somewhat above 0.6. In practice, vortex compressors of this type usually have hub ratios of 0.7 to 0.8 and axial Mach Numbers below 0.5. Referring to Fig. 2, it is seen that the mass-flow ratio for this type of compressor would amount to less than one-third of the ceiling value. With this in mind, other design methods will be discussed from the point of view of essential increase in the mass-flow ratio.

(*b*) *Free-Vortex Flow—Negative Prerotation, Axial Absolute Discharge Velocity.*—This example will show typical limiting considerations for an inlet compressor stage with free-vortex flow combined with negative prerotation—i.e., prerotation opposite to the direction of rotor rotation. This method has been widely used in axial ventilating fan practice, since it utilizes lower rotational speeds than positive prerotation and is therefore efficacious when tip speeds are limited. Positive prerotation is more widely used in gas-turbine practice where higher rotational speeds more nearly match those with high-speed turbines. Velocity diagrams for this type of flow are shown in Fig. 5, which shows the commonly used method whereby the absolute velocity leaving the rotor is axial. In other words, the prerotation vanes introduce against the rotor the same amount of spin which the rotor takes out. Using simplifying assumptions as in the previous case, the formula for the temperature coefficient is $C_T = a/(1 + a)^2$. It is seen from this formula that the cutoff of temperature rise with decreasing hub ratio has been eliminated.

(*c*) *Free-Vortex Flow—Negative Prerotation, Axial Relative Discharge Velocity at Hub.*—When the limitation of axial absolute velocity behind the rotor is removed and replaced by axial relative discharge at the rotor hub to correspond with the previously considered case of free-vortex flow with positive prerotation, the temperature coefficient is $C_T = a/(a + 1)$. It is seen that these two types with negative prerotation have smaller temperature rise or rotor work for the higher range of hub ratios than the previous positive prerotation type (see Fig. 10). However, this design method does open up a lower range of hub ratios making possible higher mass-flow capabilities. The disadvantage of negative prerotation compressors for turbojet appli-

cation is the lower rotor speeds involved. This method was used, however, in the compressor design of the Jumo 004, where low rotor speeds were also necessitated by the use of relatively low stress materials and simplified construction methods suitable for mass production at that time.

(*d*) *Free-Vortex Flow—Maximum Rotor Work.*—In the previous investigations of the free-vortex type, there was an arbitrary limitation of axial discharge velocity at the hub. Now it is of interest to investigate the potentialities of removing this limitation whereby the theoretical maximum rotor work is obtained. The analysis of this case is contained in the Appendix, and the temperature coefficient is $C_T = (1 + a)^2/4$ (see Fig. 10).

The theoretical maximum rotor work for free-vortex flow involves negative prerotation as shown in Fig. 6. However, for a practical range of hub ratios, the increase over the zero prerotation type is small.

This maximum type is given to show potential ceilings of the free-vortex principle. In actual practice, this maximum rotor work would involve considerably higher blade loading than is commonly used. Blade-loading limitations will be discussed later in this report.

A rotor of this type was designed in 1943 by the author and Elmer Johnson for wind-tunnel application. A scale model was built at Wright-Patterson Air Force Base for the Wind Tunnel Branch, Air Materiel Command.

It is noted that the blade element at the hub approaches the impulse type. Interesting investigations on the impulse type have been made by Erwin and Schulze, of the N.A.C.A.

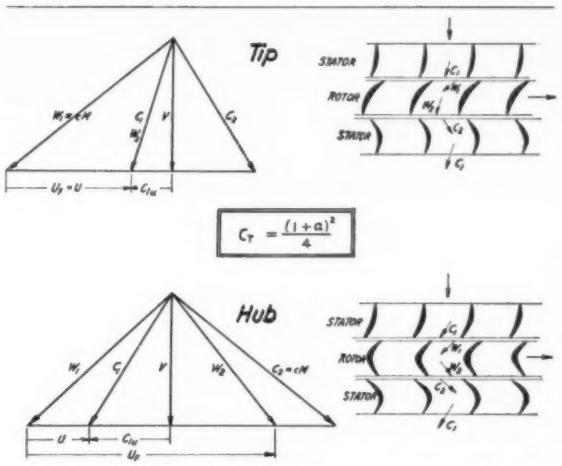

FIG. 6. Free-vortex maximum constant rotor work.

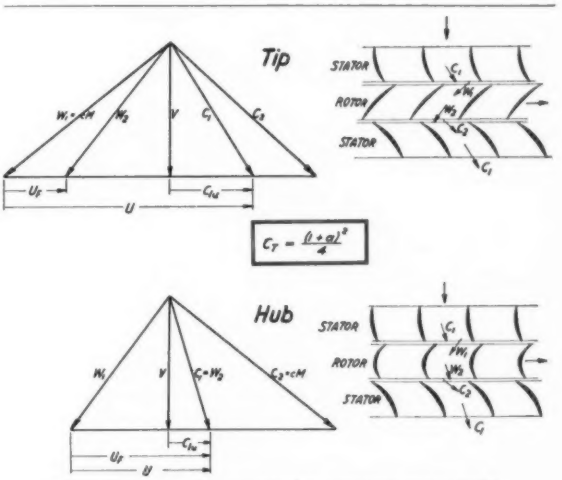

FIG. 7. Rigid body prerotation constant rotor work.

(2) *Positive Rigid Body Prerotation Constant Rotor Work*

In this type of flow, the upstream stator introduces a rigid body type of swirl into the air stream—namely, with the tangential component of absolute intake velocity directly proportional to the radial distance to the center of rotation (Fig. 7). For this type there is a deviation from the constant axial velocity distribution which is characteristic for all constant rotor work types not designed according to the free-vortex principle. This influence is not included in the present report but is being studied separately. The subject has been treated by Rannie, Wu and Wolfenstein,[6] and others.[7] The analysis has been carried out in the Appendix for two assumptions—namely, for axial relative discharge at the hub for which $C_T = a$, and for maximum constant rotor work for which $C_T = (1 + a)^2/4$. It is seen that for the axial relative discharge velocity limitation the rigid body design allows lower ranges of hub ratios to be utilized than does the corresponding free-vortex design with positive prerotation (Fig. 10). It is interesting to note, however, that the rigid body maximum constant rotor work type has exactly the same expression for temperature coefficient as the maximum free-vortex type. However, there is a significant difference between the two types in that the tangential velocity imparted by the rotor is smaller for the rigid body type. Further comparisons of the two types will be made later in this report.

(3) *Maximum Constant Rotor Work*

In the cases so far considered, the conditions of maximum rotor work were determined (1) for free-vortex prerotation and (2) for rigid body prerotation. Now it becomes of interest to investigate the more general condition of maximum constant rotor work by removing any specification as to the type of prerotation. The analysis given in the Appendix leads to a temperature coefficient of $C_T = 4a/(1 + a)^2$ (see Figs. 8 and 10). For this case the prerotation varies from positive to negative over the blade, as shown in Fig. 8. If the prerotation is restricted either to positive values over the blade length or to negative values over the blade length,

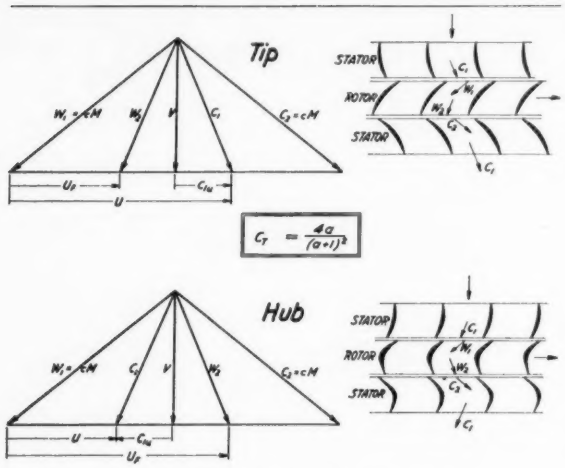

FIG. 8. Maximum constant rotor work.

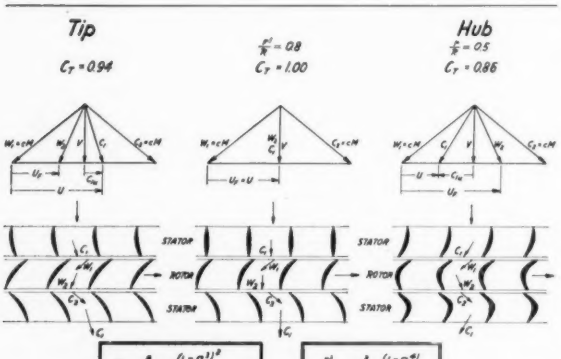

FIG. 9. Maximum unconstant rotor work.

the expression for temperature rise coefficient in both cases is $C_T = a(2 - a)$ (see Fig. 10, Curve 6).

(4) Nonconstant Distribution of Rotor Work over the Radius

In all cases investigated so far, the condition of constant rotor work was assumed throughout. This condition obviously limits the total rotor work because the work goes to zero as the hub ratio approaches zero. Therefore, an increase of total rotor work can be expected for compressor types that have the rotor work increasing toward the blade tip. Two cases will now be considered.

(*a*) *Constant Rotor Swirl, Maximum Rotor Work for a Blade Element at the Tip.*—The analysis given in the Appendix shows the temperature-rise coefficient to be $C_T = r/R$ for a blade element at radius r. For any given hub ratio, an average C_T value can be obtained by integration as follows:

$$(C_T)_{\text{av.}} = (2/3)\ [(1 - a^3)/(1 - a^2)]$$

see Fig. 10, Curve 7. This case illustrates a possible way of combining high mass flow with reasonable stage pressure or temperature rise.

(*b*) *Maximum Nonconstant Rotor Work.*—For this case all restrictions as to prerotation and work distribution over the blade length are removed and only the Mach Number limitation remains.

The analysis of this case is made in the Appendix and the resulting value of temperature coefficient is

$$(C_T)_{\text{av.}} = \frac{8}{9}\frac{(1 - a^3)^2}{(1 - a^4)\ (1 - a^2)}$$

see Figs. 9 and 10, Curve 9.

It can be seen that the value of the hub ratio has little influence on the average temperature coefficient.

(*c*) *Inducer Stages.*—An inducer stage is a preliminary rotating stage with unconstant rotor work distribution over the blade length. Its primary purpose is to achieve a desirable axial velocity distribution in a multistage compressor which deviates from the free vortex design principle.[8] Since the unconstant rotor work types are capable of high temperature rise along with high mass flow, it appears attractive to combine this characteristic with the primary function of producing a desirable axial velocity distribution. Studies in this direction are being made, and further work should be encouraged.

(5) Comparison of the Investigated Compressor Types

(*a*) *The Influence of Hub Ratio upon the Temperature Rise.*—The previously derived temperature-rise coefficients for the investigated compressor types and, in addition, the temperature-rise coefficient of a hypothetical type, which is characterized by the absence of the hub ratio effect, are plotted in Fig. 10. In comparison to this hypothetical type, the curves of the investigated compressor types show a considerable variance as to the influence of hub ratio upon the temperature-rise coefficient. The rigid body types and the free-vortex types are greatly influenced by the hub ratio, while the maximum rotor work types are little affected by the hub ratio within the practical range of hub ratios of 0.3 to 0.9. The greatest difference in temperature rise among the constant rotor work compressor types is shown by the maximum constant rotor work type and the free-vortex type with positive prerotation and axial relative discharge velocity at the hub. While the temperature rise of the latter type decreases to zero when the hub ratio decreases to 0.62, the temperature rise coefficient of the first type is still above 0.9.

Another interesting result is that the temperature-rise coefficients for the maximum free-vortex and the maximum rigid body constant rotor work types are the same. Also, the temperature rise coefficients for the maximum constant rotor work positive prerotation type and the maximum constant rotor work negative prerotation type are the same. This shows that the larger flow deflection of the negative prerotation types is compensated by the higher circumferential speed

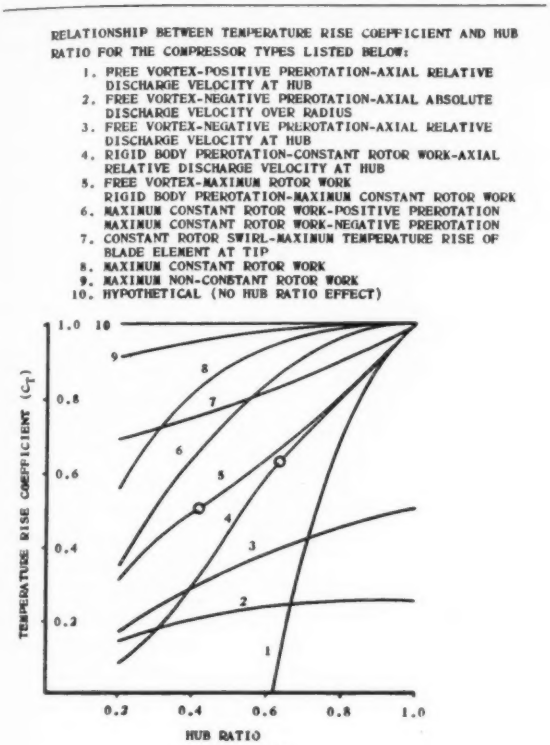
RELATIONSHIP BETWEEN TEMPERATURE RISE COEFFICIENT AND HUB RATIO FOR THE COMPRESSOR TYPES LISTED BELOW:
1. FREE VORTEX-POSITIVE PREROTATION-AXIAL RELATIVE DISCHARGE VELOCITY AT HUB
2. FREE VORTEX-NEGATIVE PREROTATION-AXIAL ABSOLUTE DISCHARGE VELOCITY OVER RADIUS
3. FREE VORTEX-NEGATIVE PREROTATION-AXIAL RELATIVE DISCHARGE VELOCITY AT HUB
4. RIGID BODY PREROTATION-CONSTANT ROTOR WORK-AXIAL RELATIVE DISCHARGE VELOCITY AT HUB
5. FREE VORTEX-MAXIMUM ROTOR WORK
RIGID BODY PREROTATION-MAXIMUM CONSTANT ROTOR WORK
6. MAXIMUM CONSTANT ROTOR WORK-POSITIVE PREROTATION
MAXIMUM CONSTANT ROTOR WORK-NEGATIVE PREROTATION
7. CONSTANT ROTOR SWIRL-MAXIMUM TEMPERATURE RISE OF BLADE ELEMENT AT TIP
8. MAXIMUM CONSTANT ROTOR WORK
9. MAXIMUM NON-CONSTANT ROTOR WORK
10. HYPOTHETICAL (NO HUB RATIO EFFECT)
TEMPERATURE RISE COEFFICIENT (C_T)
1.0
0.8
0.6
0.4
0.2
0.2
0.4
0.6
0.8
1.0
HUB RATIO

FIG. 10.

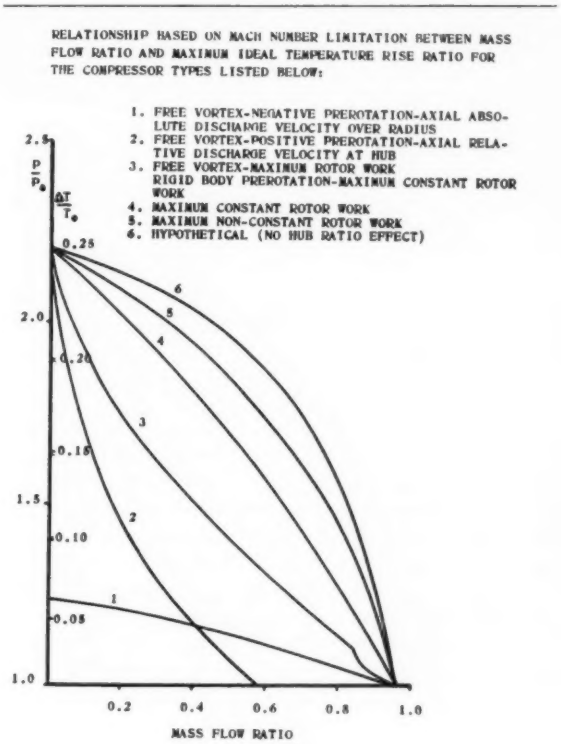

FIG. 11.

of the positive prerotation types. The problems involved with the blade loading, which is much higher for those investigated types with negative prerotation than for those with positive prerotation, will be discussed later in this paper.

(*b*) *Temperature-Rise Ratio Versus Mass-Flow Ratio.*—Having isolated the hub ratio effect, it is now of interest to combine this effect with the axial Mach Number effect to obtain the relationship between mass-flow ratio and temperature-rise ratio. This is shown in Fig. 11. These curves are derived by using Figs. 2 and 10 and are based on a limiting relative Mach Number of 0.8. For other limiting Mach Number values (M'), the curves in Fig. 11 can be used by multiplying the temperature-rise ratio by the factor $(M'/0.8)^2$ and by correcting the mass-flow ratio by using Fig. 2. Fig. 2 gives for any mass-flow ratio a manifold of hub ratio-axial Mach Number combinations. The temperature-rise ratio $\Delta T/T_0$ for each combination is given by the equation

$$\frac{\Delta T}{T_0} = \frac{c^2}{Jgc_pT_0}\,(M^2 - M^2_{ax})\,(C_T)$$

However, for one given mass-flow ratio there is only one combination of hub ratio and axial Mach Number which gives a maximum value of $\Delta T/T_0$ for each compressor type. These maximum values make up the curves of Fig. 11. The curves show that with an increasing mass-flow ratio the temperature-rise ratio decreases rapidly to zero for all compressor types, including the hypothetical type where the hub ratio has no influence on the temperature rise. Furthermore, it is apparent for higher mass-flow ratios, in a range of about 0.5 to 0.7, the maximum temperature-rise ratio is greatly influenced by the compressor type.

(6) *Investigation Based on Blade Loading Limitation and Mach Number Limitation*

In the previous investigation of several compressor types, the primary limitation was that of the intake Mach Number. This corresponds to the limiting case of infinite number of blades of infinitesimal thickness, where the intake Mach Number is the highest occurring Mach Number value and blade-loading effects do not exist. However, for a finite number of blades, the limiting intake Mach Number cannot be considered as independent of the compressor type, because the higher the blade loading which is imposed by the type of compressor, the higher will be the overvelocity at the suction side of the blades. Therefore, the higher the blade loading, the smaller will be the limiting Mach Number.

In addition, the blade loading itself is limited by the tendency of boundary-layer separation if the pressure increase in the direction of flow becomes too great.

For cascades with conventional airfoil blades, Keller[13] derived a limitation for the amount of deflection which

can be imparted to the air stream because of mutual blade interference.

If C_L is the blade lift coefficient and σ is the ratio of blade chord to spacing, then the approximate limitation proposed by Keller is

$$2U_F/W_m = \sigma(C_L) = 1.2$$

(see Fig. 12). This limiting value of flow deflection will be basic for the analysis. In addition, the same limiting Mach Number of 0.8 will be applied for comparison purpose.

An analysis is given in the Appendix for the maximum constant rotor work type as an example. The velocity diagram is shown in Fig. 13. The analysis results in the following simplified expression for the temperature-rise ratio of the maximum constant rotor work type:

$$\frac{\Delta T}{T_0} = 0.24a^2M^2\sqrt{1+\left(\frac{1-a^2}{a^2}\right)\left(\frac{M_{ax}}{M^2}\right)^2}\left[2\sqrt{1-\left(\frac{M_{ax}}{M^2}\right)^2}-0.6a^2\sqrt{1+\left(\frac{1-a^2}{a^2}\right)\left(\frac{M_{ax}}{M^2}\right)^2}\right]$$

Curves are plotted in Fig. 14 giving the relationship between maximum temperature-rise ratio and mass-flow ratio for the above example, for the free vortex positive prerotation axial relative exit velocity, for the maximum free vortex, for the maximum rigid body constant rotor work, and for the maximum nonconstant rotor work. However, these curves represent only relative values, since the limiting value $\sigma(C_L) = 1.2$ is by no means a universal constant. Its value is influenced by Reynolds Number, Mach Number, cascade configuration, etc., which have not been sufficiently investigated at this time by experimental work.[9–12]

(7) *Comparison of Compressor Types with Blade-Loading Limitation*

Fig. 14 shows that the type of compressor has great influence upon the temperature-rise ratio. This is true especially in the higher range of mass-flow ratios. In contrast to the results obtained with the Mach Number limitation only, the rigid body type with positive prerotation enables higher values of temperature rise than the free-vortex type, except for the small range of extremely high mass-flow ratios where the blade loading limitation does not come into effect. The nonconstant rotor work type gives reasonable values of stage temperature rise up to extremely high mass-flow ratio values of about 0.8.

Although it would be desirable to compare efficiencies of the various types, this is not done here, since an efficiency investigation based on two-dimensional flow theory is insufficient. The important three-dimensional effects, such as boundary layer, centrifugal effects, induced drag, gap influences, and influence of surface friction, are not sufficiently known[9] to be used in an analytical investigation.

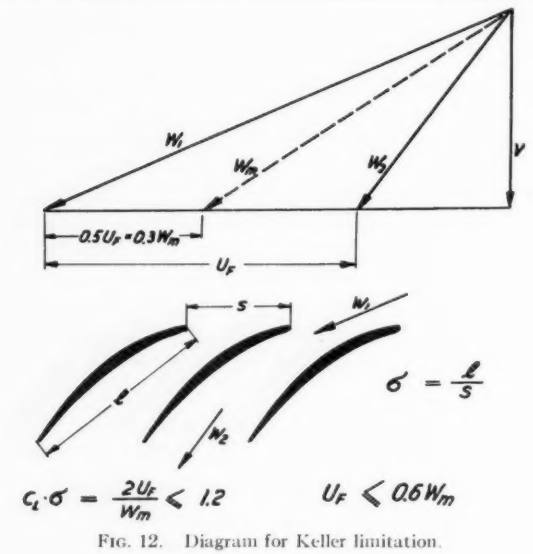

FIG. 12. Diagram for Keller limitation.

CONCLUSIONS

Simplified analyses such as presented above help research planning and integration and spotlight areas worthy of further investigation.

The following are typical research items brought out by such simplified analyses:

(1) Increasing relative Mach Number.

(2) Studying limits of loading and deflection possibilities.

(3) More complete comparative analyses with more items considered.

(4) Radial flow and equilibrium.

(5) Losses—especially mixing with work unbalances—secondary flows.

(6) Reynolds Number effects (high-altitude problems).

(7) Blade thickness effects on velocity limits.

(8) Inducer stages.

(9) Staging and matching.

Much excellent research is in progress in the above fields. It is hoped that simplified analyses like the above will give planners greater appreciation of the need for expediting and supporting present programs and for stimulating new programs.

APPENDIX

(1) *Free Vortex*

(*a*) *Positive Prerotation, Axial Relative Discharge Velocity at Hub.*—Study of the velocity diagrams (Fig. 4) shows that the limiting Mach Number (M) is attainable only for the relative intake velocity at the tip and the absolute discharge velocity at the hub. This is because the relative intake velocity decreases toward the hub, while the absolute discharge velocity increases toward the hub.

As the relative intake velocity, W_1, is limited at the tip section of the rotor by the limiting Mach Number (M), the magnitude of the tangential component $(W_1)_R$ is fixed for a given value of axial velocity (V)—i.e.,

$$(W_{1u})_R = c\sqrt{M^2 - M_{ax}{}^2}$$

If C_{1u} represents the whirl component introduced by the upstream vanes, then the blade element velocity is given by the sum of W_{1u} and C_{1u} as

$$U_r = (W_{1u})_r + (C_{1u})_r$$

At the blade tip, where $r = R$,

$$U_R = (W_{1u})_R + (C_{1u})_R$$

The blade element velocity at the hub is

$$U_{aR} = a(U_R)$$

For free vortex flow the following relationships hold:

$$(C_{1u})_{aR} = (1/a)\ (C_{1u})_R$$

and

$$(U_F)_{aR} = (1/a)\ (U_F)_R$$

Since

$$(C_2)_{aR} = (W_1)_R = cM$$

then

$$(C_{2u})_{aR} = (W_{1u})_R$$

so that

$$(C_{1u})_{aR} + (U_F)_{aR} = (W_{1u})_R$$

For vortex flow, in which case $(C_{2u})_r$ varies inversely with the radius, this can be written

$$[(C_{1u})_R/a] + [(U_F)_R/a] = (W_{1u})_R$$

From the assumption of axial relative discharge velocity at the hub, it follows that

$$aU_R = [(U_F)_R/a] + [(C_{1u})_R/a] = (W_{1u})_R$$

Multiplying by a the equation

$$[(U_F)_R/a] + [(C_{1u})_R/a] = (W_{1u})_R$$

and adding

$$U_R - (C_{1u})_R = (W_{1u})_R$$

results in

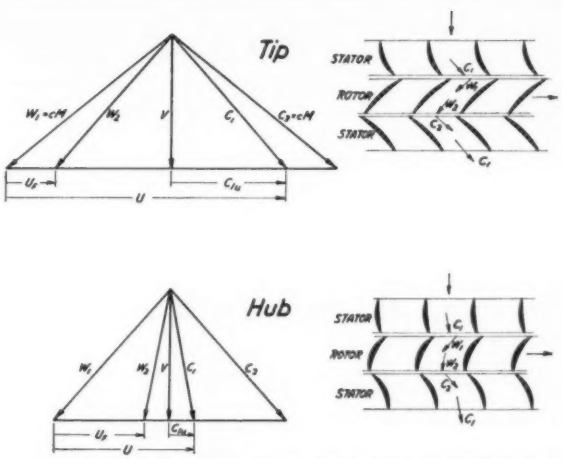

FIG. 13. Maximum constant rotor work with blade-loading limitation applied.

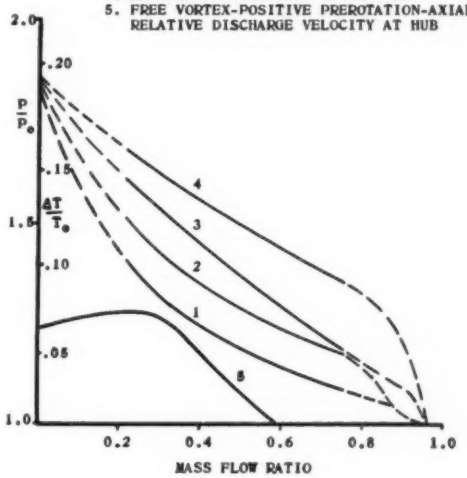

FIG. 14.

$$(U_F)_R + U_R = (1 + a)\ (W_{1u})_R$$

Substituting for U_R the value $(W_{1u})_R/a$ gives

$$(U_F)_R = [1 + a - (1/a)\ (W_{1u})_R]$$

The stage temperature rise is then given by the expression

$$Jgc_p\Delta T = U_F U_R = [1 + (1/a) - (1/a^2)]\ [c^2(M^2 - M_{ax}{}^2)]$$

For vortex flow this value is constant over the radius.

Since the formula given above for temperature rise is a product of a Mach Number effect and a hub ratio effect, comparisons may be further simplified by introducing the following coefficient that isolates the two effects—namely,

$$C_T = \frac{Jgc_p\Delta T}{c^2(M^2 - M_{ax}^2)} = 1 + \frac{1}{a} - \frac{1}{a^2}$$

(*b*) *Negative Prerotation, Axial Absolute Discharge Velocity over Blade.*—A velocity diagram for such a blade element is shown in Fig. 5.

As the absolute discharge velocity is assumed axial over the blade length,

$$(U_F)_R + U_R = (W_{1u})_R$$

so that there is no right-hand velocity triangle as in the previous case. In order to obtain the highest rotor work, $(W_{1u})_R$ must be the largest possible under the Mach Number limitation. It follows from this and from the condition of constant rotor work that $(U_F)_R$ is smaller than U_R. Otherwise, the Mach Number limitation would be violated immediately for smaller radii. Since $(W_{1u})_r$ decreases with the radius until $(U_F)_r$ equals U_r, at which point $(W_{1u})_r$ begins to increase, the Mach Number limitation will not be violated if, at the hub

$$(U_{aR} + (U_F)_{aR} \leq (W_{1u})_R$$

or

$$aU_R + [(U_F)_R/a] \leq (W_{1u})_R$$

Since

$$(U_F)_R + U_R = (W_{1u})_R$$

$$aU_R + [(U_F)_R/a] \leq U_R + (U_F)_R$$

or

$$(U_F)_R \leq aU_R$$

For maximum rotor work, $(U_F)_R$ must have the largest permissible value, so that

$$(U_F)_R = aU_R, \quad U_R(1 + a) = (W_{1u})_R$$

The stage temperature rise can now be expressed as

$$Jgc_p\Delta T = (U_F)_R U_R = [a/(a + 1)^2]c^2(M^2 - M_{ax}^2)$$

The expression for temperature-rise coefficient is

$$C_T = a(a + 1)^2$$

(*d*) *Maximum Rotor Work.*—First, in the investigation of the case of positive prerotation, it becomes evident that the relative intake velocity decreases toward the hub, since U_r is decreasing and $(C_{1u})_r$ is increasing. Also, the absolute discharge velocity increases toward the hub since both $(C_{1u})_r$ and $(U_F)_r$ are increasing. This means that, in order to attain the highest possible rotor work without violating the Mach Number condition, only the relative intake velocity at the blade tip and the absolute discharge velocity at the hub can attain the highest permissible Mach Number. Thus,

$$(W_{1u})_R = (C_{2u})_{aR}$$

$$(C_{2u})_{aR} = (U_F)_{aR} + (C_{1u})_{aR} = (W_{1u})_R$$

Since $(C_{1u})_r$ and $(U_F)_r$ vary inversely as the radius, one can be expressed as a function of the other as follows:

$$(C_{1u})_r = k(U_F)_r$$

where k must be positive for positive prerotation. Substituting $k(U_F)_{aR}$ for $(C_{1u})_{aR}$ in the above equation results in

$$(U_F)_{aR} = \frac{(W_{1u})_R}{1 + k} \quad \text{or} \quad (U_F)_R = \frac{a(w_{1u})_R}{1 + k}$$

because of constant rotor work.

Since

$$U_R = (W_{1u})_R + (C_{1u})_R$$

then

$$U_R = (W_{1u})_R + k(U_F)_R$$

so that

$$U_R = (W_{1u})_R\left(1 + \frac{ak}{1 + k}\right)$$

This gives the stage temperature rise as a function of k and hub ratio a as follows:

$$Jgc_p\Delta T = (U_F)_R\,(U_R) = c^2(M^2 - M_{ax}^2)\left(\frac{a}{1 + k}\right)\left(1 + \frac{ak}{1 + k}\right) = c^2\,(M^2 - M_{ax}^2)\,a\left[\frac{1 + k(1 - a)}{1 + k(1 - 2k)}\right]$$

Study of this equation shows that the highest stage temperature rise results when k is zero or prerotation zero. The equation for highest rotor work is then

$$Jgc_p\Delta T = ac^2\,(M^2 - M_{ax}^2)$$

The temperature rise coefficient is

$$C_T = Jgc_p\Delta T/c^2(M^2 - M_{ax}^2) = a$$

Investigating the case of negative prerotation, we find, as in the previous case of positive prerotation, that the limiting Mach Number can be achieved only for the relative intake velocity at the tip and for the absolute discharge velocity at the hub. It will be shown that, for hub ratios zero up to a definite value (0.41), the Mach Number limitation also comes into effect for the relative intake velocity at the hub.

Applying the same method as for the case of positive prerotation, the following equation is obtained for the temperature rise:

$$Jgc_p\Delta T = U_F U_R = c^2(M^2 - M_{ax}^2)\left(\frac{a}{1+k}\right)\left(1 + \frac{ak}{1+k}\right)$$

where k is negative for negative prerotation. The value of this expression is a maximum for

$$k = -[(1-a)/(1+a)]$$

Substitution of this value k into the above expression gives

$$Jgc_p\Delta T = \frac{(1+a^2)}{4}(M^2 - M_{ax}^2)(c^2)$$

The temperature rise coefficient is $C_T = (1 + a^2/4)$, see Fig. 10, Curve 5. As previously mentioned, this expression is limited to values of hub ratio a greater than or equal to 0.41. This can be shown as follows:

The Mach Number limitation will not be violated if

$$(W_{1u})_{aR} \leq (W_{1u})_R$$

which means

$$(W_{1u})_{aR} = aU_R + (1/a)(C_{1u})_R \leq (W_{1u})_R$$

Substituting the functions of $(W_{1u})_R$ for U_R and $(C_{1u})_R$ results in the equation

$$1 \leq a\{1 - [k/(1+k)][(1/a) - a]\}$$

and replacing k with $-[(1-a)/(1+a)]$ gives $a \geq \sqrt{2} - 1 = 0.41$. For hub ratios smaller than 0.41, the expression for the temperature-rise coefficient is

$$C_T = a(2+a)/(1+a)^2$$

(2) *Positive Rigid Body Prerotation—Constant Rotor Work*

(*a*) *Axial Relative Discharge at Hub.*—In this case the tangential component of the relative intake velocity decreases proportionally with the radius because of rigid body prerotation. Therefore, the Mach Number limitation will be applied at the tip for the relative intake velocity. For the absolute discharge velocities, the Mach Number limitation will not be violated if

$$U_R + (U_F)_R \leq 2(W_{1u})_R \qquad (1)$$

$$aU_R \leq (W_{1u})_R \qquad (2)$$

Eq. (2) follows from the assumption of axial relative discharge at the hub for which

$$(U_F)_{aR} = (W_{1u})_{aR} \quad \text{or} \quad (U_F)_R/a = a(W_{1u})_R$$

so that Eq. (1) now becomes

$$U_R \leq (2 - a^2)(W_{1u})_R$$

Considering the case

$$U_R \leq (2 - a^2)(W_{1u})_R \qquad (1a)$$

which means that the absolute discharge velocity at the tip is equal to the limiting Mach Number, and Eq. (2), then it follows that the hub ratio a is limited to values less than or equal to 0.63, approximately. Next, considering Eq. (2) as an equality only, which means the absolute discharge velocity at the hub is equal to the limiting Mach Number, and the Eq. (1a), then it follows that the hub ratio a is limited to values greater than or equal to 0.63, approximately.

The expression for stage temperature rise for the first case, $a \leq 0.63$, is

$$Jgc_p\Delta T = a^2(2 - a^2)(M_x^2 - M_{ax}^2)(c^2)$$

so that $C_T = a^2(2 - a^2)$.

The expression for stage temperature rise for the second case, $a \geq 0.63$, is

$$Jgc_p\Delta T = a(M^2 - M_{ax}^2)c^2$$

so that $C_T = a$ (see Fig. 10, Curve 4).

(*b*) *Maximum Constant Rotor Work.*—For positive rigid body prerotation, the relative intake velocity decreases toward the hub while the absolute discharge velocity decreases toward the tip. As in the previous case of rigid body prerotation, only the relative intake velocity at the tip and the absolute discharge velocity at the hub can attain the limiting Mach Number. However, for hub ratios smaller than 0.41, the Mach Number limitation comes into effect for the absolute discharge velocity at the tip. The analysis is as follows:

$$(W_{1u})_R = (C_{2u})_{aR} \quad \text{or} \quad (W_1)_R = (C_2)_{aR}$$

From this it follows that

$$U_R - (C_{1u})_R = (C_{1u})_{aR} + (U_F)_{aR}$$

or

$$U_R - (C_{1u})_R = a(C_{1u})_R + (1/a)(U_F)_R = C\sqrt{M^2 - M_{ax}^2}$$

Now, since $(C_{1u})_r$ and U_r vary directly as the radius, $(C_{1u})_r$ can be expressed as a constant k times U_r. Therefore,

$$U_R(1 - k - ak)a = (U_F)_R$$

$$U_R = c[\sqrt{M^2 - M_{ax}^2}/(1-k)]$$

This gives the stage temperature rise as a function of k and the hub ratio as follows:

$$U_R[(U_F)_R] = c^2\left\{(M^2 - M_{ax}^2)\frac{a[1 - k(1+a)]}{(1-k)^2}\right\}$$

The value of this expression is a maximum when $k = (1-a)/(1+a)$. Substitution of this value of k into the above expression gives

$$Jgc_p\Delta T = \frac{(1+a)^2}{4}\, c^2(M^2 - M_{ax}^2)$$

so that $C_T = (1+a)^2/4$.

(3) *Maximum Constant Rotor Work*

For maximum constant rotor work, $(W_{1u})_R$ and $(C_{2u})_R$ must be the largest possible under the Mach Number limitation. From this and from the condition of constant rotor work, $(U_F)_R$ must be smaller than U_R, otherwise the Mach Number limitation would be violated for all other radii. Thus, the sum of $(W_{1u})_r$ and $(C_{2u})_r$ decreases with the radius until $(U_F)_r$ equals U_r at which point $(W_{1u})_r$ begins to increase. However, the Mach Number limitation will not be violated at any point if at the hub

$$U_{aR} + (U_F)_{aR} \leq 2\,(W_{1u})_R$$

or

$$aU_R + [(U_F)_R/a] \leq 2\,(W_{1u})_R$$

Since

$$(U_F)_R + U_R = 2\,(W_{1u})_R$$

then

$$aU_R + [(U_F)_R/a] \leq (U_F)_R + U_R$$

or

$$(U_F)_R \leq aU_R$$

For maximum constant rotor work, $(U_F)_R$ must have the largest permissible value, so that $(U_F)_R = aU_R$. Therefore,

$$U_R + aU_R = 2(W_{1u})_R$$

or

$$U_R\,(1+a) = 2c\sqrt{M^2 - M_{ax}^2}$$

The stage temperature rise is then given by the equation

$$Jgc_p\Delta T = aU_R^2 = \frac{4a}{(1+a)^2}\,(M^2 - M_{ax}^2)\,(c^2)$$

or $C_T = 4a/(1+a)^2$.

(4) *Nonconstant Rotor Work Distribution over the Radius*

The equation of temperature rise for nonconstant work distribution is given as

$$Jgc_p\Delta T = \frac{2}{R^2(1-a^2)}\int_{aR}^{R} r(U_F)_r(U_r)\,dr$$

(*a*) *Constant Rotor Swirl—Maximum Rotor Work at Tip.*—From the assumption of maximum rotor work at the tip, it follows that

$$(U_F)_R = U_R = (W_{1u})_R = c\sqrt{M^2 - M_{ax}^2}$$

From the condition of constant rotor swirl, $(U_F)_r = (U_F)_R$.

Since

$$(U_F)_r + U_R = [1 + (r/R)]\,(W_{1u})_R$$

no Mach Number violation will occur at any radius if the prerotation is chosen properly.

For any blade radius,

$$Jgc_p\Delta T = \frac{r}{R}\,U_R\,(U_F)_R = \frac{r}{R}\,(W_{1u})_R^2$$

The expression for the temperature rise coefficient is

$$C_T = \frac{Jgc_p\Delta T}{c^2(M^2 - M_{ax}^2)} = \frac{r}{R}$$

For any given hub ratio an average value can be obtained by integration as follows:

$$(C_T)_{\text{av.}} = \frac{1}{\pi R^2(1-a^2)}\int_{aR}^{R}\frac{r}{R}\,2\pi r\,dr = \frac{2}{3}\frac{(1-a^3)}{(1-a^2)}$$

see Fig. 10, Curve 7.

(*b*) *Maximum Nonconstant Rotor Work.*—In order to obtain the maximum total rotor work, the following conditions must be considered:

(1) The Mach Number of relative intake and absolute discharge velocities over the blade length must attain the highest permissible values.

(2) The theoretical maximum work of a blade element must occur at one point r' between tip and hub. This means that U_F equals U for the radius r'. It should be noted that r' cannot be expected to coincide with blade midpoint, since the mass flow of the annulus between blade midpoint and hub is smaller than between blade midpoint and tip.

The ratio r'/R may be designated as k. The temperature rise as a function of k can be obtained as follows:

$$U_r = (W_{1u})_{r'}\left(\frac{r}{r'}\right) = (W_{1u})r'\frac{r}{k(R)}$$

and

$$(U_F)_r = 2(W_{1u})_{r'} - (W_{1u})_{r'}\frac{r}{R(k)} = (W_{1u})_{r'}\left(2 - \frac{r}{R(k)}\right)$$

Therefore

$$Jgc_p\Delta T = \frac{2(W_{1u})_{r'}^2}{R^2(1-a^2)}\left[\int_{aR}^{R} r\,\frac{r}{k(R)}\left(2 - \frac{r}{R/k}\right)dr\right]$$

$$= \frac{2(W_{1u})_{r'}^2}{(1-a^2)}\left[\frac{2(1-a^3)}{3k} - \frac{(1-a^4)}{4k^2}\right]$$

The maximum temperature rise is obtained when

$$k = 3(1-a^4)/4(1-a^3)$$

so that

$$Jgc_p\Delta T = \frac{8}{9}\frac{(1-a^3)^2}{(1-a^2)(1-a^4)}(M^2 - M_{ax}^2)c^2$$

and

$$(C_T)_{av.} = (8/9)\,[(1-a^3)^2/(1-a^2)^2(1+a^2)]$$

(6) *Maximum Constant Rotor Work with Keller Limitation*

The highest possible flow deflection U_F, according to the Keller limitation, is $U_F = 0.6W_m$. This limitation applied for rotor and stator at the hub results in

$$(1/a)\ U_F = 0.6W_m = 0.6\sqrt{(a^2/4)U^2 + V^2}$$

see Fig. 13. The Mach Number limitation comes into effect at the tip where

$$c^2M^2 = V^2 + (0.5U + 0.5U_F)^2$$

Substituting into this equation the value U_F results in

$$c^2M^2 = V^2 + \frac{1}{4}\left(U + 0.6a\sqrt{\frac{a^2U^2}{4} + V^2}\right)^2$$

$$c^2(M^2 - M_{ax}^2) = \frac{(U + 0.6a\sqrt{(a^2U^2/4) + V^2})^2}{4}$$

$$c\sqrt{M^2 - M_{ax}^2} - 0.5U = 0.3a\sqrt{(a^2U^2/4) + V^2}$$

This results in the following expression for U:

$$U = \frac{2c\sqrt{M^2 - M_{ax}^2} - 0.6a\sqrt{V^2(1 - 0.09a^4) + a^2c^2(M^2 - M_{ax}^2)}}{1 - 0.09a^4}$$

or, with good approximation,

$$U = 2c\sqrt{M^2 - M_{ax}^2} - 0.6ac\sqrt{M_{ax}^2 + a^2(M^2 - M_{ax}^2)}$$

and

$$U_F = 0.6ac\sqrt{M_{ax}^2 + a^2(M^2 - M_{ax}^2)} = 0.6a^2Mc\sqrt{1 + \frac{(1-a^2)}{a^2}\left(\frac{M_{ax}^2}{M^2}\right)}$$

This results in the following expression for $\Delta T/T_0$:

$$\frac{\Delta T}{T_0} = 0.4\frac{U(U_F)}{c^2} = 0.24a^2M^2\sqrt{1 + \frac{(1-a^2)}{a^2}\frac{(M_{ax})^2}{M^2}}\left[2\sqrt{1 - \frac{(M_{ax})^2}{M^2}} - 0.6a^2\sqrt{1 + \frac{(1-a^2)}{a^2}\frac{(M_{ax})^2}{M^2}}\right]$$

References

[1] Wattendorf, F. L., Tsien, H. S., and Duwez, Pol, *Aircraft Power Plants*, A Report of the A.A.F. Scientific Advisory Group, May, 1946 (RESTRICTED).

[2] Tsien, H. S., Sears, W. R., Ashkenas, Irving L., Hasert, C. N., and Newark, N. M., *Aerodynamics and Aircraft Design*, A Report of the A.A.F. Scientific Advisory Group, May, 1946 (RESTRICTED).

[3] Hensley, R. V., Sanders, N. D., and Kress, R. P., *Performance Potentialities of the Turbojet Engine*, Institute of Aeronautical Sciences, Preprint No. 148.

[4] Wood, G. P., *Performance Possibilities of the Turbojet System as a Power Plant for Supersonic Airplanes*, N.A.C.A. R.M. No. L7H 05a, August 26, 1947.

[5] Wattendorf, F. L., *High-Speed Flow Through Cambered Rotating Grids*, Journal of the Aeronautical Sciences, Vol. 15, No. 4, April, 1948.

[6] Wu, Chung Hua, and Wolfenstein, L., *Application of Radial Equilibrium Condition to Axial Flow Compressor and Turbine Design*, N.A.C.A. T.N. No. 1795, January, 1949.

[7] Kahane, A., *Investigation of Axial-flow Fan and Compressor Rotors Designed for Three-Dimensional Flow*, N.A.C.A. T.N. No. 1652, July, 1948.

[8] Weske, J. R., Rubin, B. Z., and Gardiner, F. J., *Theory for Design of Axial Flow Compressors*, Chrysler Corporation, Engineering Division, TR No. A-61805.57.

[9] Wu, Chung Hua, *Survey of Available Information on Internal Flow Losses Through Axial Turbo Machines*, N.A.C.A. R.M. E50J13, January 26, 1951.

[10] Weinig, F., and Eckert, B., *Uberblick Uber Forschungsergebnisse*, Bericht 171 der Lilienthal Gesellschaft, October, 1943.

[11] Ainley, D. G., *Performance of Axial-Flow Turbines*, War Emergency Issue No. 41 pub. by Inst. Mech. Eng. (London). (Reprinted in U. S. by A.S.M.E., pp. 230–244, April, 1949.)

[12] Bowen, John T., Sabersky, Rolf H., and Rannie, W. D., *Theoretical and Experimental Investigation of Axial Flow Compressors*, California Institute of Technology, U.S.N. Contract No. N6-ORI-102, January, 1949.

[13] Keller, Curt, *The Theory and Performance of Axial-Flow Fans;* McGraw-Hill Book Company, Inc., New York, 1937.

The Turbulent Boundary Layer in a Compressible Fluid with Positive Pressure Gradient*

CARLO FERRARI†

Cornell Aeronautical Laboratory, Inc.

SUMMARY

The turbulent boundary layer in compressible flow is investigated for the case where there is a pressure increase in the direction of motion in order to determine its effect upon: (a) the velocity distribution at an arbitrary cross section of the layer; (b) the variation of the thickness of the layer as one progresses along the boundary and the calculation of the corresponding drag coefficient; and (c) the phenomenon of separation of the stream from the wetted wall.

A check, resulting in close agreement, is made of the theory by comparing the velocity profiles predicted on this theoretical basis with those obtained in experiments at low speed under the influence of pressure gradients. A further numerical application is worked out for the case of a supersonic (Mach Number = 1.5) undisturbed stream velocity, but no experimental data at such high speed are at present available for confirmation.

INTRODUCTION

THE INVESTIGATION OF THE turbulent boundary layer in supersonic flow was confined in a previous report[1] to the case of flow along a flat plate, but now this restrictive assumption is relinquished in order to present methods applicable to an airfoil—i.e., to account for the presence of a positive pressure gradient.

A plausible assumption concerning the dependence of the turbulent friction stress on the kinematic and on the geometric characteristics of the average flow leads to the construction of the equation of motion, describing the flow through the "inside" portion of the layer, in the same form as that used by von Mises[2] for the case of the laminar régime. A procedure similar to that used by von Kármán[3] for incompressible flow is employed in order to obtain the solution of this equation of motion and for determining the position where the separation of the stream from the wetted wall eventually takes place.

It is further assumed that there is no heat transfer between the surface of the constraining wall and the fluid and that the flow is wholly turbulent. In addition, the equations of motion are considered to be valid only at a sufficiently great distance from the place where the increase in pressure in the direction of flow originates.

Received August 7, 1950. Extended version of manuscript submitted to Cornell Aeronautical Laboratory, Inc., on May 2, 1949.

* This research was conducted under Navy BuOrd sponsorship.

† Member of Cornell Aeronautical Laboratory consulting staff. Professor, Laboratorio di Aeronautica, Politecnico di Torino.

SYMBOLS

$\bar{R}_x$ = $U_a x/\nu_a$ = Reynolds Number of the undisturbed stream

T = absolute temperature

p = pressure; τ = tangential friction stress

μ = viscosity coefficient; ν = kinematic viscosity

ρ = density of the fluid; $\bar{\rho}_e$ = density in the external stream at a cross section of the layer having an abscissa equal to x

z = $1 - (\bar{\rho}/\bar{\rho}_e)$; $\zeta = (z_0 - z)/2$

U = component of the velocity along the x-axis; V = component of the velocity along the y-axis; $Z = (\bar{U}_e^2/U_a^2) - (\bar{U}^2/U_a^2)$; $\bar{U}_e$ = velocity of the external stream (its magnitude is taken to be equal to the component in the direction of the x-axis of the actual vector) at a location along the boundary having an abscissa equal to x

W = $\sqrt{U^2 + V^2}$; U^* = friction velocity $[U^* = (\tau_p/\rho_p)^{1/2}]$; V_l = limit velocity of the undisturbed stream when expanded to a vacuum

M = Mach Number; L = reference length; $\xi = x/L$; $\eta = y/L$; x being taken in the direction of the wetted surface

δ = thickness of the boundary layer; $\bar{\delta} = \delta/L$

$\delta^* = \delta\int_0^1 \left(1 - \frac{\rho}{\rho_e}\frac{\bar{U}}{\bar{U}_e}\right)d\frac{y}{\delta}$

$\bar{\delta}^* = \frac{\delta^*}{L}$; $\delta^{**} = \delta\int_0^1 \frac{\bar{\rho}}{\bar{\rho}_e}\frac{\bar{U}}{\bar{U}_e}\left(1 - \frac{\bar{U}}{\bar{U}_e}\right)d\frac{y}{\delta}$; $\bar{\delta}^{**} = \frac{\delta^{**}}{L}$

ψ = $\bar{\rho}\bar{U}y$ = stream function; $\psi_1 = \psi/\rho_a U_a L$; ψ_1^* = a function that is proportional to ψ_1 and defined precisely in Section (B-1)

ξ, ξ_1^* = functions of ξ defined in Sections (B-1) and (C-1)

Bars and primes will be used to denote, respectively, the mean values of the above quantities and their fluctuations about their mean values due to turbulence. The subscripts 0, p, e, and a correspond, respectively, to the stagnation condition of the undisturbed stream and to other special conditions that exist at the wall, in the external stream, and in the undisturbed stream.

(A) GENERAL EQUATIONS

(A-1) *Equations of Momentum, Energy, and Continuity*

Within the region external to the laminar sublayer and through neglect of the momentum transfer due to thermal molecular vibration in comparison to the momentum due to turbulence, one obtains

$$\left.\begin{aligned} -\frac{\partial}{\partial x}\bar{p} &= \frac{\partial}{\partial x}(\overline{\rho U^2}) + \frac{\partial}{\partial y}(\overline{\rho UV}) \\ -\frac{\partial}{\partial y}\bar{p} &= \frac{\partial}{\partial x}(\overline{\rho UV}) + \frac{\partial}{\partial y}(\overline{\rho V^2}) = 0 \end{aligned}\right\} \quad (1)$$

It is being assumed here that the curvature of the surface of the obstacle along which the boundary layer is built up is sufficiently small to permit the supposition that the tangent to the surface, at every point P, is parallel to the x-axis for all intents and purposes. Because

$$\overline{\rho U^2} = \overline{(\bar{\rho} + \rho')(\bar{U} + U')^2} \cong \bar{U}(\bar{\rho}\bar{U} + 2\,\overline{\rho' U'}) \cong \bar{\rho}\bar{U}^2 \quad (2)$$

inasmuch as it is generally true that $\bar{\rho}\bar{U} \gg \overline{\rho' U'}$, while, also,

$$\overline{\rho UV} \cong \bar{\rho}\bar{U}\bar{V} + \bar{U}\,\overline{\rho' V'} + \bar{\rho}\,\overline{U'V'} \quad (2')$$

then one obtains

$$-\frac{\partial \bar{p}}{\partial x} \cong \frac{\partial}{\partial x}(\bar{\rho}\bar{U}^2) + \frac{\partial}{\partial y}(\bar{\rho}\bar{U}\bar{V}) + \frac{\partial}{\partial y}(\bar{\rho}\,\overline{U'V'} + \bar{U}\,\overline{\rho' V'}) \quad (3)$$

Analogously and with the same approximation, one derives, from the equation of energy,

$$\frac{\partial}{\partial x}\left[\overline{\rho U\left(i + \frac{1}{2}W^2\right)}\right] + \frac{\partial}{\partial y}\left[\overline{\rho V\left(i + \frac{1}{2}W^2\right)}\right] = 0$$

Let $H = i + (1/2)\,W^2$ in the above expression and, upon noting that

$$\overline{\rho UH} \cong \bar{\rho}\bar{U}\bar{H} + \bar{\rho}\,\overline{U'H'} + \overline{\rho' U'}\,\bar{H} + \overline{\rho' H'}\,\bar{U}$$

and

$$\overline{\rho VH} \cong \bar{\rho}\bar{V}\bar{H} + \bar{H}\,\overline{\rho' V'} + \bar{\rho}\,\overline{V'H'}$$

it results that

$$\frac{\partial}{\partial x}(\bar{\rho}\bar{U}\bar{H}) + \frac{\partial}{\partial x}(\bar{\rho}\overline{U'H'} + \overline{\rho' U'}\,\bar{H} + \overline{\rho' H'}\,\bar{U}) + \frac{\partial}{\partial y}(\bar{\rho}\bar{V}\bar{H}) + \frac{\partial}{\partial y}(\bar{\rho}\overline{V'H'} + \bar{H}\,\overline{\rho' V'}) = 0 \quad (4)$$

Finally, from the equation of continuity, it is found that

$$\frac{\partial}{\partial x}(\bar{\rho}\bar{U}) + \frac{\partial}{\partial y}(\bar{\rho}\bar{V}) + \frac{\partial}{\partial x}(\overline{\rho' U'}) + \frac{\partial}{\partial y}(\overline{\rho' V'}) = 0 \quad (5)$$

It should be observed that, in the case of flow past a flat plate (i.e., with pressure gradient equal to zero at a sufficiently large distance from the transition point from laminar to turbulent flow), it has been found[1] admissible to write $\overline{\rho' V'} = \text{const.}$ Bearing in mind that in the problem now under consideration the pressure gradient is assumed to be independent of y, it still appears allowable to write $(\partial/\partial y)(\overline{\rho' V'}) = 0$ or at least to consider this derivative so small as to be negligible.

It follows that $\overline{\rho' U'}$ may be neglected in comparison with $\bar{\rho}\bar{U}$, and, hence,

$$(\partial/\partial x)(\bar{\rho}\bar{U}) + (\partial/\partial y)(\bar{\rho}\bar{V}) = 0 \quad (6)$$

while one may write

$$\overline{\rho' V'} = c_1 \bar{\rho}_e \bar{U}_e \quad (7)$$

as was done previously in the case of flow along a flat plate.

(A-2) *First Integral of Energy*

By comparison of Eq. (4) with Eq. (5) and remembering that if $\bar{H}$ is a constant it is likely to be true that $\overline{U'H'} = \overline{\rho' H'} = \overline{V'H'} = 0$, one finds that

$$\bar{H} = \bar{\imath} + (1/2)\bar{U}^2 = \text{const.} = i_p = i_0 = \bar{\imath}_e + (1/2)\bar{U}_e^2 \quad (8)$$

is a particular integral of Eq. (4). This integral corresponds to the case of a nonconducting wall, and the following investigation is restricted to this condition.

(A-3) *Turbulent Friction Stress*

From Eq. (3) it may be inferred that the turbulent friction stress is given by

$$\tau = -(\bar{\rho}\,\overline{U'V'} + \bar{U}\,\overline{\rho' V'}) \quad (9)$$

If one admits that $\overline{U'V'}$, at every given point of the flow, depends only upon the average stream characteristics, one can generalize the formula used in the previous note[1] of this series. Letting

$$\overline{U'V'} = (\partial\bar{U}/\partial y)\, f(\bar{U}, \partial\bar{U}/\partial y, \ldots)$$

and expanding f in a power series of the parameters on which it depends, and keeping only the first terms, one may write

$$\overline{U'V'} = -(\partial\bar{U}/\partial y)(C_1 U^* + C_2\bar{U}) \quad (10)$$

where U^* is a velocity depending on the velocity U_a at infinity but independent, at least formally, of the local velocity $\bar{U}$. The use of Eq. (10) in the case of turbulent flow along a flat plate, with pressure gradient equal to zero, led previously[1] to the replacement of U^* by the friction velocity in contact with the wall, which is written here as

$$U^* = U_p^* = \sqrt{\tau_p/\bar{\rho}_e} \quad (11)$$

On the other hand, in proximity to the wall, if $d\bar{p}/dx$ is taken equal to zero, Eq. (10) reduces to

$$\overline{U'V'} = -(\partial\bar{U}/\partial y)\, C_1 U^* \quad (10')$$

It follows that C_1 must depend on $d\bar{p}/dx$ and vanish along with it. Furthermore, because of the fact that (again in proximity to the obstacle S) the physical quantities that probably affect C_2, at least for the sections of the boundary layer far from the one at which separation occurs, are the thickness, δ, of the boundary layer (at the same cross section, viz., for the same value

of x, as that defining the point P of S in the neighborhood of which we are evaluating C_2), the friction velocity, U_p^*, and the kinematic viscosity ν_p, then one obtains, because of the principle of homogeneity of the physical equations,

$$C_2 = k_2 \frac{d\bar{p}}{dx} \frac{1}{\bar{\rho}_e \bar{U}_e^2} \frac{\delta \nu_p}{U_p^*} = -k_2 \frac{1}{\bar{U}_e} \frac{d\bar{U}_e}{dx} \frac{\delta \nu_p}{U_p^*} \quad (11')$$

where y must be sufficiently small and x must not be too close to the value defining the location at which separation occurs.

At a sufficient distance from the wall S and therefore in proximity to the outer contour of the boundary layer, C_2, as well as C_1, is to be considered as independent of those parameters that are more directly bound to the viscosity of the fluid, as, for example, the coefficient of kinematic viscosity, ν.

It seems allowable, therefore, to set simply

$$C_2 = h_2 \delta \quad \text{and} \quad C_1 = h_1 \delta \quad (12)$$

for y large enough.

Thus it appears that one may write

$$\begin{aligned} \overline{U'V'} &= -\frac{\partial \bar{U}}{\partial y}\left(k_1 y U_p^* - k_2 \frac{1}{\bar{U}_e}\frac{d\bar{U}_e}{dx}\frac{\delta \nu_p}{U_p^*}\bar{U}\right) && \text{for } y \text{ small enough} \\ \overline{U'V'} &= -(\partial \bar{U}/\partial y)\,\delta\,(h_1 U_p^* + h_2 \bar{U}_e) && \text{for } y \text{ large enough} \end{aligned} \quad (13)$$

Now, if $-d\bar{U}_e/dx$ is large enough in order that the related values of y require the use of the first of Eqs. (13), $k_1 y$ and

$$-k_2(1/\bar{U}_e)\,(d\bar{U}_e/dx)\,(\delta \nu_p/U_p^*)$$

are of the same order of magnitude. It is further worthy of note that $\bar{U}$, in general, is much larger than U_p^*; thus it will be possible to neglect in Eqs. (13) the terms containing k_1 and h_1 with respect to those containing k_2 and h_2. Thus it will be true that

$$\begin{aligned} \overline{U'V'} &= \frac{\partial \bar{U}}{\partial y} k_2 \frac{1}{\bar{U}_e}\frac{d\bar{U}_e}{dx}\frac{\delta \nu_p}{U_p^*}\bar{U} && \text{for } y \text{ small enough} \\ \overline{U'V'} &= -(\partial \bar{U}/\partial y)\, h_2 \delta \bar{U}_e && \text{for } y \text{ large enough} \end{aligned} \quad (13')$$

This assumption enables one to write

$$\begin{aligned} \tau &= -\bar{\rho}\frac{\partial \bar{U}}{\partial y} k_2 \frac{1}{\bar{U}_e}\frac{d\bar{U}_e}{dx}\frac{\delta \nu_p}{U_p^*}\bar{U} - c_1 \bar{\rho}_e \bar{U}_e \bar{U} && \text{for small values of } y \\ \tau &= -\bar{\rho}\,(\partial \bar{U}/\partial y) h_2 \delta \bar{U}_e - c_1 \bar{\rho}_e \bar{U}_e \bar{U} && \text{for large values of } y \end{aligned} \quad (14)$$

On the other hand, the investigation carried out in the previous report[1] of this series showed that, in the case of flow along a flat plate, the term corresponding to $c_1 \bar{\rho}_e \bar{U}_e \bar{U}$ in the expression for τ is of the same order of magnitude as that corresponding to $-k_1 y U_p^* (\partial \bar{U}/\partial y)$. Because the latter term has been neglected in the present investigation, it is permissible, therefore, to neglect the former also, and it is thus deduced that

$$\begin{aligned} \tau &= -\bar{\rho}\frac{\partial \bar{U}}{\partial y} k_2 \frac{1}{\bar{U}_e}\frac{d\bar{U}_e}{dx}\frac{\delta \nu_p}{U_p^*}\bar{U} && \text{for small values of } y \\ \tau &= -\bar{\rho}\,(\partial \bar{U}/\partial y)\, h_2 \delta \bar{U}_e && \text{for large values of } y \end{aligned} \quad (14')$$

The assumption being made here is not essential to the aims of the present investigation, however, since a procedure like that followed in the succeeding paragraphs would be possible even if the term involving c_1 were retained.

It should be noted that the results now attained, particularly in the simplified form of Eqs. (14′), may hold only at sufficiently large distances from the profile (cross section of the boundary layer) at which $d\bar{p}/dx$ becomes positive, in order that, away from such a profile, the influence of the pressure gradient on the motion of turbulent vibration will be of such a magnitude as to offset the effect of the friction stress at the wall upon this motion. On the other hand, at least in regard to the first of Eqs. (14′), the remark already made holds—i.e., this equation is only applicable to those sections that are not close to the place where separation occurs.

The derivation of Eqs. (14′) was just accomplished by following a wholly formal procedure based on the assumption that the component of the double tensor of correlation between the turbulent fluctuations of the velocity, to which the tangential friction stress is due, depends solely on the average flow characteristics. These relations may, however, be given the following physical interpretation:

Near the cross section Σ of the boundary layer at which $d\bar{U}_e/dx < 0$, the influential effect of the friction in contact with the wall still prevails in determining the correlation between U' and V', especially within the region closest to the wall itself (region of wall turbulence). Moving away from this region and also from the above-mentioned cross section Σ, the influence that the pressure variation $d\bar{p}/dx$ has on the correlation increases in importance and probably tends to produce a dependence of the correlation itself on the mean velocity, analogous to that occurring in the region of free turbulence,[4] as is substantially characterized by the second of Eqs. (14′). These considerations lead one to foresee that the nearer the section under investigation is to the place where separation occurs, the larger will be the region within which the second of Eqs. (14′) holds. Thus it is implied that, downstream of a certain section, at least, it will be possible to assume that this equation defines τ within the whole layer.

(B) Reduction of the Equation of Motion Within the Boundary Layer to the Equation of von Mises—External and Internal Solutions—Separation Point

(B-1) *Transformation of Eq. (3)*

In accordance with the method suggested by von Mises,[2] which has been improved by von Kármán[3] and applied to the study of the laminar boundary layer in flow with a pressure gradient for the case of an incompressible fluid, ξ and the reduced stream function $\psi_1 = \psi/\rho_a U_a L$ are taken as independent variables, instead of $\xi = x/L$ and $\eta = y/L$. It is found that

$$\frac{\partial}{\partial \xi}(\bar{\rho}\bar{U}^2) + \frac{\partial}{\partial \eta}(\bar{\rho}\bar{U}\bar{V}) = \bar{\rho}\bar{U}\frac{\partial}{\partial \xi}\bar{U}(\xi, \psi_1)$$

while it is also true that

$$\frac{\partial \bar{p}}{\partial \xi} + \frac{1}{2}\bar{\rho}\frac{\partial}{\partial \xi}\bar{U}^2 = \frac{\bar{p}_e^2}{2\bar{p}}\left[-\frac{\bar{p}}{\bar{p}_e}\frac{\partial}{\partial \xi}\bar{U}_e^2 + \frac{\bar{p}^2}{\bar{p}_e^2}\frac{\partial \bar{U}^2}{\partial \xi}\right] \quad (15)$$

Since

$$\frac{\bar{p}}{\bar{p}_e} = \frac{\bar{T}_e}{\bar{T}} = \frac{i_0 - (1/2)\bar{U}_e^2}{i_0 - (1/2)\bar{U}^2} = \frac{1 - (\bar{U}_e^2/V_l^2)}{1 - (\bar{U}^2/V_l^2)} \quad (16)$$

then, consequently,

$$\frac{\partial}{\partial \xi}\left(\frac{\bar{p}}{\bar{p}_e}\right) = \frac{1}{1 - (\bar{U}_e^2/V_l^2)}\frac{1}{V_l^2} \times \left[-\frac{\bar{p}}{\bar{p}_e}\frac{\partial \bar{U}_e^2}{\partial \xi} + \frac{\bar{p}^2}{\bar{p}_e^2}\frac{\partial \bar{U}^2}{\partial \xi}\right] \quad (17)$$

From Eqs. (17) and (15) it is found that

$$\frac{\partial \bar{p}}{\partial \xi} + \frac{1}{2}\bar{p}\frac{\partial \bar{U}^2}{\partial \xi} = \frac{\bar{p}_e^2}{2\bar{p}}\left(1 - \frac{\bar{U}_e^2}{V_l^2}\right)V_l^2\frac{\partial}{\partial \xi}\left(\frac{\bar{p}}{\bar{p}_e}\right) \quad (18)$$

On the other hand, by considering now the *external solution* of the equation of motion within the boundary layer and, consequently, by assuming τ to be equal to the expression given as the second of Eqs. (13), one obtains

$$\frac{\partial \tau}{\partial \eta} = h_2\bar{\delta}\bar{U}_e\frac{\partial}{\partial \eta}\left(\bar{\mu}\frac{\partial \bar{U}}{\partial \eta}\right) = h_2\bar{\delta}\bar{U}_e\frac{\bar{p}_e^2}{\rho_a}\frac{\partial}{\partial \eta}\left(\frac{\bar{\rho}^2}{\bar{p}_e^2}\frac{\bar{U}}{U_a}\frac{\partial \bar{U}}{\partial \psi_1}\right)$$
$$= h_2\bar{\delta}\frac{\bar{U}_e}{U_a}\frac{\bar{p}_e^2}{\rho_a}\frac{1 - (\bar{U}_e^2/V_l^2)}{2}V_l^2\frac{\bar{\rho}\bar{U}}{\rho_a U_a}\frac{\partial^2}{\partial \psi_1^2}\left(\frac{\bar{\rho}}{\bar{p}_e}\right)$$

Hence, taking Eq. (18) into account, one infers that

$$\frac{\partial}{\partial \xi}\left(\frac{\bar{\rho}}{\bar{p}_e}\right) = h_2\bar{\delta}\frac{\bar{U}_e^2}{U_a^2}\frac{\bar{U}}{\bar{U}_e}\frac{\bar{\rho}^2}{\bar{p}_e^2}\frac{\bar{p}_e^2}{\rho_a^2}\frac{\partial^2}{\partial \psi_1^2}\left(\frac{\bar{\rho}}{\bar{p}_e}\right) \quad (19)$$

Letting

$$\bar{\rho}/\bar{p}_e = 1 - z$$

$$\frac{1}{\bar{\delta}}\frac{U_a^2}{\bar{U}_e^2}\frac{\rho_a^2}{\bar{p}_e^2}\frac{\partial}{\partial \xi}\left(\frac{\bar{\rho}}{\bar{p}_e}\right) = \frac{\partial}{\partial \xi_1}\left(\frac{\bar{\rho}}{\bar{p}_e}\right) \quad (20)$$

and, hence,

$$(1/\bar{\delta})(U_a^2/\bar{U}_e^2)(\rho_a^2/\bar{p}_e^2) = d\xi/d\xi_1 \quad (21)$$

that is,

$$\xi_1 = \int_0^{\xi}(\bar{\delta}\bar{U}_e^2\bar{p}_e^2/U_a^2\rho_a^2)d\xi \quad (21')$$

Now setting

$$1 - z_0 = \rho_p/\bar{p}_e = 1 - (\bar{U}_e^2/V_l^2)$$

one finds that

$$\bar{U}/\bar{U}_e = (z_0 - z)^{1/2}/z_0^{1/2}(1 - z)^{1/2} \quad (22)$$

and, hence, Eq. (19) yields

$$\frac{\partial z}{\partial \xi_1} = (1 - z)^{3/2}\left(\frac{z_0 - z}{z_0}\right)^{1/2}\frac{\partial^2 z}{\partial \psi_1^{*2}} \quad (23)$$

where

$$\psi_1^* = \psi_1/\sqrt{h_2} \quad (24)$$

(B-2) *External Solution of the Equation of von Mises*

It is evident that Eq. (23) has the same form as the equation of von Mises[2] for the case of laminar flow in an incompressible fluid. Thus there may be found an *external* solution—that is, a solution holding in the outer portion of the boundary layer and rigorously on the very outer contour of the layer. This solution may be easily determined as indicated below.

Following the procedure suggested by von Kármán[3] for treating the analogous equation just mentioned [and upon letting z take on the value that it attains on the outer contour—i.e., from Eq. (20), $z = 0$] one obtains

$$\partial z_e/\partial \xi_1 = \partial^2 z_e/\partial \psi_1^{*2} \quad (25)$$

wherein z_e denotes the function z corresponding to the *external* solution. This equation is the same as the equation of heat propagation within a medium having unit diffusivity (in accordance with the interpretation

given by Lord Kelvin). In order to determine z_e unequivocally, it is still necessary to assign the boundary conditions. Now, one of these conditions, which has already been made use of (viz., the one corresponding to $\psi_1^* = \infty$), is given straight off by $z_e = 0$ for all values of ξ_1.

In order to establish the other boundary condition corresponding to $\psi_1^* = 0$, it may first of all be said that, according to what has been stated in Section (A-3), the region within which the second of Eqs. (14′) holds is supposed to be large for those cross sections of the boundary layer that are sufficiently far away from the initial section Σ. It follows that, by imposing the same boundary condition upon z_e that conforms with the one existing for the internal solution of Eq. (3), one may expect to obtain a solution describing the fluid motion within practically the whole turbulent layer with sufficient accuracy. If attention is now focused upon the boundary of the laminar sublayer, it is evident that the values of ψ_1^* are so small here that it is permissible to set them equal to zero. If one then imposes the condition that the turbulent shearing stress at this boundary be a given multiple m of the viscous stress, for m suitably large, the first of Eqs. (14′) yields

$$-\rho_p \frac{\partial \bar{U}}{\partial y} k_2 \frac{1}{\bar{U}_e} \frac{d\bar{U}_e}{dx} \frac{\delta \nu_p}{U_p^*} \bar{U} = m\mu_p \frac{\partial \bar{U}}{\partial y}$$

whence

$$-\frac{1}{\bar{U}_e}\frac{d\bar{U}_e}{d\xi}\frac{\bar{\delta}}{}\frac{\bar{U}}{U_p^*} = \frac{m}{k_2} = c \tag{26}$$

and, consequently, for $\psi_1^* = 0$,

$$\bar{U}/\bar{U}_e = -c\,[U_p^*/\bar{\delta}(d\bar{U}_e/d\xi)] \tag{26′}$$

wherein c is a constant whose value can be obtained from experiments. Because of the way in which c has been introduced, it is likely to be independent of the compressibility of the fluid. Noting that

$$z = [1 - (\bar{U}/\bar{U}_e^2)]/[(V_1^2/\bar{U}_e^2) - (\bar{U}^2/\bar{U}_e^2)] \tag{27}$$

thus Eq. (27), together with Eq. (26′), affords the means of obtaining the distribution of the values of z for $\psi_1^* = 0$; these values are denoted here by z_1. The function z_e satisfying Eq. (25), together with the boundary conditions just defined, is given by

$$z_e = \frac{\psi_1^*}{2\sqrt{\pi}} \int_0^{\xi_1} z_1(x_1) \frac{e^{-\psi_1^{*2}/4(\xi_1 - x_1)}}{(\xi_1 - x_1)^{3/2}}\, dx_1 \tag{28}$$

If the function $z_1(x_1)$ may be expanded in a power series having the form

$$z_1 = \sum_{r=0}^{n} B_r\, x_1^r \tag{29}$$

(which is now assumed to be possible), the second member of Eq. (28) may be evaluated, and one finds that

$$z_e = \sum_{r=0}^{n} B_r\, 2^{2r}\, r!\, \xi_1^r \left[i^{2r} \operatorname{erfc}\left(\frac{\psi_1^*}{2\sqrt{\xi_1}}\right)\right] \tag{30}$$

where, according to the notation used by Carslaw,[5] $\operatorname{erfc} x = 1 - \operatorname{erf} x$ and i^n represents the nth integral of the complement of the error function.

(*B-3*) *Complete Solution of von Mises' Equation*

For those cross sections that are not too close to the section at which separation occurs, the complete solution of Eq. (23) may be worked out by the method of successive approximations suggested by von Kármán in his paper[3] already referred to above. Writing Eq. (23) in the form

$$\frac{\partial z}{\partial \xi_1} - \frac{\partial^2 z}{\partial \psi_1^{*2}} = \frac{\partial^2 z}{\partial \psi_1^{*2}}\left[(1-z)^{3/2}\left(1 - \frac{z}{z_0}\right)^{1/2} - 1\right] = H(z) \tag{23′}$$

and replacing z in the second member of Eq. (23′) by z_e, one obtains for z a further approximation as a result of solving the equation

$$\frac{\partial z}{\partial \xi_1} - \frac{\partial^2 z}{\partial \psi_1^{*2}} = H(z_e)$$

This solution is formally given by

$$z = z_e - \frac{1}{2\sqrt{\pi}} \int_0^{\infty} d\eta \int_0^{\xi_1} dx_1 \left[e^{-(\psi_1^* - \eta)^2/4(\xi_1 - x_1)} - e^{-(\psi_1^* + \eta)^2/4(\xi_1 - x_1)}\right] \frac{H(x_1, \eta)}{\sqrt{\xi_1 - x_1}} \tag{31}$$

The calculations required by Eq. (31), in order to obtain the values of z in the whole field, are undoubtedly laborious; on the other hand, if one denotes by $H_{max.}$ the maximum absolute value of H, the maximum absolute value of $z - z_e$ resulting from Eq. (31) is found to be

$$|z - z_e|_{max.} < \frac{1}{2\sqrt{\pi}} H_{max.} \int_0^{\infty} d\eta \int_0^{\xi_1} dx_1 \left[e^{-(\psi_1^* - \eta)^2/4(\xi_1 - x_1)} - e^{-(\psi_1^* + \eta)^2/4(\xi_1 - x_1)}\right] \frac{1}{\sqrt{\xi_1 - x_1}} =$$

$$\frac{1}{2} 4H_{max.}\, \xi_1 \left\{\operatorname{erfc} x + 2x(i \operatorname{erfc} x) + (2i^2 \operatorname{erfc} x) - [2i^2 \operatorname{erfc}(0)]\right\} \tag{31′}$$

where, for sake of simplicity, the symbol x represents $\psi_1^*/2\sqrt{\xi_1}$. Now, for x comprised in the intervals 1.5 to 1.0 and from 1.0 to 0.5, the coefficient of $4H_{max.}$ falls in the intervals 0.2479 to 0.2355 and 0.2355 to 0.18, respec-

tively; and because, as a result of calculations to be described in the following Sections (C-1) and (C-2), it appears that $4H_{max.}$ is small besides, it is allowable to conclude that, for the sections of the boundary layer not too close to the section in which separation takes place, even the first approximation $z = z_e$ yields good results over the whole interval of variation of ψ_1^*.

In fact the error is certainly somewhat smaller than that resulting from Eq. (31′) because not only is H not constant but it reverses its sign within the range of variation of ψ_1^* [as one may observe from the calculations presented in Sections (C-1) and (C-2)]. Furthermore, H approaches zero for large values of ψ_1^*—that is, it approaches zero right where [according to Eq. (31′)] the coefficient of the error attains its largest values.

In proximity to the section in which separation occurs and particularly for the purpose of determining the separation point, the above given approximation corresponding to the *external* solution is no longer sufficient. In order to determine such a separation point, a procedure is suggested herewith which is similar to that used by von Kármán. In fact, the condition to be satisfied for $\psi_1^* = 0$ is now $z = z_0$; this situation is identical with that dealt with by von Kármán in his above-mentioned paper.

Letting

$$\zeta = (z_0 - z)/2 \tag{32}$$

be the independent variable, Eq. (23) becomes

$$\frac{\partial^2\zeta}{\partial\psi_1^{*2}} = -\frac{z_0^{1/2}}{2\cdot 2^{1/2}(1 - z_0 + 2\zeta)^{3/2}}\frac{\partial z_0/\partial\xi_1}{\zeta^{1/2}} \times \left[1 - 2\frac{\partial\zeta/\partial\xi_1}{\partial z_e/\partial\xi_1}\right] \tag{33}$$

which, for ζ small enough, is approximated by

$$\partial^2\zeta/\partial\psi_1^{*2} = [A(\xi_1)/\zeta^{1/2}]\,[1 - (a\sqrt{\zeta})] \tag{34}$$

The latter equation is obtained by setting

$$A(\xi_1) = -[z_0^{1/2}/2^{3/2}(1 - z_0)^{3/2}]\,(\partial z_0/\partial\xi_1)$$

and by replacing the coefficient of $A/\zeta^{1/2}$ in the second member of Eq. (33) by a function of ζ only (in accordance with the procedure used by von Kármán). This function of ζ attains, for $\psi_1^* = 0$, the same value as the coefficient itself does. Furthermore, let a denote a constant or, better, a function of ξ_1 only, which is left undetermined and which will be at free disposal to be employed when convenient in order to ensure the connection between the *internal* solution given by Eq. (34) and the *external* solution presented by Eq. (30).

Setting

$$B_1 = (\partial\zeta/\partial\psi_1^*)_{\psi_1^*=0} \tag{35}$$

one obtains

$$\partial\zeta/\partial\psi_1^* = \sqrt{B_1^2 + 4A\sqrt{\zeta} - 2Aa\zeta} \tag{36}$$

and

$$\psi_1^* = \frac{1}{aA}(B_1 - \sqrt{B_1^2 + 4A\sqrt{\zeta} - 2Aa\zeta}\,) + \sqrt{\frac{2}{A}}\frac{1}{a^{3/2}}\left[\arcsin\frac{1}{\sqrt{1 + (B_1^2/2A)a}} - \arcsin\frac{1 - a\sqrt{\zeta}}{\sqrt{1 + (B_1^2/2A)a}}\right] \tag{37}$$

In order to join the *internal* to the *external* solution, the following method is proposed: The *external* solution is assumed to hold up to a value of ψ_1^* which is close to the one $(\psi_1^*)_f$ for which the velocity profile $(z_e, \psi_1^*/2\sqrt{\xi_1})$ has a point of inflection and corresponding to a value of ζ (denoted here by ζ_f) which is small enough with respect to $z_0/2$ so as to permit the replacement of Eq. (33) by Eq. (34). The values of B_1 and of a are then to be determined. This determination requires that, for $\zeta = \zeta_f$, the following conditions be satisfied simultaneously: (a) that ψ_1^*, obtained from Eq. (37), be equal to $(\psi_1^*)_f$, corresponding to the value $\zeta = \zeta_f$, given by the *external* solution; and (b) that $(\partial\zeta/\partial\psi_1^*)_{\zeta=\zeta_f}$, calculated from Eq. (36), be equal to the analogous value given by the *external* solution.

Since it seems likely that the complete profile of z (or of ζ) for every ξ_1 would have only one point of inflection, the point of inflection related to Eq. (34), given by $\sqrt{\zeta} = 1/a$, will be associated with a value of $\psi_1^* \geq (\psi_1^*)_f$ or, at least, it will be close to $(\psi_1^*)_f$. It is hardly necessary to remark that the method described here cannot be applied to cross sections of the boundary layer which are too close to the one at which separation occurs, because for these sections ζ is everywhere too large and substitution of Eq. (34) for Eq. (33) is no longer allowable.

(*B-4*) *Separation Point of the Stream*

The location of the cross section at which separation occurs can be obtained by following a method analogous to that suggested earlier by von Kármán. In fact, such a section is always defined by the condition that $B_1 = 0$, since it is true that

$$\frac{\partial\zeta}{\partial\psi_1^*} = \frac{1}{z_0}\frac{V_i^2}{\bar{U}_e^2}\frac{2}{(V_i^2/\bar{U}_e^2) - (U^2/\bar{U}_e^2)}\frac{\rho_a}{\bar{\rho}}\frac{U_a^2}{\bar{U}_e^2}\frac{\partial}{\partial\eta}\frac{\bar{U}}{U_a}$$

at such a point of separation.

In the case of supersonic flow, however, it should be pointed out that the demarcation of the separation point, evolved with aid of the same assumptions upon which the theory of the boundary layer is based, is somewhat less correct than in the case of subsonic flow. In the latter case, in fact, separation ameliorates the causes that produce it, because of the fact that, when the divergence of the stream tube flowing along the wall decreases, the component of grad p in the direction of motion decreases as well. In the former case, however, separation increases the convergence of the tube, thus

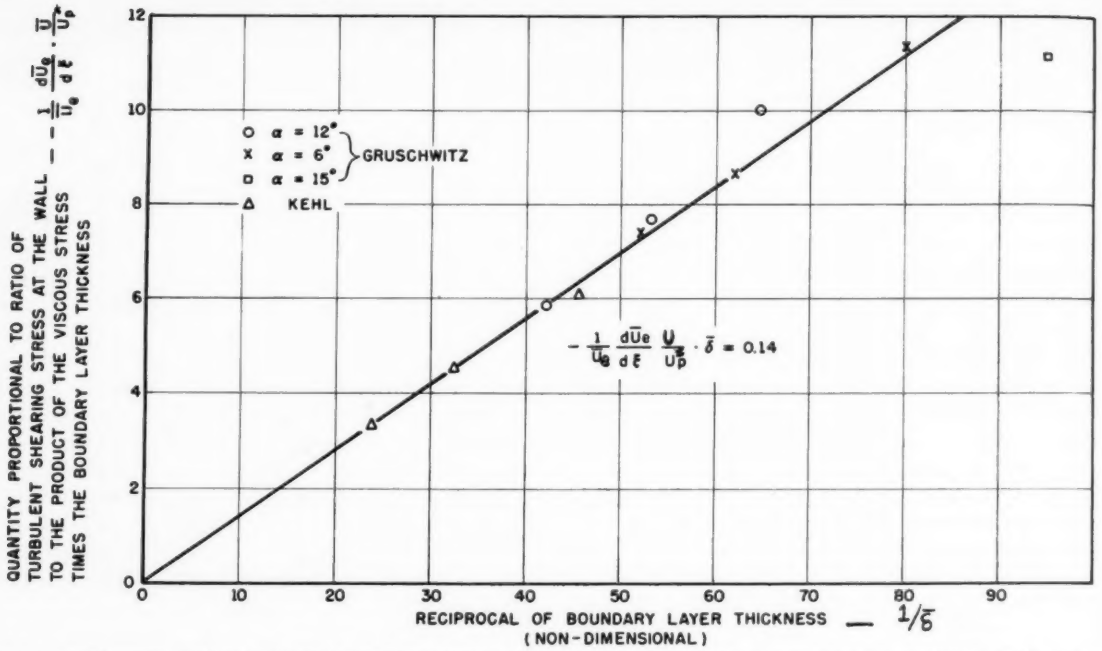

FIG. 1. Experimental verification that the turbulent shearing stress is proportional to the viscous stress and elicitation of the value of c in Eq. (26).

rendering matters worse. This state of affairs gives rise to an inconsistency, and in order to eliminate it the flow must become *subsonic;* however, this alteration of the flow cannot happen without the generation of a shock wave. This wave must start in front of the separation point (which would be determined by applying the present theory) in order that the stream may still have the kinetic energy necessary to overcome the rapid increase of pressure corresponding to the formation of the shock wave. On the other hand, one must take into consideration the fact that the increase in pressure is felt upstream of the wave through the subsonic boundary layer.

For this reason, the actual separation point will be shifted upstream of that which is predicted by the calculations based on the foregoing assumptions.

(*B-5*) *Experimental Verification of Eq.* (*26*) *and Determination of c*

Before showing how the formulas obtained above may be applied to the determination of the motion within the boundary layer, it is advisable to ascertain whether the experimental tests confirm Eq. (26). As a consequence of such verification, the value of c will be deduced. With this desirable objective in mind, one should remember that in establishing Eq. (26) no assumption regarding the compressibility of the fluid was made; it is therefore reasonable to expect that c does not depend on this property of the flow. In order to check the above equations, one may thus refer to the results obtained for streams having a very small Mach Number. In view of this likelihood of slight compressibility effect on c, the experiments of Gruschwitz[6] and Kehl[7] are selected for analysis.

The values of $-(1/\bar{U}_e)\ (d\bar{U}_e/d\xi)\ (\bar{U}/U_p^*)$, calculated on the basis of the above-mentioned experimental results, are shown in Fig. 1 as a function of the corresponding values of $1/\bar{\delta}$ derived from these experiments.† It clearly appears that the experimental points lie close to the straight line.

$$\frac{1}{\bar{U}_e}\frac{d\bar{U}_e}{d\zeta}\frac{\bar{U}}{U_p^*}+0.14\,\frac{1}{\bar{\delta}}=0$$

so that Eq. (26) is sufficiently satisfied, and the constant is determined as $c = 0.14$.‡

(*B-6*) *Approximate Evaluation a priori of* $\bar{\delta}$ *and of* U_p^*

In order to apply Eq. (28) to the determination of the motion in the boundary layer, it is necessary to know *a priori* the friction velocity U_p^* for the various values of ξ, as well as the thickness $\bar{\delta}$ of the layer. It would appear at first glance that these two quantities are actually only known *a posteriori.*

An approximate value *a priori* for U_p^* is now obtained by regarding the friction coefficient c_f as constant

† The length of the experimental wing is taken as the reference length, L, for the experiments by Gruschwitz; while for those by Kehl, referring to the rectangular channel designated as AK III, the value $L = 172.5$ cm. has been assumed.

‡ The detailed steps in the calculation of these data, as well as those presented in subsequent tables, are contained in an extended version of this investigation which is available from The Johns Hopkins University, Applied Physics Laboratory as reference 8

over the whole portion of the wing along which the flow is certainly turbulent and where the further restriction is enforced that such a region be not too close to that cross section where separation occurs. The coefficient of friction is obtained from the formula that is applicable for a flat plate ($d\bar{p}/d\xi = 0$). The Reynolds Number employed in the formula is taken as the one corresponding to the final section of this portion of the wing, and the value of the velocity U_{me} is selected to lie intermediately between those related to the first and last sections of the portion of wing now being considered.

As far as the variation of the thickness δ of the layer is concerned (considering first the case of an incompressible fluid), one obtains, from the equation

$$\frac{\tau_p}{\rho \bar{U}_e^2} = \frac{1}{\bar{U}_e}\frac{d\bar{U}_e}{dx}(\delta^* + 2\delta^{**}) + \frac{d\delta^{**}}{dx} \qquad (38)$$

wherein $\delta^* = c_1\delta$ and $\delta^{**} = c_2\delta$, that

$$\frac{1}{2}c_f = \frac{1}{\bar{U}_e}\frac{d\bar{U}_e}{dx}\delta(c_1 + 2c_2) + c_2\frac{d\delta}{dx} + \delta\frac{dc_2}{dx} \qquad (38')$$

Since $dc_2/dx = 0$ if p is constant, let

$$dc_2/dx = -b(1/\bar{U}_e)(d\bar{U}_e/dx)$$

and hence write

$$\frac{d\delta}{dx} = \frac{1}{2c_2}c_f - \frac{1}{\bar{U}_e}\frac{d\bar{U}_e}{dx}\frac{c_1 + 2c_2 - b}{c_2}\delta \qquad (38'')$$

Furthermore, assuming that it is permissible to consider c_f/c_2, as well as the coefficient of $(1/\bar{U}_e)(d\bar{U}_e/dx)$, as constant (or at least by assuming it is permissible to substitute for the variable values a constant mean value), it follows that

$$\delta = a_1 x - a_2\int_0^x \frac{\delta}{\bar{U}_e}\frac{d\bar{U}_e}{dx}dx \cong a_1 x - a_2 a_1 \times \int_0^x \frac{x}{\bar{U}_e}\frac{d\bar{U}_e}{dx}dx \qquad (39)$$

From the above-mentioned experiments by Gruschwitz and by Kehl it is possible to deduce the values of c_1, c_2, and b and, hence, of $(c_1 + 2c_2 - b)/c_2$. The variation of the values of the last parameter is not small, since its value ranges between 1.32 and 2.158; however, this variation is of little consequence as long as the second term in the second member of Eq. (38″) is sufficiently small in comparison with the first.

Thus it is justifiable to take for this coefficient a mean value deduced from those presented above [for which purpose the value 1.7 is selected to represent $(c_1 + 2c_2 - b)/c_2$]. Furthermore, because of the fact that, for the case of flow along a flat plate, the term $d\bar{U}_e/dx$ vanishes, one has simply $\delta = 0.38\sqrt{c_f}\,x$, so it is proposed to take

$$\delta = 0.38\sqrt{c_f}\left(x - 1.7\int_0^x \frac{x}{\bar{U}_e}\frac{d\bar{U}_e}{dx}dx\right) \qquad (39')$$

as a first approximation to the evaluation of δ.

If the values of U_p^* and of δ obtained in a first approximation by means of the above-suggested methods are compared with those obtained from the experiments of Gruschwitz and of Kehl, it appears that, in spite of the crude processes employed in obtaining the formulas that yield U_p^* and δ, the values deduced are in satisfactory agreement with the experimental ones; thus it is apparent that these methods may be applied to advantage despite their inelegance.

As a typical example one may cite here a comparison between the calculated and the experimental values that apply in the case of the experiments by Gruschwitz for the wing with 12° angle of attack and for a cross-section location having an abscissa $\xi = 0.587$.

It is found that $(U_p^*)_{\text{calc.}} = 177$ cm. per sec., while $(U_p^*)_{\text{exp.}} = 180$ cm. per sec.; and $(\delta)_{\text{calc.}} = 0.626$ cm., while $(\delta)_{\text{exp.}} = 0.62$ cm. If the stream is compressible, Eq. (38) is replaced[9] by

$$\frac{d\delta^{**}}{dx} = \frac{1}{\bar{\rho}\bar{U}_e^2}\frac{d}{dx}(\bar{\rho}_e\bar{U}_e^2)\delta^{**} + \frac{1}{\bar{U}_e}\frac{d\bar{U}_e}{dx}\delta^* = \frac{1}{2}c_f \qquad (40)$$

Letting $\delta^* = c_1\delta$ and $\delta^{**} = c_2\delta$ and noting that

$$\frac{dc_2}{dx} = -b\frac{1}{\bar{\rho}_e\bar{U}_e^2}\frac{d}{dx}(\bar{\rho}_e\bar{U}_e^2)$$

one obtains (by following the same procedure as in the case for which the Mach Number is zero)

$$\delta = a\sqrt{c_f}\left[1 - a_1\int_0^x \frac{1}{\bar{U}_e}\frac{d\bar{U}_e}{dx}x\,dx + a_2\int_0^x \frac{1}{\bar{U}_e}\frac{d\bar{U}_e}{dx}xM^2\,dx\right] \qquad (40')$$

wherein a is a function of the Mach Number, which may be given the value derived in the first report[1] of this series. Experimental data are lacking which would enable one to determine approximately the values of the coefficients a_1 and a_2 analogously to what has just been done in the case of an incompressible fluid. It is proposed, therefore, for the time being, to use Eq. (39′) in the case of compressible fluid flows. After having performed the calculations, one can always check the values of δ and U_p^* to see whether they are sufficiently good approximations.

(C) Numerical Application and Variation of the Drag Coefficient Along the Boundary Layer

(C-1) *Numerical Application; Case of an Incompressible Fluid*

In order to compare the numerical results that are derived upon the basis of theory just expounded with those obtained from experiment, a detailed application will now be made for the conditions under which the

TABLE 1

Computation of the Velocity Parameter z_1 As a Function of the Integrated Thickness Parameter ξ_1^*—Case of Incompressible Flow

ξ	$= 0.396$	0.484	0.587	0.676	0.780	0.872
$\frac{\bar{U}_e}{U_a}$	$= 1.51$	1.41	1.31	1.21	1.14	1.06
$\frac{d\bar{U}_e}{d\xi}$	$= -3{,}950$ cm. per sec.	$-3{,}430$	$-3{,}340$	$-2{,}800$	$-2{,}530$	$-2{,}100$
δ	$= 0.80 \times 10^{-2}$	1.15×10^{-2}	1.55×10^{-2}	1.88×10^{-2}	2.37×10^{-2}	2.95×10^{-2}
$\frac{d\xi_1}{d\xi}$	$= 1.83 \times 10^{-2}$	2.29×10^{-2}	2.66×10^{-2}	2.76×10^{-2}	2.08×10^{-2}	3.31×10^{-2}
ξ_1	$= 0.0096 \times 10^{-2}$	0.1928×10^{-2}	0.444×10^{-2}	0.687×10^{-2}	0.991×10^{-2}	1.286×10^{-2}
$\frac{U_1}{U_a}$	$= 1.182$	0.885	0.629	0.570	0.472	0.424
$10^2\xi_1$	$= \xi_1^* = 0.0096$	0.1928	0.444	0.687	0.991	1.286
z_1	$= 0.883$	1.205	1.321	1.139	1.076	0.964

experiments conducted by Gruschwitz were carried out. In particular, the test speed is low, so that the numerical application applies in this instance to the case of an incompressible fluid. The velocity distribution assumed to exist just external to the boundary layer is taken to be identical with that which Gruschwitz determined to exist around the airfoil he tested, when it was at a 12° angle of attack. Then, for $\rho_a = \rho_e$, Eq. (21) yields

$$d\xi_1/d\xi = \delta\,(\bar{U}_e^2/U_a^2)$$

The values of $\bar{U}_e/U_a$, ξ, $d\bar{U}_e/d\xi$, and δ, taken as the starting point for the calculations, are given in Table 1. The values of $d\xi_1/d\xi$ [obtained from Eq. (21)], of ξ_1 (deduced from the preceding quantities by graphical integration), of $U_1/U_a = (\bar{U}/U_a)_{\psi_1^*=0}$ [evaluated from Eq. (26) by taking $c = 0.14$ and $U_p^* = 177$ cm. per sec. as determined in Section (B-6)], and, lastly, of $z_1 = (\bar{U}_e^2/U_a^2) - (U_1^2/U_a^2)$ are also given in the same table.

Because of the difficulty encountered in the determination of a polynomial in ξ_1^* which approximates sufficiently well the function $z_1(\xi_1^*)$ corresponding to the above values at every point of the interval through which ξ_1 varies, the values of z_1 have been represented by a polynomial of third degree just in the first part of the interval only

$$P_3(\xi_1^*) = 0.90 + 2.31\,\xi_1^* - 4.32\,\xi_1^{*2} + 2.13\,\xi_1^{*3} \quad (\text{for } 0 \le \xi_1^* \le 0.69) \tag{41}$$

In order to evaluate z_e in the interval for which ξ_1^* is external to $\xi_1^* = 0.69$, the quantity $z_1(\xi_1^*)$ has been approximated by the function

$$R(\xi_1^*) = \begin{cases} 0.90 + 1.558\,\xi_1^* \\ \qquad (\text{for } 0 \le \xi_1^* \le 0.28) \\ 1.442 - 0.379\,\xi_1^* \\ \qquad (\text{for } 0.28 \le \xi_1^* \le 1.286) \end{cases} \tag{42}$$

The broken line defined by Eq. (42) and the cubic defined by Eq. (41) are plotted in Fig. 2, on which the

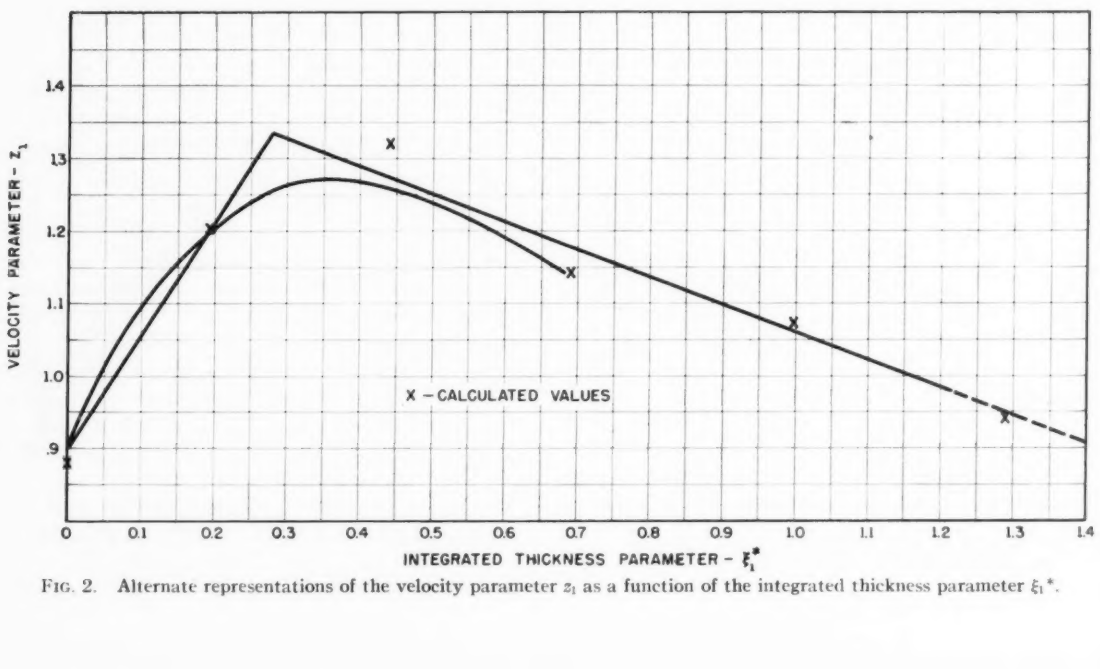

FIG. 2. Alternate representations of the velocity parameter z_1 as a function of the integrated thickness parameter ξ_1^*.

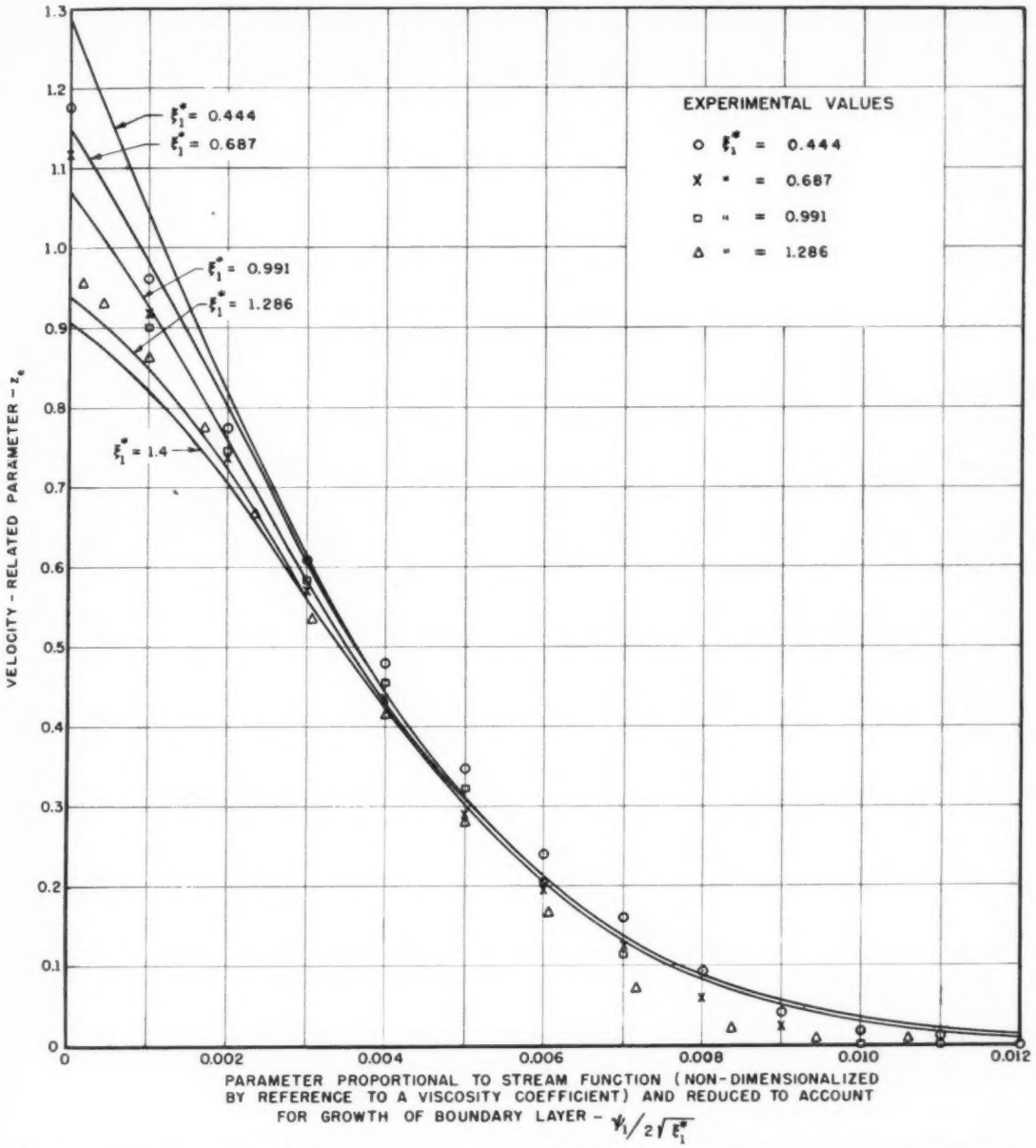

FIG. 3. Variation of the reduced stream function upon traverse of the boundary layer as related to a velocity parameter.

points corresponding to the calculated values of z_1 are marked by crosses.

Let $z_1 = P_2(\xi_1^*)$. One obtains, from Eq. (30),

$$z_e\left(\frac{\psi_1^*}{2\sqrt{\xi_1^*}}\right) = \sum_{r=0}^{3} B_r \xi_1^{*2} G_r\left(\frac{\psi_1^*}{2\sqrt{\xi_1^*}}\right) \qquad (30')$$

wherein the constant h_2 contained in the expression for ψ_1^* includes the factor 10^{-2} which arises upon substitution of ξ_1^* for ξ_1 in Eq. (30) itself. Furthermore, $G_n(x) = 2^{2n} n!(i^{2n}\ \text{erfc}\ x)$. The functions $i^{2n}\ \text{erfc}\ x$ have already been partially tabulated by Hartree.[10] Because the values of such functions for values of x larger than those considered in Hartree's Tables are needed, the tabulation has now been extended by completing the entries up to the value $n = 5$. In carrying out this work, the following recurrence formula is employed:

$$2(n+1)(n+2)\, i^{2n+2}\ \text{erfc}\ x = (1 + 2n + 2x^2) i^n\ \text{erfc}\ x - \frac{i^{n-2}\ \text{erfc}\ x}{2}$$

whence

$$G_{n+1} = \frac{1}{2n+2}(1 + 4n + 2x^2)G_n - \frac{2n}{2n+1} G_{n-1}$$

The functions G_n are given in the Appendix. The profiles corresponding to the locations for which ξ_1^* equals 0.444 and 0.687 are computed by means of Eq. (30′) and are plotted in Fig. 3.

Assuming $z_1(\xi_1^*)$ to be given by Eq. (42), one finds for z_e that

$$z_e\left(\frac{\psi_1^*}{2\sqrt{\xi_1^*}}\right) = 0.90\ \mathrm{erfc}\left(\frac{\psi_1^*}{2\sqrt{\xi_1^*}}\right) + 1.558\xi_1^*\left[4i^2\ \mathrm{erfc}\ \frac{\psi_1^*}{2\sqrt{\xi_1^*}}\right] - (1.558 + 0.379)\times(\xi_1^* - 0.28)\left[4i^2\ \mathrm{erfc}\ \frac{\psi_1^*}{2\sqrt{\xi_1^* - 0.28}}\right] \quad (30'')$$

The profiles corresponding to the locations for which ξ_1^* equals 0.991 and 1.286 are computed by means of Eq. (30″) and are plotted in Fig. 3.

The determination of z_e has also been worked out for $\xi_1^* = 1.4$, corresponding to $\xi = 0.95$, although for this value of ξ no experimental graph of $\bar{U}/U_a$ in terms of y is given. This extra computation has been performed in order to determine the point of separation of the stream.

In Fig. 3 are given the profiles of z_e in terms of $\psi_1^*/2\sqrt{\xi_1^*}$ deduced from the experiments by Gruschwitz. By comparing these results with those obtained from the calculations, one finds that $\sqrt{h_2} = 0.00625$. It appears that the agreement is generally satisfactory within the range of variation of ψ_1 and for all the values of ξ_1^* considered. The fact that the deviation of $(z_e)_{\text{theor.}}$ from the experimental values appears to be greater for the larger values of ψ_1 is due to circumstances already pointed out in Section (B-3), while it should be noticed that an error in the experimental determination of the velocity, even if small, in this region of the boundary layer gives rise to a relatively large error in the determination of z_e. On the other hand, the value of $z_e = 0$ corresponds theoretically to $\psi_1 = \infty$, while, experimentally, $\bar{U} = \bar{U}_e$ at an actually finite distance from the wetted wall. It is worth mentioning that, at a sufficient distance from the wall, the theoretical values of z_e are but slightly different from one another for equal values of $\psi_1^*/2\sqrt{\xi_1^*}$ but for varying ξ_1^*. This tendency to uniformity is also in agreement with the experimental results.

From the profiles of z_e in terms of $\psi_1/2\sqrt{\xi_1^*}$, the velocity diagrams of $\bar{U}/U_a$ in terms of y/L have then been computed.

From the relation $\bar{U}/U_a = \partial\psi_1/\partial\eta$, one gathers that

$$\eta = 2\sqrt{\xi_1^*}\int_0^{\psi_1/2\sqrt{\xi_1^*}} \frac{d(\psi_1/2\sqrt{\xi_1^*})}{\sqrt{z_0 - z_e}} \quad (43)$$

where $z_0 = \bar{U}_e^2/U_a^2$; and, consequently,

$$\eta = \begin{Bmatrix}1.333\\1.658\\1.991\\2.268\\2.366\end{Bmatrix} \int_0^{\psi_1/2\sqrt{\xi_1^*}} \frac{d(\psi_1/2\sqrt{\xi_1^*})}{\sqrt{z_0 - z_e}} \quad \text{for } \xi_1^* = \begin{Bmatrix}0.444\\0.687\\0.991\\1.286\\1.4\end{Bmatrix} \quad \text{or } \xi = \begin{Bmatrix}0.587\\0.676\\0.780\\0.872\\0.95\end{Bmatrix} \quad (43')$$

In the determination of η by means of Eq. (43′) the graph of z_e in terms of $\psi_1/2\sqrt{\xi_1^*}$ has been completed up to $\psi_1 = 0$ by extending the velocity diagram through the laminar sublayer; it has been assumed here that within this layer the variation of the velocity is linear and the slope is equal to that at the value of U_p^* under consideration. This assumption yields simply a linear variation of z_e in terms of $\psi_1/2\sqrt{\xi_1^*}$. On the other hand, since

$$(\partial z_e/\partial\psi_1)_{\psi_1=0} = -2(\partial/\partial\eta)\ (\bar{U}/U_a)$$

while

$$\frac{\tau_p}{\rho U_a^2} = \frac{\mu}{\rho U_a^2}\left(\frac{\partial U}{\partial y}\right)_{y=0} = \frac{1}{R_e}\left(\frac{\partial}{\partial\eta}\frac{\bar{U}}{U_a}\right)_{\eta=0} = \frac{U_p^{*2}}{U_a^2}$$

one infers that

$$[(\partial/\partial\eta)\ (\bar{U}/U_a)]_{\eta=0} = R_e\ (U_p^{*2}/U_a^2)$$

wherein $R_e = U_aL/\nu$ is the Reynolds Number of the asymptotic (at an infinite distance) stream. One may conclude thus that

$$(\partial z_e/\partial\psi_1)_{\psi_1=0} = -2R_e\ (U_p^{*2}/U_a^2)$$

or

$$D = \left[\frac{\partial z_e}{\partial(\psi_1/2\sqrt{\xi_1^*})}\right]_{\psi_1=0} = -2R_e\frac{U_p^{*2}}{U_a^2}2\sqrt{\xi_1^*}$$

and, hence,

$$D = -2\left[\frac{3{,}080\ (40)}{0.15}\right]\left(\frac{177^2}{3{,}080^2}\right)2\sqrt{\xi_1^*} = -10{,}640\sqrt{\xi_1^*}$$

This expression allows the extension, mentioned above, of the velocity profile to the "inside" of the laminar sublayer.

In order to carry out the integration required in the second member of Eq. (43′), the interval of integration is subdivided into two parts, the first corresponding to the laminar sublayer and the second to the turbulent layer. For the former it is true that $z = z_0 - D\ (\psi_1 \div 2\sqrt{\xi_1^*})$, while for the latter $z = z_e$ varies accordingly to the law deduced above. The results of the calculations are given in the graphs of Fig. 4, upon which the points corresponding to the experimental results are also plotted. For the section at $\xi_1^* = 1.4$ it is found,

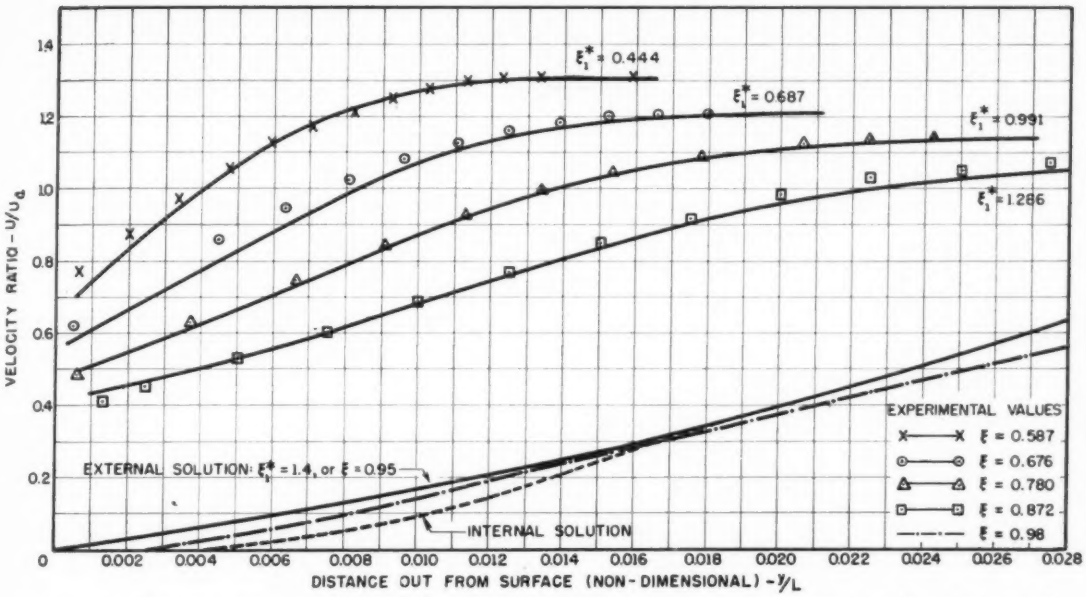

FIG. 4. Comparison of theoretical and experimental velocity profiles at various stations along airfoil (Gruschwitz data).

by extrapolation of the linear profile depicted in Fig. 2, that $z_1 = 0.9115$ there.

On the other hand, for the value $\xi = 0.95$, corresponding to this value of ξ_1^*, the experimental results obtained by Gruschwitz show that $\bar{U}_e/U_a = 0.95$; and, consequently, it may be assumed that for this section $z_0 = z_1$ closely. From the form of the profile $(\bar{U}/U_a, \eta)$ for $\xi_1^* = 1.4$, it appears that this cross section is close to the one where separation occurs. The determination of the *internal* solution for this section is completed, therefore, by following the procedure suggested in Section (B-3).

Taking into account Eqs. (36) and (43), one obtains

$$\eta = \frac{1}{\sqrt{2}}\int_0^{\psi_1} \frac{d\psi_1}{\sqrt{\zeta}} = \frac{0.0125}{\sqrt{2}}\,\frac{1}{\sqrt{2Aa}} \times \left[\arcsin \frac{2A}{\sqrt{4A^2 + 2AaB_1^2}} - \arcsin \frac{2A(1 - a\sqrt{\zeta})}{\sqrt{4A^2 + 2AaB_1^2}}\right] \quad (43'')$$

From the profiles determined by Gruschwitz, the value of A is derived as

$$A = -\frac{z_0^{1/2}}{2^{3/2}}\frac{\partial z_0}{\partial \xi_1^*} = -\frac{2}{2^{3/2}}\left(\frac{\bar{U}_e}{U_a}\right)^2 \frac{\partial}{\partial \xi}\left(\frac{\bar{U}_e}{U_a}\right)\frac{d\xi}{d\xi_1^*} = \left(\frac{0.9155}{1.41}\right)\left(\frac{0.55}{3.31}\right) = 0.107$$

For the point of connection between the *external* and the *internal* solution (see the profile of Fig. 4), the one for which the coordinates are $\bar{U}/U_a = 0.4$, $\eta = 0.02$ is selected; this location is somewhat close to the inflection point.

From the same profile one perceives that, at this inflection point, $(d/d\eta)\,(\bar{U}/U_a) = 30.2$, and, since

$$\frac{d\zeta}{d\psi_1^*} = \frac{d\zeta}{d\eta}\frac{d\eta}{d\psi_1}\frac{d\psi_1}{d\psi_1^*} = 0.00625\,\frac{d}{d\eta}\frac{\bar{U}}{U_a}$$

it results that $\sqrt{B_1^2 + 4A}\,\sqrt{\zeta_i} - 2Aa\zeta_1 = (0.00625) \times (30.2) = 0.189$ or $a = 4.92 - 58.5B_1^2$; while, from Eq. (43''), we obtain

$$0.02 = \frac{0.00625}{\sqrt{0.526 - 6.26B_1^2}}\left(\arcsin \frac{1}{\sqrt{1 + 22.95B_1^2 - 273B_1^4}} - \arcsin \frac{-0.39 + 16.55B_1^2}{\sqrt{1 + 22.95B_1^2 - 273B_1^4}}\right)$$

Now the function consisting of the second member of this equation decreases as B_1 increases, and since, for $B_1 = 0$, its value is already equal to 0.01715, it is obvious that the junction is impossible. It therefore appears evident that separation has already taken place by the time this cross section is reached. Then, if it is assumed that $B_1 = 0$ and it is admitted that $\bar{U}/U_a$ vanishes for $\eta = 0.02 - 0.0175 \doteq 0.00285$, the value of a is obtained as 4.92. By use of this value of a and by means of Eq. (43''), values in Table 2 are found.

The graph describing this internal solution is shown as a dotted line in Fig. 4, on which the experimental profile obtained for $\xi = 0.98$ is also drawn (dash-dot

TABLE 2
Velocity Distribution for Internal Region of Boundary Layer

$\bar{U}/U_a$ = 0.4	0.3	0.2	0.1	0.05	0
η = 0.2	0.01675	0.01382	0.01029	0.00802	0

TABLE 3
Computation of the Velocity Parameter z_1 As a Function of the Integrated Thickness Parameter, ξ_1^*—Case of Compressible Flow

ξ = 0.396	0.484	0.587	0.676	0.780
δ = 1.048×10^{-2}	1.505×10^{-2}	2.03×10^{-2}	2.46×10^{-2}	3.86×10^{-2}
$\frac{\bar{U}_e}{U_a}$ = 1.51	1.41	1.31	1.21	1.14
$\frac{\rho_e}{\rho_a}$ = 0.1175	0.2298	0.379	0.556	0.696
$\frac{d\xi_1}{d\xi}$ = 0.033×10^{-2}	0.158×10^{-2}	0.498×10^{-2}	1.12×10^{-2}	2.43×10^{-2}
ξ_1^* = 0	0.0077	0.0384	0.111	0.292
$\frac{U_1}{\bar{U}_e}$ = 0.598	0.481	0.365	0.36	0.254
$\frac{\bar{U}_e^2}{V_l^2}$ = 0.707	0.617	0.532	0.455	0.404
z_1 = 0.606	0.557	0.495	0.42	0.388

line). The qualitative and the quantitative agreement between the two curves appears to be excellent.

(C-2-1) *Numerical Application: Case of a Compressible Fluid*

In order to show how the methods described in the preceding Sections may be applied to the case of a compressible fluid for the case of a supersonic velocity external to the layer, a fluid flow having a Mach Number at an infinite distance upstream equal to 1.5 (M_a = 1.5) is now investigated. It is assumed that the stream attains the same values of $\bar{U}_e/U_a$ at the same locations, ξ, as considered in Section (C-1), for the region comprised between the velocity just external to the layer and the velocity at infinity.

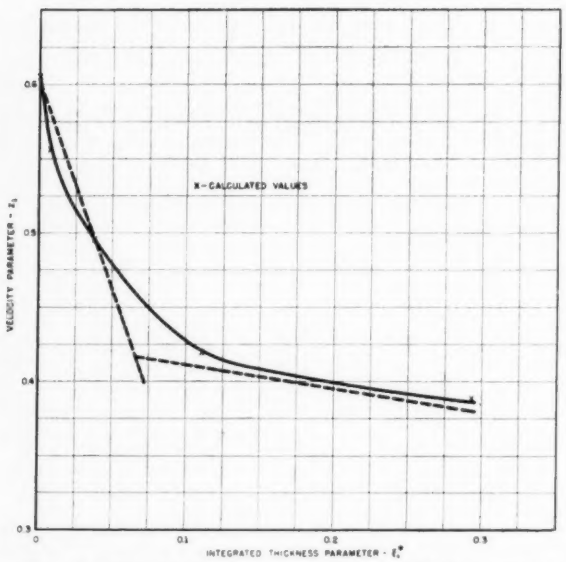

FIG. 5. Calculated curve and two straight-line segment representation of velocity parameter z_1 as a function of the integrated thickness parameter ξ_1^*.

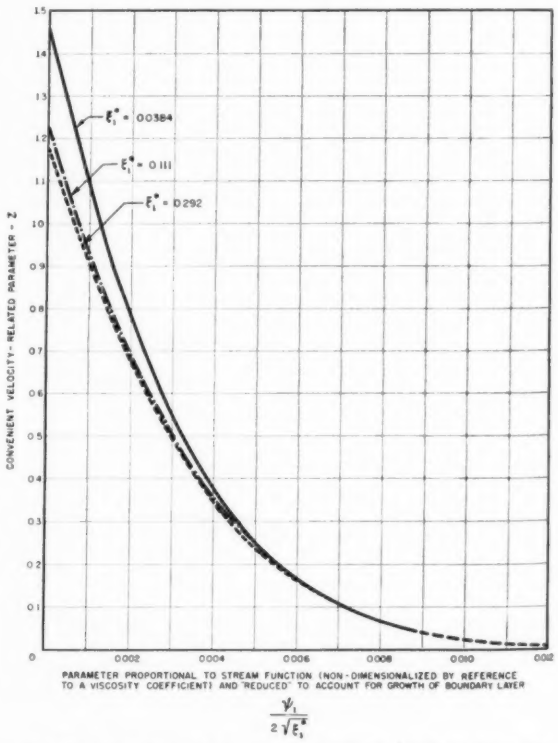

FIG. 6. Variation of the reduced stream function upon traverse of the boundary layer as related to a convenient velocity parameter.

In order to calculate the approximate values of δ by means of Eq. (40′), the following values are employed: $a = 0.5$, $a_1 = 1.7$, and $a_2 = 0$. The same value as employed in Section (C-1) is assumed for c_f. The value of a is the same as that obtained in the first report[1] of this series, at $M_a = 1.5$, for the case of turbulent flow along a flat plate.

The values of $\bar{\delta}$ in the case now considered are obtained at once from those calculated in Section (C-1) just through multiplication by $0.56/0.38 = 1.31$. Because

$$\frac{\bar{\rho}_e}{\rho_a} = \left[1 + \frac{\gamma - 1}{2} M_a^2 \left(1 - \frac{\bar{U}_e^2}{U_a^2}\right)\right]^{1/(\gamma-1)}$$

the values of $d\xi_1/d\xi$ may be easily obtained. The results of the calculations are listed in Table 3, where the values of $\xi_1^* = 10^2\xi_1$; U_1/U_a (assuming $U_p^*/U_a = 177/3{,}080 = 0.0575$, as in the previously considered case of an incompressible fluid);

$$\frac{\bar{U}_e^2}{V_l^2} = \frac{U_e^2}{U_a^2} \frac{1}{1 + [2/(\gamma - 1)]\,(1/M_a^2)}$$

and

$$z_1 = \frac{\bar{U}_e^2}{V_l^2} \frac{1 - (U_1^2/\bar{U}_e^2)}{1 - (U_1^2/\bar{U}_e^2)\,(\bar{U}_e^2/V_l^2)}$$

are also given.

The profile showing the variation of z_1 with respect to ξ_1^* is given in Fig. 5, where the broken line with which $z_1(\xi_1^*)$ was approximated (used in the determination of z_e) is also given. This broken line describes the function

$$L(\xi_1^*) = \begin{cases} 0.600 - 2.864\xi_1^* & (\text{for } 0 \leq \xi_1^* \leq 0.0636) \\ 0.428 - 0.166\xi_1^* & (\text{for } 0.0636 \leq \xi_1^* \leq 0.292) \end{cases}$$

The reduced velocity z_e then takes on the following form:

$$z_e = 0.600 \operatorname{erfc} \frac{\psi_1^*}{2\sqrt{\xi_1^*}} - 2.864\xi_1^* \left[4i^2 \operatorname{erfc} \frac{\psi_1^*}{2\sqrt{\xi_1^*}}\right] \quad (\text{for } 0 \leq \xi_1^* \leq 0.0636)$$

$$z_e = 0.600 \operatorname{erfc} \frac{\psi_1^*}{2\sqrt{\xi_1^*}} - 2.864\xi_1^* \left[4i^2 \operatorname{erfc} \frac{\psi_1^*}{2\sqrt{\xi_1^*}}\right] + (2.8645 - 0.1657)\,(\xi_1^* - 0.0636)\left[4i^2 \operatorname{erfc} \frac{\psi_1^*}{2\sqrt{\xi_1^* - 0.0636}}\right] \quad (\text{for } 0.0636 \leq \xi_1^* \leq 0.292)$$

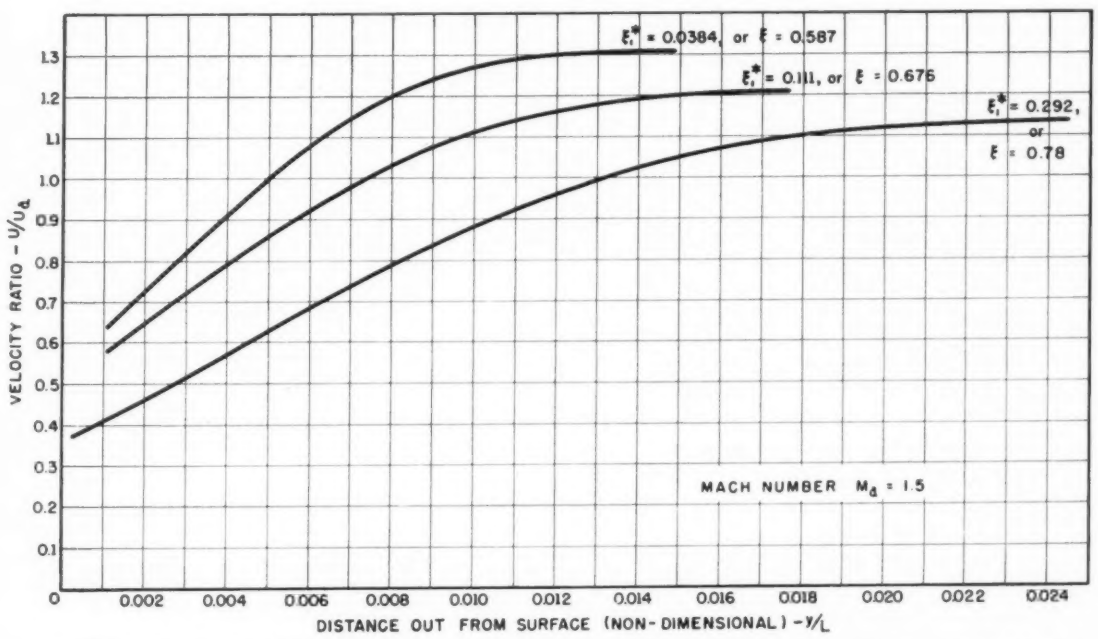

FIG. 7. Supersonic flow velocity profiles calculated for three of the same locations on airfoil as previously computed for the incompressible case.

The calculation of z_e for the different values of the parameter $\psi_1^*/2\sqrt{\xi_1^*}$ has been carried out for $\xi_1^* = 0.0384$, 0.111, and 0.292. Starting from these values of z_e, the corresponding values of $\bar{U}/U_a$ will now be calculated. Let

$$Z = (\bar{U}_e^2/U_a^2) - \bar{U}^2/U_a^2$$

then one obtains

$$Z = (V_l^2/U_a^2)\,[1 - (\bar{U}_e^2/V_l^2)]\,[z_e/(1 - z_e)] \tag{44}$$

and, consequently, upon noting that $V_l^2/U_a^2 = 3.22$, one has

$$Z = \left.\begin{matrix}1.51\\1.755\\1.92\end{matrix}\right\} \quad z_e/(1 - z_e) \qquad \text{for} \qquad \xi_1^* = \begin{cases}0.0384\\0.111\\0.292\end{cases} \tag{45}$$

The graphs of Fig. 6 depict the final result of calculating Z in terms of $\psi_1/2\sqrt{\xi_1^*} = 0.00625\,(\psi_1^*/2\sqrt{\xi_1^*})$, where the same value of h_2 is employed as that derived in Section (C-1).

Letting $Z_0 = \bar{U}_e^2/U_a^2$, one has

$$\eta = 2\sqrt{\xi_1^*}\int_0^{\psi_1/2\sqrt{\xi_1^*}} \frac{1}{\frac{\bar{\rho}}{\rho_a}\frac{\bar{U}}{U_a}}\, d\left(\frac{\psi_1}{2\sqrt{\xi_1^*}}\right) = 2\sqrt{\xi_1^*}\int_0^{\psi_1/2\sqrt{\xi_1^*}} \frac{\rho_a}{\bar{\rho}_e}\frac{1}{1 - z}\frac{1}{\sqrt{Z_0 - Z}}\, d\left(\frac{\psi_1}{2\sqrt{\xi_1^*}}\right) =$$

$$\left.\begin{matrix}1.035\\1.2\\1.55\end{matrix}\right\} \int_0^{\psi_1/2\sqrt{\xi_1^*}} \frac{1}{1 - z}\frac{1}{\sqrt{Z_0 - Z}}\, d\left(\frac{\psi_1}{2\sqrt{\xi_1^*}}\right) \qquad \text{for } \xi_1^* = \begin{cases}0.0384\\0.111\\0.292\end{cases} \tag{46}$$

The evaluation of η from Eq. (46) is accomplished by following the same procedure as described in the preceding Section. The slope of the straight-line portion on the graph of Z versus $\psi_1/2\sqrt{\xi_1^*}$, which correspond to the laminar sublayer, is now

$$(\partial Z/\partial\psi_1)_{\psi_1=0} = -2(\rho_a/\bar{\rho}_e)\,(\bar{\rho}_e/\bar{\rho}_p)^2\,R_p\,(U_p^{*2}/U_a^2)$$

and since

$$(\bar{\rho}_e/\rho_p)^2 = 1/[1 - (\bar{U}_e^2/V_l^2)]^2$$

and

$$R_p = LU_a/\nu_p = R_a\,(\bar{\rho}_e/\rho_a)\,(\mu_a/\bar{\mu}_e)\,(\nu_e/\nu_p)$$

while

$$\mu_a/\bar{\mu}_e = (T_a/T_e)^n = \left\{1 + 0.2M_a^2\left[1 - \left(\frac{\bar{U}_e^2}{U_a^2}\right)\right]\right\}^{-n}$$

and

$$\nu_e/\nu_p = [1 - (\bar{U}_e^2/V_l^2)]^{1+n}$$

it is found that

$$\left[\frac{\partial Z}{\partial\left(\frac{\psi_1}{2\sqrt{\xi_1^*}}\right)}\right]_{\psi_1=0} = -(2)2\sqrt{\xi_1^*}R_a\frac{U_p^{*2}}{U_a^2}\left\{\frac{1}{\left(1 - \frac{\bar{U}_e^2}{V_l^2}\right)^2}\frac{1}{\left[1 + 0.2M_a^2\left(1 - \frac{\bar{U}_e^2}{U_a^2}\right)\right]^n}\left(1 - \frac{\bar{U}_e^2}{V_l^2}\right)^{1+n}\right\}$$

It appears from the form of this expression that the slope of this portion of the curve is obtained from that calculated in the preceding Section, multiplied by the term standing between the brackets. If this adjusting term is denoted by the symbol E, then, for $\xi_1^* = 0.0384$:

$$E = \left[\frac{1}{(1 - 0.532)^2}\right]\frac{1}{1 + (0.2)2.25(1 - 1.716)^{0.75}}\,(1 - 0.532)^{1.75} = 1.62$$

for $\xi_1^* = 0.111$:

$$E = \left[\frac{1}{(1 - 0.455)^2}\right]\frac{1}{1 + (0.2)2.25(1 - 1.465)^{0.75}}\,(1 - 0.455)^{1.75} = 1.39$$

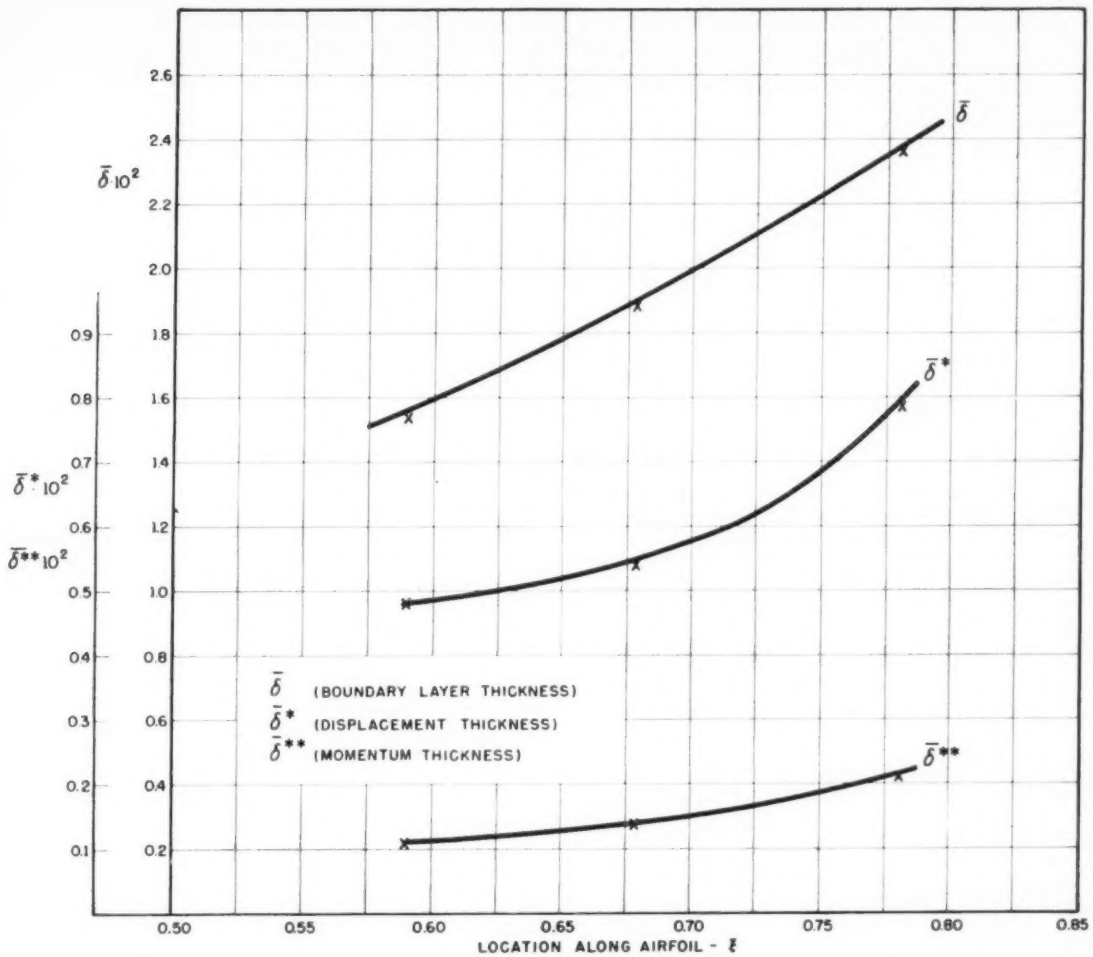

FIG. 8. Theoretical variation along airfoil of boundary-layer thickness parameters for the case of compressible ($M_a = 1.5$) flow.

for $\xi_1^* = 0.292$:

$$E = \left[\frac{1}{(1 - 0.404)^2}\right] \frac{1}{1 + (0.2)2.25(1 - 1.3)^{0.75}} (1 - 0.404)^{1.75} = 1.27$$

where n has been assumed to be equal to 0.75.

The profiles giving the law of variation of $\bar{U}/U_a$ in terms of η, calculated from Eq. (46), are presented in Fig. 7. From these graphs it appears that the value of $\bar{\delta}$ assumed *a priori* for evaluating ξ_1, as well as for determining Z_1, is somewhat larger than that resulting *a posteriori* from the above calculation. The magnitude of $\bar{\delta}$ evinced in Fig. 8 is practically equal to that obtained in the case of an incompressible fluid; this agreement justifies the statement made at the end of Section (B-6).

(C-2-2) *Drag Law*

The graphs presenting $\bar{U}/U_a$ versus η and the values of $\bar{\rho}/\rho_a$ calculated in the preceding Section allow us to determine δ^* and δ^{**}. By graphical integration it is found that, for $\xi_1^* = 0.0384$:

$$\frac{\delta^*}{\bar{\delta}} = 0.31; \quad \frac{\delta^{**}}{\bar{\delta}} = 0.0718; \quad \bar{\delta} = 1.55 \times 10^{-2}; \quad \bar{\delta}^* = 0.481 \times 10^{-2}; \quad \bar{\delta}^{**} = 0.1114 \times 10^{-2}$$

for $\xi_1^* = 0.111$:

$$\frac{\delta^*}{\delta} = 0.285; \quad \frac{\delta^{**}}{\delta} = 0.0775; \quad \bar{\delta} = 1.88 \times 10^{-2}; \quad \bar{\delta}^* = 0.536 \times 10^{-2}; \quad \bar{\delta}^{**} = 0.1459 \times 10^{-2}$$

for $\xi_1^* = 0.292$:

$$\frac{\delta^*}{\delta} = 0.3325; \quad \frac{\delta^{**}}{\delta} = 0.091; \quad \bar{\delta} = 2.37 \times 10^{-2}; \quad \bar{\delta}^* = 0.789 \times 10^{-2}; \quad \bar{\delta}^{**} = 0.216 \times 10^{-2}$$

The values of $\bar{\delta}$, $\bar{\delta}^*$, and $\bar{\delta}^{**}$ in terms of ξ are presented in the plots of Fig. 8. From these diagrams one can estimate that, for $\xi = 0.587$:

$$\frac{d\bar{\delta}^{**}}{d\xi} = 0.0023; \quad \text{while } \frac{\bar{\rho}_e \bar{U}_e^2}{\rho_a U_a^2} = 0.65; \quad \frac{d}{d\xi}\left(\frac{\bar{\rho}_e}{\rho_a}\frac{\bar{U}_e^2}{U_a^2}\right) = 2.4; \quad \frac{1}{\bar{U}_e}\frac{d\bar{U}_e}{d\xi} = -0.828$$

for $\xi = 0.676$:

$$\frac{d\bar{\delta}^{**}}{d\xi} = 0.00534; \quad \text{while } \frac{\bar{\rho}_e \bar{U}_e^2}{\rho_a U_a^2} = 0.815; \quad \frac{d}{d\xi}\left(\frac{\bar{\rho}_e}{\rho_a}\frac{\bar{U}_e^2}{U_a^2}\right) = 1.16; \quad \frac{1}{\bar{U}_e}\frac{d\bar{U}_e}{d\xi} = -0.75$$

for $\xi = 0.780$:

$$\frac{d\bar{\delta}^{**}}{d\xi} = 0.00835; \quad \text{while } \frac{\bar{\rho}_e}{\rho_a}\frac{\bar{U}_e^2}{U_a^2} = 0.905; \quad \frac{d}{d\xi}\left(\frac{\bar{\rho}_e}{\rho_a}\frac{\bar{U}_e^2}{U_a^2}\right) = 0.38; \quad \frac{1}{\bar{U}_e}\frac{d\bar{U}_e}{d\xi} = -0.722$$

Appendix

Values of the Functions $G_n(\psi_1^*/2\sqrt{\xi_1^*})$†

$\frac{\psi_1^*}{2\sqrt{\xi_1^*}}$	G_0	G_1	G_2	G_3	G_4	G_5
0	1	1	1	1	1	1
0.05	0.943628	0.8921	0.8591	0.8337	0.8124	0.7940
0.1	0.887537	0.7936	0.7363	0.6933	0.6585	0.6290
0.15	0.832004	0.7040	0.6292	0.5749	0.5321	0.4967
0.2	0.777297	0.6227	0.5362	0.4753	0.4285	0.3907
0.25	0.723674	0.5491	0.4556	0.3922	0.3449	0.3077
0.3	0.671373	0.4828	0.3861	0.3226	0.2764	0.2409
0.35	0.620618	0.4233	0.3263	0.2647	0.2212	0.1884
0.4	0.571608	0.3699	0.2748	0.2165	0.1764	0.1471
0.45	0.524518	0.3223	0.2308	0.1765	0.1402	0.1141
0.5	0.479500	0.2799	0.1934	0.1435	0.1111	0.0884
0.55	0.436677	0.2423	0.1616	0.1164	0.0878	0.0683
0.6	0.396144	0.2090	0.1344	0.0941	0.0692	0.0526
0.65	0.357971	0.1798	0.1116	0.0758	0.0544	0.0404
0.7	0.322199	0.1541	0.0992	0.0609	0.0426	0.0309
0.75	0.288844	0.1316	0.0761	0.0487	0.0332	0.0235
0.8	0.257899	0.1120	0.0625	0.0389	0.0257	0.0176
0.85	0.229332	0.0950	0.0512	0.0309	0.0198	0.0132
0.9	0.203092	0.0803	0.0419	0.0246	0.0154	0.0100
0.95	0.179109	0.0677	0.0341	0.0196	0.0122	0.0081
1.0	0.157299	0.0568	0.0277	0.0154	0.0093	0.0060
1.1	0.119795	0.0396	0.0180	0.0094	0.0052	0.0029
1.2	0.089686	0.0272	0.0116	0.0058	0.0032	0.0020
1.3	0.065992	0.0184	0.0074	0.0035	0.0020	0.0014
1.4	0.047715	0.0122	0.0046	0.0022	0.0012	0.0009
1.5	0.033895	0.0080	0.0028	0.0012	0.0006	0.0004
1.6	0.023652	0.0052	0.0017	0.0008	0.0004	
1.7	0.016210	0.0033	0.0011	0.0005		
1.8	0.010909	0.0021	0.0006			
1.9	0.007210	0.0013	0.0004			
2.0	0.004678	0.0008	0.0002			
2.1	0.002979	0.0005	0.0001			
2.2	0.001863	0.0003				

† NOTE: The values of G_0 and G_1 are given here for sake of convenience. They have been reproduced from Carslaw and Jaeger, *Conduction of Heat in Solids*, page 373, Appendix III. The values of G_2, G_3, G_4, and G_5 are given to four decimal places, although the fourth place is not accurate because of the inaccuracy inherent in the fifth decimal place in the expansion for G_1, from which the G's of higher ordered subscripts are derived by means of a recurrence formula. This inaccuracy is aggravated at the larger value of $\psi_1^*/2\sqrt{\xi_1^*}$.

From Eq. (40) it follows that, for $\xi = 0.587$:

$$0.0023 + \frac{2.4}{0.65}(0.001114) - 0.828(0.00481) = 0.0024 = \frac{1}{2}c_f$$

whence $c_f = 0.0048$ and $U_p^*/U_a = (\bar{U}_e/U_a)\sqrt{0.0024} = 0.0641$.

For $\xi = 0.676$:

$$0.00534 + \frac{1.16}{0.815}(0.001459) - 0.75(0.00536) = 0.00339$$

so $c_f = 0.00678$ and $U_p^*/U_a = 0.0705$.

For $\xi = 0.78$:

$$0.00835 + \frac{0.38}{0.705}(0.00216) - 0.722(0.00789) = 0.00392$$

so $c_f = 0.00784$ and $U_p^*/U_a = 0.0713$.

The values of U_p^*/U_a just found are slightly larger than those assumed in carrying out the first approximation, but, on the other hand, it also turns out that the assumed values of δ are larger than those calculated. Because these trends yield values of δ^* and δ^{**} larger than the correct values, it may be presumed that the deviation between the assumed values of U_p^*/U_a and the actual ones is smaller than that now in evidence.

REFERENCES

[1] Ferrari, C., *Study of the Boundary Layer at Supersonic Speeds in Turbulent Flow—Case of Flow Along a Flat Plate*, Quarterly of Applied Mathematics, Vol. VIII, No. 1, April, 1950.

[2] von Mises, R., *Bemerkungen zur Hydrodynamik*, Z.A.M.M., Vol. 7, No. 6, p. 425, 1927.

[3] von Kármán, T., and Milliken, C. B., *On the Theory of Laminar Boundary Layers Involving Separation*, N.A.C.A. T.R. No. 504, 1934.

[4] Mattioli, G. D., *Teoria Dinamica dei Regimi Fluidi Turbolenti*, Chapt. xii, p. 275; Casa Editrice Dott. Antonio Milani, Padova, 1937.

[5] Carslaw, H. S., and Jaeger, J. C., *Conduction of Heat in Solids;* The Clarendon Press, Oxford, 1947.

[6] Gruschwitz, E., *Die Turbulente Reibungsschicht in Ebener Stroemung bei Druckabfall und Druckanstieg*, Ingenieur Archiv, Vol. 2, p. 321, 1931.

[7] Kehl, A., *Untersuchungen ueber Konvergente und Divergente Turbulente Reibungsschichten*, Ingenieur Archiv, Volume xiii, p. 293, 1943.

[8] Ferrari, C., *The Turbulent Boundary Layer in a Compressible Fluid with Positive Pressure Gradient*, Cornell Aeronautical Laboratory CAL/CM-560 (available from The Johns Hopkins University, Applied Physics Laboratory, Silver Spring, Md.), September, 1949.

[9] Ackeret, J., Feldmann, F., and Rott, N., *Untersuchungen an Verdichtungsstoessen und Grenzschichten in Schnellbewegten Gasen*, Mitt. aus dem Institut fuer Aerodynamik, No. 10, Zürich, 1946. Also translated as *Tests on Compression Shocks and Boundary Layers in Fast-Moving Gases*, N.A.C.A. T.M. No. 1113, January, 1947.

[10] Hartree, D. R., *Tables of the Error Function*, Mem. and Proc. Manchester Lit. and Phil. Soc., Vol. 80, p. 85, 1935. (Reference is made here to the Hartree Tables given on page 373 of reference 5, because it has been impossible to locate the original tables.)

Changes of Address

Since the Post Office Department does not as a rule forward magazines to forwarding addresses, it is important that the Institute be notified of changes in address 30 days in advance of publishing date to ensure receipt of every issue of the JOURNAL and REVIEW.

Notices should be printed legibly and sent directly to:

Institute of the Aeronautical Sciences, Inc.

2 East 64th Street, New York 21, New York

Tables of the Theodorsen Circulation Function for Generalized Motion*

YUDELL L. LUKE† AND MAX A. DENGLER‡

Midwest Research Institute

(1) SUMMARY

Important in all stability, aeroelastic, and flutter problems is the Theodorsen $C(k)$ function. Tables of this function are well known if the motion is harmonic. Heretofore, tables of the Theodorsen function for generalized motion have not been available. In this report, the latter tables are given for a range that should be sufficient to meet the needs of aerodynamicists. W. P. Jones has given a discussion of the generalized Theodorsen function, but his results appear incorrect, for, in his analysis, the Theodorsen function as derived by approaching harmonic motion from the side of stability and from the side of instability is distinct. If the Jones analysis were true, the nonuniqueness of the Theodorsen function would imply that the Bessel functions are not continuous, which is indeed false. The difficulty is clarified in this paper.

(2) INTRODUCTION

ONE OF THE MOST BASIC FUNCTIONS in subsonic unsteady aerodynamics is the Theodorsen function.[1] This function is important in all types of stability, aeroelastic, and flutter problems. In the case of incompressible flow, it is needed to compute the values of the flutter coefficients. Employing an iterative method, Dietze[2] uses the function to calculate flutter coefficients for subsonic flow. An alternative iterative procedure for calculating subsonic flutter coefficients has been suggested by Miles,[3] and here, too, the starting point is a knowledge of the Theodorsen function. Another application is found in the aerodynamic theory of oscillating wings of finite span.[4–6] The curt discussion rendered is by no means complete but is presented only to show the significance of the Theodorsen function.

(3) DEVELOPMENT OF THE THEODORSEN CIRCULATION FUNCTION FOR GENERALIZED MOTION

In the treatment of aerodynamic oscillatory problems, it is assumed that the motion follows the law e^{ikt}, where t is the time variable and

$$ik = \mu + i\omega \tag{1}$$

Thus, ω gives the frequency of motion, while μ defines the damping. If $\mu < 0$, the motion is convergent or stable; if $\mu > 0$, the motion is divergent or unstable. When $\mu = 0$, the motion is of constant amplitude and is said to be neutrally stable.

Heretofore, for the most part, the nature of the Theodorsen function has only been considered when $\mu = 0$. In a paper by Jones,[7] the generalization of this function is studied. His conclusions are rather disturbing, and it seems appropriate at this time that the difficulties be clarified. To accomplish this effectively, a derivation of the Theodorsen function $C(k)$ for general motions will be presented. For a starting point, consider the equality[8]

$$C(k) = \int_1^\infty \frac{x}{\sqrt{x^2-1}}\,U\,dx \Big/ \int_1^\infty \frac{x+1}{\sqrt{x^2-1}}\,U\,dx \tag{2}$$

where it is supposed that

$$U = U_0 e^{i[k(s/b - x) + \phi]} \tag{3}$$

and that $\omega > 0$. It is well known in the theory of Bessel functions[9] that

$$K_n(z) = \int_0^\infty e^{-z\cosh y}\cosh ny\,dy \tag{4}$$

which is valid if $|\arg z| < \pi/2$. This requires that $Re(z) > 0$. Let

$$z = ik \tag{5}$$

Thus, if $Re(z) > 0$, it follows that $\mu > 0$, so that the motion is assumed to be divergent. Combining Eqs. (2) through (5) with the well-known relation

$$K_n(z) = (\pi/2)\,ie^{(1/2)n\pi i}H_n^{(1)}(iz) \tag{6}$$

it is readily deduced that

$$C(k) = H_1^{(2)}(k)/[H_1^{(2)}(k) + iH_0^{(2)}(k)] \tag{7}$$

which is the generalized Theodorsen $C(k)$ function. It is true that, in the development of Eq. (7), it was necessary to require that $\mu > 0$. However, Eq. (7) has no need for such a restriction, and therefore, by the method of analytic continuation, one can argue that Eq. (7) is valid for all μ's.

In the preceding analysis the frequency of the motion was taken as positive. If, in Eq. (3), i is replaced by $-i$ so that Eq. (1) is replaced by its complex conjugate, then it is easy to show that the Theodorsen function is given by the complex conjugate of Eq. (7), which is

$$\overline{C(k)} = H_1^{(1)}(k)/[H_1^{(1)}(k) - iH_0^{(1)}(k)] \tag{8}$$

Received July 5, 1950. Revised December 22, 1950.

* The authors desire to thank Elizabeth Kahn, Gloria Flake, and Dolores Ufford, all of the computing staff of the Midwest Research Institute, for the computations reported here.

† Research Mathematician.

‡ Research Engineer.

TABLE 1

Tables of the Theodorsen Circulation Function for Generalized Motion

	$\theta = -5°$		$\theta = 0°$		$\theta = 5°$		$\theta = 10°$	
ρ	$F(\rho e^{i\theta})$	$-G(\rho e^{i\theta})$	$F(\rho e^{i\theta})$	$-G(\rho e^{i\theta})$	$F(\rho e^{i\theta})$	$-G(\rho e^{i\theta})$	$F(\rho e^{i\theta})$	$-G(\rho e^{i\theta})$
0	1.0	0	1.0	0	1.0	0	1.0	0
0.01	0.97949 42	0.04396 04	0.98242 15	0.04565 21	0.98549 60	0.04717 45	0.98871 13	0.04851 44
0.02	0.95958 24	0.07107 24	0.96372 52	0.07520 79	0.96833 68	0.07839 16	0.97323 65	0.08136 36
0.03	0.93993 12	0.09298 43	0.94501 10	0.07971 35	0.95048 58	0.10269 36	0.95637 13	0.10729 86
0.04	0.92127 37	0.10967 36	0.92670 18	0.11600 13	0.93260 31	0.12225 04	0.93900 62	0.12839 71
0.05	0.90350 68	0.12308 30	0.90900 90	0.13064 44	0.91503 33	0.13821 25	0.92162 01	0.14576 94
0.06	0.88665 35	0.13395 84	0.89203 97	0.14259 44	0.89797 19	0.15132 68	0.90468 45	0.15909 51
0.07	0.87070 45	0.14281 93	0.87584 27	0.15238 17	0.88153 00	0.16212 89	0.88782 24	0.17206 30
0.08	0.85563 25	0.15004 84	0.86043 18	0.16040 21	0.86576 68	0.17102 38	0.87169 73	0.18192 70
0.09	0.84139 97	0.15593 78	0.84579 92	0.16696 15	0.85070 83	0.17832 92	0.85618 78	0.19006 56
0.10	0.82796 32	0.16071 67	0.83192 41	0.17230 22	0.83635 89	0.18429 96	0.84132 73	0.19674 41
0.11	0.81527 81	0.16456 76	0.81877 79	0.17661 95	0.82270 87	0.18914 23	0.82712 77	0.20218 13
0.12	0.80329 92	0.16763 88	0.80632 73	0.18007 27	0.80973 89	0.19302 83	0.81358 69	0.20655 96
0.13	0.79198 23	0.17005 10	0.79453 72	0.18279 33	0.79742 48	0.19609 96	0.80069 26	0.21003 19
0.14	0.78128 51	0.17190 45	0.78337 15	0.18489 04	0.78573 82	0.19847 53	0.78842 69	0.21272 77
0.15	0.77116 71	0.17328 26	0.77279 46	0.18645 56	0.77464 93	0.20025 57	0.77676 64	0.21475 66
0.16	0.76159 04	0.17425 48	0.76277 19	0.18756 59	0.76412 76	0.20152 57	0.76568 61	0.21621 22
0.17	0.75251 93	0.17488 01	0.75326 99	0.18828 65	0.75414 26	0.20235 76	0.75515 91	0.21717 45
0.18	0.74392 07	0.17520 81	0.74425 70	0.18867 27	0.74466 47	0.20281 28	0.74515 89	0.21771 24
0.19	0.73576 36	0.17528 13	0.73570 31	0.18877 18	0.73566 50	0.20294 44	0.73565 74	0.21788 42
0.20	0.72801 92	0.17513 56	0.72757 99	0.18862 42	0.72711 59	0.20279 72	0.72662 89	0.21774 11
0.21	0.72066 07	0.17480 22	0.71986 08	0.18826 47	0.71899 12	0.20241 10	0.71804 69	0.21732 70
0.22	0.71366 36	0.17430 74	0.71252 11	0.18772 32	0.71126 59	0.20181 90	0.70988 75	0.21668 02
0.23	0.70700 48	0.17367 44	0.70553 73	0.18702 55	0.70391 66	0.20105 03	0.70212 62	0.21583 31
0.24	0.70066 32	0.17292 28	0.69888 79	0.18619 40	0.69692 11	0.20013 03	0.69474 13	0.21481 47
0.25	0.69461 90	0.17206 98	0.69255 26	0.18524 80	0.69025 86	0.19908 08	0.68771 04	0.21364 96
0.26	0.68885 39	0.17113 02	0.68651 25	0.18420 43	0.68390 96	0.19792 10	0.68101 42	0.21235 97
0.27	0.68335 11	0.17011 70	0.68075 02	0.18307 76	0.67785 59	0.19666 75	0.67463 30	0.21096 37
0.28	0.67809 48	0.16904 16	0.67524 91	0.18188 07	0.67208 05	0.19533 48	0.66854 96	0.20947 84
0.29	0.67307 06	0.16791 35	0.66999 42	0.18062 46	0.66656 71	0.19393 53	0.66274 63	0.20791 75
0.30	0.66826 47	0.16674 15	0.66497 11	0.17931 91	0.66130 10	0.19248 04	0.65720 81	0.20629 43
0.32	0.65925 90	0.16429 47	0.65556 86	0.17659 29	0.65145 54	0.18944 11	0.64686 76	0.20290 27
0.34	0.65098 70	0.16175 05	0.64694 60	0.17375 80	0.64244 24	0.18628 06	0.63741 98	0.19937 58
0.36	0.64337 04	0.15914 69	0.63902 00	0.17085 75	0.63417 33	0.18304 78	0.62877 00	0.19576 92
0.38	0.63634 06	0.15651 31	0.63171 79	0.16792 44	0.62657 03	0.17978 00	0.62083 48	0.19212 55
0.40	0.62983 82	0.15387 14	0.62497 63	0.16498 40	0.61956 55	0.17650 60	0.61354 07	0.18847 72
0.42	0.62381 06	0.15123 91	0.61873 92	0.16205 57	0.61309 89	0.17324 76	0.60682 32	0.18484 91
0.44	0.61821 22	0.14862 92	0.61295 75	0.15915 43	0.60711 77	0.17002 15	0.60062 52	0.18125 98
0.46	0.61300 22	0.14605 18	0.60758 79	0.15629 10	0.60157 53	0.16684 03	0.59489 64	0.17772 35
0.48	0.60814 49	0.14351 42	0.60259 21	0.15347 40	0.59643 05	0.16371 30	0.58959 22	0.17425 06
0.50	0.60360 86	0.14102 21	0.59793 61	0.15070 95	0.59164 67	0.16064 67	0.58467 30	0.17084 84
0.55	0.59349 44	0.13501 33	0.58759 22	0.14405 33	0.58106 19	0.15327 49	0.57383 76	0.16268 29
0.60	0.58485 35	0.12934 36	0.57880 16	0.13778 52	0.57211 97	0.14634 82	0.56474 49	0.15502 89
0.65	0.57740 81	0.12401 93	0.57126 71	0.13191 06	0.56450 10	0.13987 06	0.55705 02	0.14788 87
0.70	0.57094 35	0.11903 21	0.56475 95	0.12641 89	0.55796 00	0.13382 82	0.55048 91	0.14124 39
0.75	0.56529 16	0.11436 61	0.55909 99	0.12129 05	0.55230 52	0.12819 74	0.54485 59	0.13506 60
0.80	0.56031 94	0.11000 14	0.55414 66	0.11650 24	0.54738 56	0.12295 10	0.53998 90	0.12932 26
0.85	0.55592 01	0.10591 73	0.54978 66	0.11203 01	0.54308 11	0.11806 02	0.53576 00	0.12398 02
0.90	0.55200 74	0.10209 30	0.54592 86	0.10784 96	0.53929 48	0.11349 72	0.53206 60	0.11900 61
0.95	0.54851 09	0.09850 85	0.54249 83	0.10393 77	0.53594 82	0.10923 53	0.52882 39	0.11436 94
1.00	0.54537 26	0.09514 49	0.53943 48	0.10027 29	0.53297 69	0.10524 96	0.52596 57	0.11004 17
1.50	0.52606 27	0.07045 55	0.52101 32	0.07356 41	0.51559 65	0.07642 70	0.50980 34	0.07900 88
2.00	0.51721 41	0.05561 26	0.51295 48	0.05769 13	0.50843 14	0.05951 18	0.50364 62	0.06104 38
2.50	0.51238 79	0.04580 94	0.50874 40	0.04729 69	0.50490 39	0.04853 74	0.50087 53	0.04950 59
3.00	0.50944 74	0.03888 56	0.50628 00	0.04000 39	0.50296 19	0.04089 26	0.49950 39	0.04153 13
3.50	0.50751 23	0.03374 95	0.50471 92	0.03462 23	0.50180 75	0.03528 34	0.49878 89	0.03571 63
4.00	0.50616 45	0.02979 45	0.50367 09	0.03049 61	0.50108 18	0.03100 27	0.49840 94	0.03130 07
5.00	0.50444 46	0.02411 44	0.50239 72	0.02459 86	0.50028 47	0.02491 64	0.49811 86	0.02505 83
6.00	0.50341 73	0.02023 91	0.50168 46	0.02059 55	0.49990 47	0.02080 81	0.49808 84	0.02086 98
7.00	0.50274 71	0.01742 98	0.50124 70	0.01770 50	0.49971 11	0.01785 40	0.49814 96	0.01787 12
8.00	0.50228 10	0.01530 21	0.50095 96	0.01552 20	0.49960 99	0.01562 99	0.49824 16	0.01562 10
9.00	0.50194 22	0.01363 53	0.50076 09	0.01381 61	0.49955 78	0.01389 59	0.49834 08	0.01387 15
10.00	0.50168 48	0.01229 46	0.50061 78	0.01244 67	0.49953 29	0.01250 69	0.49843 75	0.01247 29

Here the frequency of the motion is negative. In all problems involving the Theodorsen function, current practice is to assume that the frequency part of the motion is positive. In this manner, many difficulties can be avoided.

If the motion is nonoscillatory but divergent so that $\omega = 0$ and $\mu > 0$, then,

$$C(\mu) = K_1(\mu)/[K_1(\mu) + K_0(\mu)] \tag{9}$$

If the motion is nonoscillatory and convergent, then Eq. (9) must be replaced by

$$C(\mu) = \frac{K_1(\mu) + \pi i I_1(\mu)}{K_1(\mu) - K_0(\mu) + \pi i[I_1(\mu) + I_0(\mu)]} \tag{10}$$

where μ is now treated as a positive number.

TABLE 2
Tables of the Theodorsen Circulation Function for Generalized Motion

	$\theta = 15°$		$\theta = 20°$		$\theta = 25°$		$\theta = 30°$	
ρ	$F(\rho e^{i\theta})$	$-G(\rho e^{i\theta})$	$F(\rho e^{i\theta})$	$-G(\rho e^{i\theta})$	$F(\rho e^{i\theta})$	$-G(\rho e^{i\theta})$	$F(\rho e^{i\theta})$	$-G(\rho e^{i\theta})$
0	1.0	0	1.0	0	1.0	0	1.0	0
0.01	0.99206 01	0.04965 82	0.99553 36	0.05059 20	0.99912 17	0.05130 20	1.00281 29	0.05177 39
0.02	0.97842 52	0.08409 88	0.98390 25	0.08657 02	0.98966 56	0.08874 85	0.99570 96	0.09060 23
0.03	0.96268 22	0.11169 82	0.96943 31	0.11585 83	0.97663 69	0.11974 03	0.98430 49	0.12330 07
0.04	0.94594 13	0.13441 22	0.95343 98	0.14026 15	0.96153 35	0.14590 42	0.97025 50	0.15129 23
0.05	0.92881 33	0.15329 25	0.93666 02	0.16075 28	0.94521 21	0.16811 41	0.95452 27	0.17533 21
0.06	0.91167 80	0.16904 21	0.91956 81	0.17799 25	0.92823 74	0.18697 28	0.93775 96	0.19594 84
0.07	0.89478 31	0.18218 25	0.90248 35	0.19248 14	0.91000 37	0.20294 77	0.92043 42	0.21356 23
0.08	0.87829 12	0.19312 30	0.88562 69	0.20462 04	0.89379 32	0.21642 38	0.90289 20	0.22853 18
0.09	0.86230 80	0.20219 53	0.86914 99	0.21474 18	0.87680 76	0.22772 70	0.88538 98	0.24116 99
0.10	0.84689 91	0.20967 30	0.85315 52	0.22312 47	0.86019 09	0.23713 84	0.86811 75	0.25175 38
0.11	0.83210 18	0.21578 56	0.83770 94	0.23000 71	0.84404 34	0.24490 23	0.85121 36	0.26053 04
0.12	0.81793 37	0.22072 61	0.82285 30	0.23559 28	0.82843 28	0.25123 11	0.83477 75	0.26771 92
0.13	0.80439 79	0.22465 88	0.80860 73	0.24005 68	0.81340 17	0.25631 08	0.81887 77	0.27351 58
0.14	0.79148 73	0.22772 40	0.79497 94	0.24355 04	0.79897 44	0.26030 37	0.80355 90	0.27809 34
0.15	0.77918 84	0.23004 12	0.78196 61	0.24620 41	0.78516 10	0.26335 16	0.78884 79	0.28160 58
0.16	0.76748 18	0.23171 38	0.76955 67	0.24813 10	0.77196 11	0.26557 87	0.77475 68	0.28418 88
0.17	0.75634 62	0.23282 99	0.75773 55	0.24942 92	0.75936 65	0.26709 34	0.76128 74	0.28596 23
0.18	0.74575 73	0.23346 61	0.74648 31	0.25018 36	0.74736 37	0.26799 04	0.74843 35	0.28703 21
0.19	0.73569 07	0.23368 82	0.73577 78	0.25046 82	0.73593 49	0.26835 27	0.73618 27	0.28749 10
0.20	0.72612 11	0.23355 34	0.72559 64	0.25034 72	0.72506 00	0.26825 25	0.72451 86	0.28742 10
0.21	0.71702 36	0.23311 13	0.71591 54	0.24987 64	0.71471 68	0.26775 33	0.71342 18	0.28689 38
0.22	0.70837 38	0.23240 46	0.70671 08	0.24910 46	0.70488 26	0.26691 02	0.70287 07	0.28597 24
0.23	0.70014 78	0.23147 08	0.69795 89	0.24807 42	0.69553 40	0.26577 16	0.69284 27	0.28471 22
0.24	0.69232 28	0.23034 23	0.68963 66	0.24682 20	0.68664 77	0.26437 98	0.68331 46	0.28316 16
0.25	0.68487 68	0.22904 75	0.68172 14	0.24538 06	0.67820 07	0.26277 17	0.67426 30	0.28136 32
0.26	0.67778 73	0.22761 02	0.67419 16	0.24377 79	0.67017 05	0.26097 97	0.66566 46	0.27935 43
0.27	0.67103 96	0.22605 42	0.66702 66	0.24203 86	0.66253 55	0.25903 21	0.65749 67	0.27716 74
0.28	0.66460 96	0.22439 60	0.66020 63	0.24018 43	0.65527 47	0.25695 36	0.64973 71	0.27483 11
0.29	0.65848 13	0.22265 30	0.65371 22	0.23823 38	0.64836 82	0.25476 58	0.64236 46	0.27237 04
0.30	0.65263 79	0.22083 93	0.64752 62	0.23620 35	0.64179 67	0.25248 77	0.63535 85	0.26980 72
0.32	0.64174 38	0.21704 88	0.63601 22	0.23195 93	0.62958 74	0.24772 47	0.62236 79	0.26444 75
0.34	0.63181 18	0.21310 74	0.62554 01	0.22754 68	0.61851 24	0.24277 37	0.61061 91	0.25887 79
0.36	0.62273 97	0.20907 85	0.61599 95	0.22303 82	0.60845 16	0.23771 79	0.59998 06	0.25319 43
0.38	0.61443 76	0.20501 05	0.60729 25	0.21848 92	0.59929 81	0.23262 08	0.59033 46	0.24746 97
0.40	0.60682 60	0.20094 04	0.59933 26	0.21394 16	0.59095 68	0.22753 03	0.58157 62	0.24175 91
0.42	0.59983 47	0.19689 62	0.59204 34	0.20942 74	0.58334 38	0.22248 28	0.57361 26	0.23610 37
0.44	0.59340 19	0.19289 92	0.58535 70	0.20497 05	0.57638 46	0.21750 51	0.56636 12	0.23053 41
0.46	0.58747 28	0.18896 49	0.57921 36	0.20058 84	0.57001 31	0.21261 71	0.55974 88	0.22507 25
0.48	0.58199 88	0.18510 51	0.57356 00	0.19629 41	0.56417 10	0.20783 32	0.55371 06	0.21973 48
0.50	0.57693 69	0.18132 79	0.56834 92	0.19209 66	0.55880 64	0.20316 32	0.54818 94	0.21453 19
0.55	0.56584 42	0.17227 91	0.55699 58	0.18206 19	0.54719 42	0.19202 44	0.53632 72	0.20215 34
0.60	0.55660 58	0.16382 00	0.54762 14	0.17270 89	0.53770 03	0.18167 66	0.52673 87	0.19069 58
0.65	0.54884 81	0.15594 97	0.53981 92	0.16403 24	0.52987 92	0.17210 81	0.51893 34	0.18013 89
0.70	0.54228 50	0.14864 44	0.53327 82	0.15600 18	0.52339 18	0.16327 98	0.51254 02	0.17043 22
0.75	0.53669 48	0.14186 98	0.52775 87	0.14857 51	0.51797 76	0.15514 01	0.50727 51	0.16151 21
0.80	0.53190 41	0.13558 68	0.52307 35	0.14170 59	0.51343 45	0.14763 32	0.50291 88	0.15331 19
0.85	0.52777 53	0.12975 63	0.51907 53	0.13534 76	0.50960 37	0.14070 42	0.49930 03	0.14576 60
0.90	0.52419 89	0.12434 01	0.51564 68	0.12945 57	0.50635 98	0.13430 07	0.49628 50	0.13881 27
0.95	0.52108 64	0.11930 23	0.51269 40	0.12398 85	0.50360 26	0.12837 42	0.49376 60	0.13239 56
1.00	0.51836 60	0.11461 00	0.51014 08	0.11890 78	0.50125 14	0.12288 04	0.49165 77	0.12646 29
1.50	0.50362 58	0.08126 98	0.49705 73	0.08316 52	0.49009 40	0.08464 49	0.48273 53	0.08565 25
2.00	0.49860 38	0.06225 44	0.49331 16	0.06310 75	0.48778 00	0.06356 40	0.48202 38	0.06358 14
2.50	0.49666 87	0.05017 60	0.49229 71	0.05051 97	0.48777 71	0.05050 72	0.48312 90	0.05010 74
3.00	0.49591 88	0.04189 87	0.49222 20	0.04197 32	0.48843 22	0.04173 21	0.48457 11	0.04115 26
3.50	0.49567 73	0.03590 37	0.49248 87	0.03582 86	0.48924 21	0.03547 38	0.48595 91	0.03482 23
4.00	0.49566 74	0.03137 62	0.49287 21	0.03121 56	0.49004 15	0.03080 57	0.48719 63	0.03013 39
5.00	0.49591 21	0.02501 48	0.49367 99	0.02477 70	0.49143 83	0.02433 68	0.48920 54	0.02368 73
6.00	0.49624 77	0.02077 38	0.49439 59	0.02051 41	0.49254 72	0.02008 56	0.49071 73	0.01948 44
7.00	0.49657 33	0.01775 17	0.49499 38	0.01749 14	0.49342 39	0.01708 72	0.49187 70	0.01653 67
8.00	0.49686 44	0.01549 20	0.49548 90	0.01523 97	0.49412 63	0.01486 23	0.49278 82	0.01435 85
9.00	0.49711 88	0.01373 98	0.49590 14	0.01349 88	0.49469 83	0.01314 73	0.49352 02	0.01268 47
10.00	0.49733 97	0.01234 22	0.49624 81	0.01211 33	0.49517 17	0.01178 56	0.49411 98	0.01135 90

(4) JONES'S DISCUSSION OF THE THEODORSEN CIRCULATION FUNCTION FOR GENERALIZED MOTION

The essential starting point for Jones's discussion of the Theodorsen function is Eq. (9). He replaces μ by $\mu + i\omega$ and employs the form of Eq. (6). These equations are then combined with the following formula given by Watson:[10]

$$H_n^{(1)}(ze^{m\pi i}) = \frac{\sin(1-m)n\pi}{\sin n\pi} H_n^{(1)}(z) - e^{-n\pi i}\frac{\sin mn\pi}{\sin n\pi} H_n^{(2)}(z) \quad (11)$$

If $\mu > 0$, Jones takes $m = 1$ and derives the form of Eq. (7); but, for $\mu < 0$, $m = -1$ in Eq. (11) is used, and the result is different from Eq. (7). By letting

TABLE 3

Table of the Theodorsen Circulation Function for Harmonic Motion

k	$F(k)$	$-G(k)$	k	$F(k)$	$-G(k)$	k	$F(k)$	$-G(k)$	k	$F(k)$	$-G(k)$
0	1.0	0	0.072	0.87269 76	0.15411 63	0.340	0.64694 60	0.17375 80	0.940	0.54315 33	0.10469 96
0.002	0.99670 96	0.01257 97	0.074	0.86958 41	0.15578 31	0.350	0.64290 06	0.17231 37	0.950	0.54249 83	0.10393 77
0.004	0.99325 79	0.02225 66	0.076	0.86650 19	0.15738 48	0.360	0.63902 00	0.17085 75	0.960	0.54185 81	0.10318 56
0.006	0.98970 82	0.03077 52	0.078	0.86345 12	0.15892 36	0.380	0.63171 79	0.16792 44	0.980	0.54061 97	0.10171 05
0.008	0.98608 97	0.03851 30	0.080	0.86043 18	0.16040 21	0.400	0.62497 63	0.16498 40	1.000	0.53943 48	0.10027 29
0.010	0.98242 15	0.04565 21	0.082	0.85744 35	0.16182 23	0.420	0.61873 92	0.16205 57	1.100	0.53421 47	0.09360 62
0.012	0.97871 74	0.05230 15	0.084	0.85448 62	0.16318 64	0.440	0.61295 75	0.15915 43	1.200	0.52995 60	0.08770 89
0.014	0.97498 80	0.05853 45	0.086	0.85155 99	0.16449 63	0.450	0.61022 37	0.15771 73	1.300	0.52643 67	0.08246 43
0.016	0.97124 18	0.06440 43	0.088	0.84866 43	0.16575 41	0.460	0.60758 79	0.15629 10	1.400	0.52349 57	0.07777 59
0.018	0.96748 56	0.06995 15	0.090	0.84579 92	0.16696 15	0.480	0.60259 21	0.15347 40	1.500	0.52101 32	0.07356 41
0.020	0.96372 52	0.07520 79	0.092	0.84296 44	0.16812 03	0.500	0.59793 61	0.15070 95	1.600	0.51889 92	0.06976 29
0.022	0.95996 37	0.08019 99	0.094	0.84015 97	0.16923 22	0.520	0.59358 96	0.14800 19	1.700	0.51708 45	0.06631 74
0.024	0.95621 11	0.08494 91	0.096	0.83738 49	0.17029 88	0.540	0.58952 58	0.14535 41	1.800	0.51551 56	0.06318 17
0.026	0.95246 51	0.08947 42	0.098	0.83463 98	0.17132 16	0.550	0.58759 22	0.14405 33	1.900	0.51415 02	0.06031 72
0.028	0.94873 08	0.09379 10	0.100	0.83192 41	0.17230 22	0.560	0.58572 05	0.14276 82	2.000	0.51295 48	0.05769 13
0.030	0.94501 10	0.09791 35	0.110	0.81877 79	0.17661 95	0.580	0.58215 22	0.14024 50	2.500	0.50874 40	0.04729 69
0.032	0.94130 79	0.10185 41	0.120	0.80632 73	0.18007 27	0.600	0.57880 16	0.13778 52	3.000	0.50628 00	0.04000 39
0.034	0.93762 38	0.10562 38	0.130	0.79453 72	0.18279 33	0.620	0.57565 12	0.13538 85	3.500	0.50471 92	0.03462 23
0.036	0.93396 03	0.10923 23	0.140	0.78337 15	0.18489 04	0.640	0.57268 53	0.13305 44	4.000	0.50367 09	0.03049 61
0.038	0.93031 92	0.11268 88	0.150	0.77279 46	0.18645 56	0.650	0.57126 71	0.13191 06	4.500	0.50293 41	0.02723 63
0.040	0.92670 18	0.11600 13	0.160	0.76277 19	0.18756 59	0.660	0.56988 98	0.13078 22	5.000	0.50239 72	0.02459 86
0.042	0.92310 94	0.11917 72	0.170	0.75326 99	0.18828 65	0.680	0.56725 18	0.12857 08	5.500	0.50199 44	0.02242 16
0.044	0.91954 30	0.12222 33	0.180	0.74425 70	0.18867 27	0.700	0.56475 95	0.12641 89	6.000	0.50168 46	0.02059 55
0.046	0.91600 36	0.12514 61	0.190	0.73570 31	0.18877 18	0.720	0.56240 26	0.12432 52	6.500	0.50144 14	0.01904 21
0.048	0.91249 21	0.12795 13	0.200	0.72757 99	0.18862 42	0.740	0.56017 12	0.12228 82	7.000	0.50124 70	0.01770 50
0.050	0.90900 90	0.13064 44	0.210	0.71986 08	0.18826 47	0.750	0.55909 99	0.12129 05	7.500	0.50108 94	0.01654 23
0.052	0.90555 50	0.13323 04	0.220	0.71252 11	0.18772 32	0.760	0.55805 67	0.12030 65	8.000	0.50095 96	0.01552 20
0.054	0.90213 07	0.13571 41	0.230	0.70553 73	0.18702 55	0.780	0.55605 09	0.11837 84	8.500	0.50085 17	0.01461 96
0.056	0.89873 65	0.13810 00	0.240	0.69888 79	0.18619 40	0.800	0.55414 66	0.11650 24	9.000	0.50076 09	0.01381 61
0.058	0.89537 27	0.14039 21	0.250	0.69255 26	0.18524 80	0.820	0.55233 69	0.11467 70	9.500	0.50068 38	0.01309 58
0.060	0.89203 97	0.14259 44	0.260	0.68651 25	0.18420 43	0.840	0.55061 58	0.11290 05	10.000	0.50061 78	0.01244 67
0.062	0.88873 77	0.14471 06	0.270	0.68075 02	0.18307 76	0.850	0.54978 66	0.11203 01	20.000	0.50015 58	0.00624 32
0.064	0.88546 68	0.14674 43	0.280	0.67524 91	0.18188 07	0.860	0.54897 74	0.11117 14	30.000	0.50006 94	0.00416 46
0.066	0.88222 74	0.14869 86	0.290	0.66999 42	0.18062 46	0.880	0.54741 66	0.10948 83	40.000	0.50003 90	0.00312 42
0.068	0.87901 93	0.15057 68	0.300	0.66497 11	0.17931 91	0.900	0.54592 86	0.10784 96	50.000	0.50002 50	0.00249 96
0.070	0.87584 27	0.15238 17	0.320	0.65556 86	0.17659 29	0.920	0.54450 89	0.10625 38	100.000	0.50000 62	0.00124 99
									∞	0.50000 00	0.00000 00

$\mu \to 0$ from both the positive and negative sides, two different limits of the Theodorsen function for real argument are obtained. Actually, no limiting process is required, since the Hankel functions are regular in the complex plane except at zero and infinity. A *prima facie* examination shows that his results are incorrect, for, if not, one then concludes that the Bessel functions are not continuous, which is false. It can be shown that the correct branch of the Hankel function is taken when $m = 1$. By utilizing the principle of analytic continuation, the resulting form of the Theodorsen function is valid for all μ's.

(5) Discussion of the Tables of the Theodorsen Circulation Function for Generalized Motion

In the sequel, the Theodorsen function is defined as

$$C(z) = \frac{H_1^{(2)}(z)}{H_1^{(2)}(z) + iH_0^{(2)}(z)} = F(\rho, \theta) + iG(\rho, \theta) \quad (12)$$

where

$$z = \rho e^{i\theta} = \omega - i\mu = k, \quad \rho \geq 0, \quad |\theta| \leq \pi/2 \quad (13)$$

Thus, if the motion is convergent, $0 < \theta \leq \pi/2$; if the motion is divergent, $-\pi/2 \leq \theta < 0$. However, if the motion is harmonic, $\theta = 0$ and, therefore, $\rho = k$. In this case, values of $C(k)$ are well known.[11] However, if it is desired to study an aerodynamic system for nonharmonic motion, it is then necessary to know the value of $C(z)$ for general z. Heretofore, tables of $C(z)$ have not been available. Many studies in stability have been hypothesized on a pseudo-expansion of $C(k)$ about $k = 0$. That this can lead to serious discrepancies is the subject of a recent report by Goland.[12] In other studies, the necessity of tables of $C(z)$ has been obviated by using curve fits of $C(k)$ for k real and then substituting $z = \rho e^{i\theta}$ for k in the curve fit expressions. An example of this approach is to be found in a paper by Goland and Luke.[13]

Since the tendency in aerodynamics is always toward greater accuracy and refinement, it has become apparent that a table of $C(z)$ would prove most useful for future research. In Tables 1 and 2, $C(z)$ is tabulated for the following range of ρ and θ:

ρ: 0(0.01)0.3(0.02)0.5(0.05)1.0(0.5)10.0
θ: $-5°(5°)30°$

For $\theta = 0$, the range of values is a bit more extensive than that given above. All the tables were computed using values of the Bessel functions tabulated in refer-

FIG. 1 - PLOT OF THE THEODORSEN FUNCTION FOR GENERALIZED MOTION. $F(\rho,\theta)$ VS. ρ FOR DIFFERENT θ.

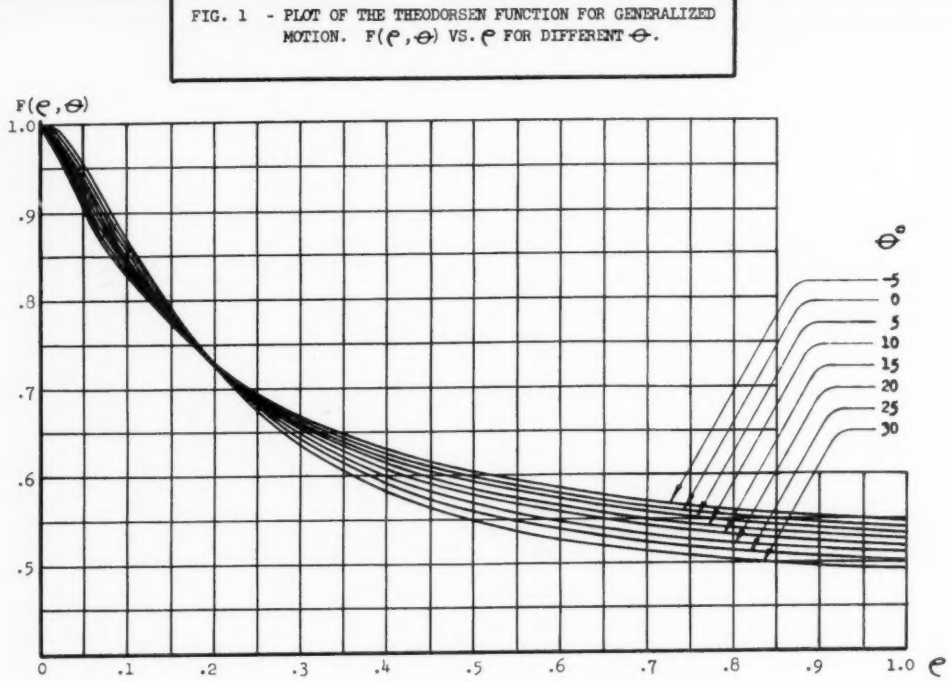

FIG. 2 - PLOT OF THE THEODORSEN FUNCTION FOR GENERALIZED MOTION. $G(\rho,\theta)$ VS. ρ FOR DIFFERENT θ.

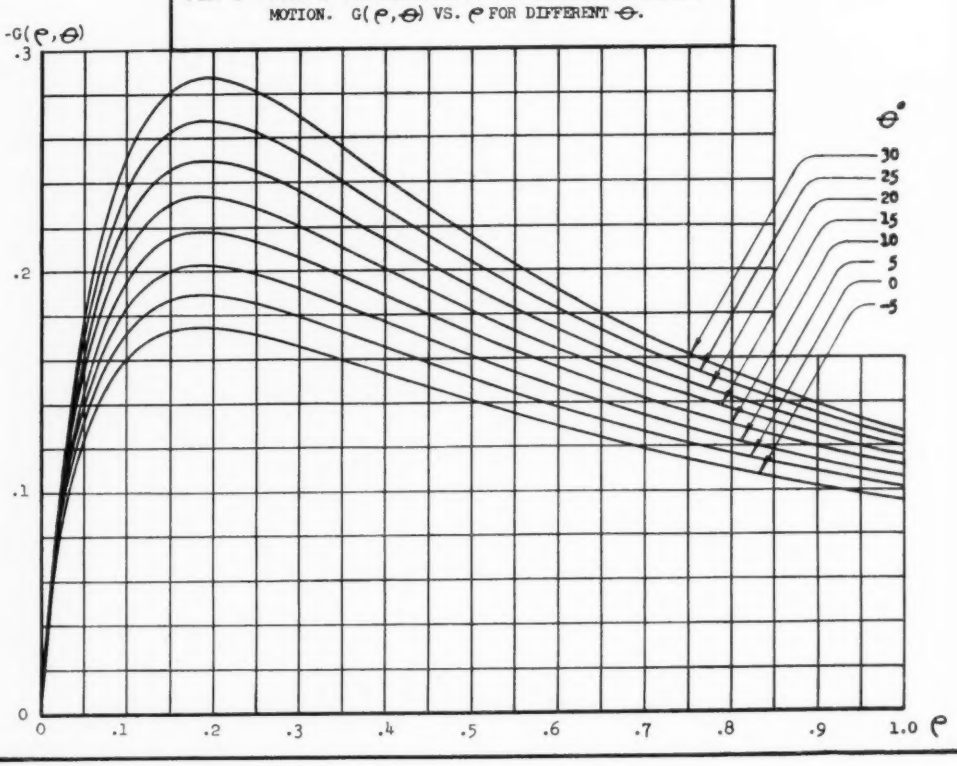

ences 14, 15, 16, and 17. Seven decimals were carried, and it is estimated that the error is $\leq 3 \times 10^{-7}$. It is believed that the present range is sufficiently large to cover current needs. The range of θ can easily be extended using the last two references. Plots of F and G versus ρ for different θ are shown in Figs. 1 and 2.

For a number of applications, linear single or double interpolation, as the case may be, will afford sufficiently reliable results. To achieve greater accuracy, one can employ the series expansions of the Hankel functions in the neighborhood of the origin. Elsewhere, Taylor series expansions of $C(z)$ are valid, for, if z is small, neglecting terms of second order and higher,

$$C(z) \sim 1 + iz[\log (z/2) + \gamma + i(\pi/2)] \quad (14)$$

$$dC/dz \sim i[\log (z/2) + \gamma + i(\pi/2)] \quad (15)$$

where γ is Euler's constant. Thus, dC/dz does not exist at the origin. It follows from Eq. (14) that

$$F(\rho, \theta) \sim 1 - \rho\left[\left(\log \frac{\rho}{2} + \gamma\right) \sin \theta + \left(\frac{\pi}{2} + \theta\right) \cos \theta\right] \quad (16)$$

$$G(\rho, \theta) \sim \rho\left[\left(\log \frac{\rho}{2} + \gamma\right) \cos \theta - \left(\frac{\pi}{2} + \theta\right) \sin \theta\right] \quad (17)$$

Thus, $\lim_{z \to 0} C(z) = 1$. Note further that $\lim_{\rho \to 0} |\partial G/\partial \rho| \to \infty$ for all θ and that $\lim_{\rho \to 0} |\partial F/\partial \rho| \to \infty$ for $\theta \neq 0$. But, if $\theta = 0$, then the latter limit becomes $-\pi/2$. It can easily be shown that the higher derivatives of F with respect to ρ do not exist at the origin. Differentiating Eq. (12), one easily derives that

$$z(dC/dz) = C(C - 1) + iz(2C - 1) \quad (18)$$

and, therefore, calculation of all higher derivatives is simple.

If z is real,

$$k(dG/dk) = (2F - 1)(G + k) \quad (19)$$

and

$$k(dF/dk) = F(F - 1) - G^2 - 2Gk \quad (20)$$

It can be shown that

$$F(F - 1) + G^2 = \frac{2G}{\pi k}\left(\frac{1}{Y_0 Y_1 + J_0 J_1}\right) \quad (21)$$

and, if Eq. (21) is placed in Eq. (20), then dF/dk has the form as given by Rauscher and Heilenday.[15] This reference contains a typographical error in that the coefficient of $J_0 J_1$ should be positive.

Values of $C(z)$ for z large can be calculated rapidly by employing the asymptotic expansions of the Hankel functions. By employing these expansions, it is readily deduced that $\lim_{z \to \infty} C(z) = 1/2$.

References

[1] Theodorsen, Th., *General Theory of Aerodynamic Instability and the Mechanism of Flutter*, N.A.C.A. T.R. No. 496, 1940.

[2] Dietze, F., *Die Luftkraefte des Harmonisch schwingenden Fleugels im kompressiblen Medium bei Unterschallgeschwindigeit (Plane Problems). Part I. Method of Computation*, ZWB FB 1733, January, 1943. Translation by A.A.F. No. F-TS-506-RE, November, 1946.

[3] Miles, J. W., *A Note on a Solution to Possio's Integral Equation for an Oscillating Airfoil in Subsonic Flow*, Quart. of Appl. Math., Vol. 7, pp. 213–216, July, 1949.

[4] Biot, M. A., and Boehnlein, C. T., *Aerodynamic Theory of the Oscillating Wing of Finite Span*, Report No. 5 for submittal to the Army Air Forces, September, 1942.

[5] Reissner, E., *Effect of Finite Span on the Airload Distributions for Oscillating Wings. Part I—Aerodynamic Theory of Oscillating Wings of Finite Span*, N.A.C.A. T.N. No. 1194, March, 1947.

[6] Reissner, E., and Stevens, J. E., *Effect of Finite Span on the Airload Distributions for Oscillating Wings. Part II—Methods of Calculation and Examples of Application*, N.A.C.A. T.N. No. 1195, October, 1947.

[7] Jones, W. P., *Aerodynamic Forces on Wings in Non-Uniform Motion*, R. & M. No. 2117, August, 1945.

[8] Reference 1 of this section, p. 8.

[9] Watson, G. N., *A Treatise on the Theory of Bessel Functions*, 2nd Ed., p. 181; Cambridge University Press, 1945.

[10] *Ibid.*, p. 75.

[11] Kassner, R., and Fingado, H., *The Two-Dimensional Problem of Wing Vibrations*, Jour. Royal Aero. Soc., Vol. 41, 1937. See also Luke, Y. L., *Tables of Coefficients for Compressible Flutter Calculations*, Midwest Research Institute, Kansas City, Mo., Report No. R111E-108, August, 1949 (Prepared for U.S.A.F.).

[12] Goland, M., *The Quasi-Steady Air Forces for Use in Low-Frequency Stability Calculations*, Journal of the Aeronautical Sciences, Vol. 17, No. 10, p. 601, October, 1950.

[13] Goland, M., and Luke, Y. L., *A Study of the Bending-Torsion Aeroelastic Modes for Aircraft Wings*, Journal of the Aeronautical Sciences, Vol. 16, No. 7, p. 389, July, 1949.

[14] *Bessel Functions, Part I, Functions of Order Zero and Unity;* British Association for the Advancement of Science, Cambridge University Press, 1937.

[15] *Tables of the Bessel Functions $Y_0(x)$, $Y_1(x)$, $K_0(x)$, $K_1(x)$, $0 \leq x \leq 1$;* National Bureau of Standards, Appl. Math. Series—1, Washington, February, 1948.

[16] *Table of the Bessel Functions $J_0(z)$ and $J_1(z)$ for Complex Arguments*, 2nd Ed.; Mathematical Tables Project, National Bureau of Standards, Columbia University Press, 1947.

[17] *Table of the Bessel Functions $Y_0(z)$ and $Y_1(z)$ for Complex Arguments;* Mathematical Tables Project, National Bureau of Standards, Columbia University Press, 1950.

[18] Rauscher, M., and Heilenday, F., Jr., *Theoretical and Experimental Methods of Flutter Analysis*, Vol. VI, p. 57; Massachusetts Institute of Technology, June 15, 1949.

Three-Dimensional Shock-Wave Reflections*

E. MIGOTSKY† AND M. V. MORKOVIN‡
University of Michigan

SUMMARY

Reflections of steady shock waves from three-dimensional bodies are analyzed by applying the sweepback principle locally along the intersection between shock and body. It is found that the mathematical analyses of two important special cases—namely, a plane shock intersecting a circular cylinder and a conical shock impinging on a plane surface—are identical because of the underlying similarity of local geometries. In both cases it is concluded that some type of Mach reflection must occur over part of the body even if regular reflection is possible at the point where the shock first reaches the body. Furthermore, the existence of an expansion wave originating on the lee side of the circular cylinder is indicated. The practical significance of these phenomena and their possible modifications in presence of a boundary layer are briefly discussed.

INTRODUCTION

SHOCK-WAVE REFLECTION in steady two-dimensional supersonic flow has been studied at length both theoretically[1–3] and experimentally.[3–5, 8] No work, theoretical or experimental, on reflection of steady shock waves from three-dimensional bodies has yet been reported in accessible literature. The extension of the relatively meager results to three dimensions is likely to be slow; the considerable difficulties encountered in the two-dimensional problem are here further complicated for both the experimental and analytical approach. Yet, there are some configurations of practical interest where the knowledge of the three-dimensional reflection would be useful: wing-body interactions, static pressure probes in proximity of shock waves, three-dimensional models in closed supersonic wind tunnels, etc. In the present paper, the principle of local sweepback is developed for the study of these reflections in absence of boundary layer. This principle is applied to the case of a plane shock impinging on an infinite cylinder aligned with the free stream and to the case of a conical shock, with its axis parallel to the free stream, reflected from a plane wall (which is equivalent to the case of intersection between two equal, symmetrically placed conical shocks). In both cases it is found that, at all Mach Numbers and at all skewed shock orientations, there exists a region where regular shock reflection cannot occur; if the shock remained plane for this irregular region, there would also be a region where no reflection at all is possible. It is planned to follow this theoretical study with experimental investigations in the University of Michigan Supersonic Wind Tunnel in the near future.

Received July 24, 1950.

* The authors wish to express their appreciation to the U.S. Air Force for sponsoring the investigation. Parts of this paper were taken from E. Migotsky's Ph.D. thesis at the University of Michigan.

† Research Associate, University of Michigan Supersonic Wind Tunnel.

‡ Associate Professor, Department of Aeronautical Engineering.

LIST OF SYMBOLS

$\boldsymbol{i}$	= curve along which the shock-wave surface intersects the body surface
$\boldsymbol{t}$	= tangent to $\boldsymbol{i}$
$\boldsymbol{n}$	= normal to the body
c	= a constant (equal to component of Mach vector normal to shock wave)
$\boldsymbol{q}$	= velocity
M	= Mach Number
θ	= shock-wave angle
δ	= angle of velocity deflection through a shock wave
ψ	= angle of yaw of $\boldsymbol{t}$ (Fig. 2)
ω	= meridian angle (Fig. 4 and 6)
S	= plane tangent to the shock surface
T	= plane tangent to the body
N	= plane normal to $\boldsymbol{t}$
V	= plane containing the local Mach vector and a generator of the body surface
x, y, z	= right-handed rectangular coordinates (Fig. 4 and 6)

Subscripts

0	= region upstream of oncoming shock
1	= downstream of oncoming shock, upstream of reflected shock
2	= downstream of reflected shock
01	= across oncoming shock
12	= across reflected shock
e	= "effective"
m	= maximum
n	= normal
t	= tangential

Prime denotes parallelism to unprimed element.

(1) TWO-DIMENSIONAL SHOCK REFLECTIONS

In absence of the boundary layer, the supersonic flow is tangent to the body upstream of the line, $\boldsymbol{i}$, where the shock impinges on the wall. Regular (also called simple) reflection of the shock is determined by the condition that the flow remain tangential to the boundary downstream from $\boldsymbol{i}$. Thus, the deflection angle δ_{01} across the oncoming shock must be equal and opposite in sense to the deflection angle δ_{12} across the reflected shock (Fig. 1).

It is well known that, for a range of upstream Mach Numbers M_0 and of oncoming shock angles θ_{01}, such de-

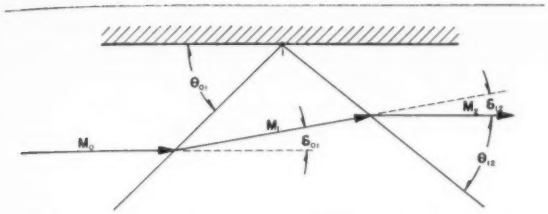

FIG. 1. Flow fields for regular shock reflection in two dimensions.

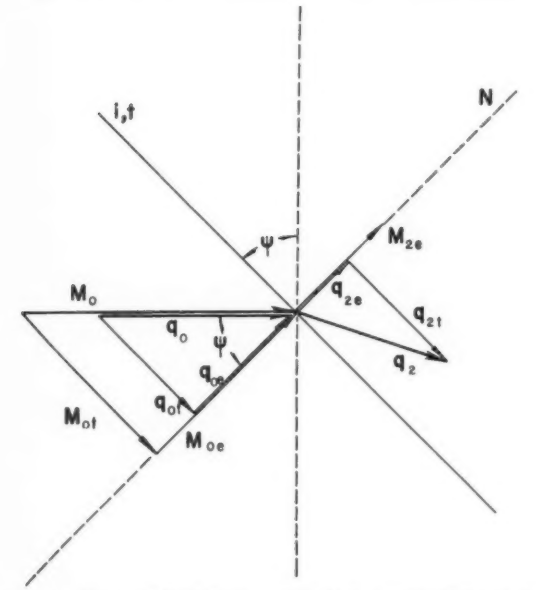

FIG. 2. Initial and final flows viewed in the plane of the wall.

flections δ_{01} and "middle" Mach Numbers M_1 (upstream M of a regularly reflected shock) occur that the maximum deflection δ_{12m} across the regularly reflected shock is less than δ_{01} and the condition of tangency is violated. The boundary of this "forbidden" range is represented by the curve A of Fig. 7; it is also given in terms of the critical δ_{01} and M_0 in Fig. 4.14 of reference 2. A second, somewhat fictitious boundary also exists; this is the curve that represents the condition for which the Mach Number M_1 behind the initial shock is equal to unity. If the shock could continue straight all the way to the wall, then this curve, denoted by B in Fig. 7, would represent the limit for any reflection, inasmuch as the flow beyond the first shock is no longer supersonic. Presumably, a Mach-type reflection occurs when the parameters M_0 and θ_{01} are in the region between A and B. It is often forgotten that steady-state reflection in the form of a Mach Y with straight shocks (which is equivalent to the "stationary" Mach reflection of reference 1) is then also impossible. Either the stem of the Y curves or the boundary-layer interaction transforms the reflection more radically, skewing the Y pattern or producing λ- and X-type patterns, often accompanied by separation. At present, such cases cannot be handled by analytical methods. In the analogous three-dimensional situation, we shall therefore restrict ourselves to the location of the forbidden zones on the body.

(2) Basic Principle of Three-Dimensional Reflection

The transition from two-dimensional to three-dimensional treatment is accomplished by first applying the sweepback principle to shock reflection. In Fig. 2, a plane skewed shock S impinges on a flat wall T (parallel to the paper) along the line $\boldsymbol{i}$ yawed by an angle ψ from the perpendicular to the free-stream M_0 direction. Since the component $\boldsymbol{q}_{0t}$ (parallel to $\boldsymbol{i}$) of the velocity vector is tangent to both the oncoming and reflected shock, it remains unchanged and therefore tangent to the body. The actual condition of tangency needs to be imposed only upon the velocity component $\boldsymbol{q}_{2e}$ in the plane N normal to $\boldsymbol{i}$. Hence, in this normal plane, one can apply directly the two-dimensional analysis corresponding to Fig. 1, using the "effective" Mach Numbers M_{0e} for the upstream Mach Number M_0 and measuring the "effective" angles θ_{01e}, δ_{01e}, etc., in N. Clearly, one has

$$M_{0e} = M_0 \cos \psi \tag{1}$$

Furthermore, dropping a plane perpendicular to the shock plane S through M_{0t}, one forms (Fig. 3) the following three triangles: one in the vertical plane V containing θ_{01}; one in the horizontal (i.e., tangential) plane T containing ψ; and one in the normal plane N containing θ_{01e}. From these triangles, it follows that

$$\sin \theta_{01e} \cos \psi = \sin \theta_{01} \tag{2}$$

Eliminating ψ between Eqs. (1) and (2), the important relation

$$M_{0e} \sin \theta_{01e} = M_0 \sin \theta_{01} \tag{3}$$

is obtained. The two sides of Eq. (3) are merely the expression for the component of the Mach vector perpendicular to the shock wave, which should govern the whole phenomenon. Therefore, Eq. (3) expresses the fact that, by considering the reflection in the normal plane N, nothing of the essential character of the phenomenon has been omitted. It also indicates that the basic parameter governing the reflection is the product $M_0 \sin \theta_{01}$ rather than M_0 and θ_{01} separately.

When the oncoming shock forms a continuously curved surface, the line $\boldsymbol{i}$ is curved and has a continuously changing tangent $\boldsymbol{t}$. It can be shown rigorously that the previous analysis still applies *locally* at any point on the curve of impingement if, in Fig. 2, the straight line $\boldsymbol{i}$ is interpreted as the tangent line $\boldsymbol{t}$. This is analogous to the application of the sweepback principle to the local direction of the sharp leading edge of a supersonic wing with variable sweepback. The proof rests on the fact that finite changes across the

shocks at the reflection curve $\boldsymbol{i}$ occur within an "infinitesimal" distance, whereas the changes in the same quantites associated with a comparable distance along $\boldsymbol{i}$ are only "infinitesimal."

A similar argument applies if the curve $\boldsymbol{i}$ is a space curve in three dimensions. The plane of Fig. 2 now becomes the plane T tangent to the body, defined by the local upstream Mach vector M_0 and the tangent line $\boldsymbol{t}$, since the condition of tangency behind the reflected shock now demands that the resulting velocity vector $\boldsymbol{q}_2$ remain in T. In Fig. 3, S represents the plane tangent to the shock surface at the point and N the plane normal to the local space direction $\boldsymbol{t}$.

Eqs. (1), (2), and (3) remain valid. From them, the basic reason for the anomaly of the reflection (say, in the case of a conical shock impinging on a flat wall in an otherwise uniform supersonic stream) can be understood. The curve $\boldsymbol{i}$ is a hyperbola with a vertex at the point nearest the apex of the cone. At the vertex there is no yaw. Let us assume that M_{01} and θ_{01} are such that at the vertex regular reflection occurs. As one follows the hyperbola on the wall, the tangent $\boldsymbol{t}$ turns continuously and the angle of yaw ψ increases. Then, according to Eqs. (1) and (2), the effective Mach Number M_{0e} in the normal plane decreases, while the effective shock angle increases. It is clear that the effective deflection angles δ_{01e} and δ_{12e} also change and that the "forbidden" range of parameters M_{0e} and θ_{01e} might be entered at some point on the hyperbola. That this is actually always the case will be shown later.

Just what would happen beyond the critical point on the hyperbola an analysis of the present type cannot show. It should be added that, during testing of cones in rectangular supersonic wind tunnels, the conical shock is not usually of constant strength, since it is softened by the expansion wave originating at the shoulder of the finite cone. Also, there is usually a well-developed boundary layer on the wall of the tunnel which may "accommodate" the needed flow deflection well beyond the critical point predicted by the above theory.

(3) Special Cases

Consider a uniform supersonic flow with an infinitely long circular cylinder oriented along the horizontal axis directed upstream (Fig. 4). A plane shock wave S, generated, say, by an unyawed two-dimensional wedge, impinges upon the cylinder at the angle θ_{01} which is measured, as customary, in a vertical plane V parallel to the $\boldsymbol{xy}$-plane. For the regular reflection, the curve of impingement $\boldsymbol{i}$, is then the elliptical intersection of the cylindrical surface with the shock plane S. At any point P on $\boldsymbol{i}$, a plane T tangent to the cylinder can be constructed; this plane contains the free-stream Mach vector M_0 attached to P and the line $\boldsymbol{t}$ tangent to $\boldsymbol{i}$. As explained in the previous section, it is now possible to apply the sweepback principle locally and

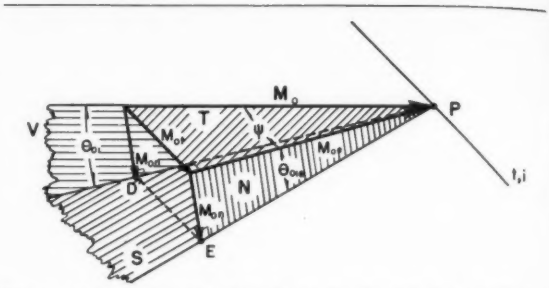

Fig. 3. Nominal and effective Mach Numbers and shock angles according to the sweepback principle.

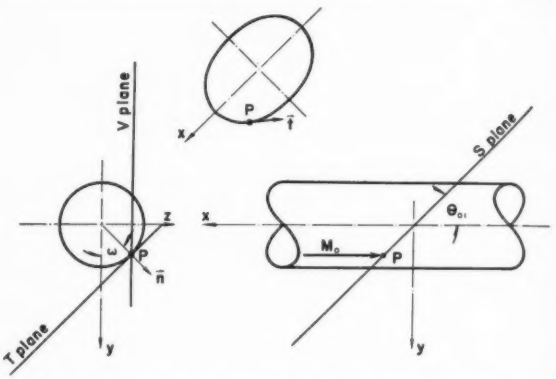

Fig. 4. Plane shock wave impinging on a circular cylinder.

to obtain Eqs. (1), (2), and (3) with the aid of a construction completely analogous to that of Fig. 3.

It is still necessary to express the two fundamental "effective" variables, M_{0e} and θ_{01e}, as functions of the location of the point P on the intersection curve $\boldsymbol{i}$. In the present case of a uniform flow and a plane shock wave, the component of the Mach vector normal to the shock, $M_0 \sin \theta_{01}$, has a constant magnitude larger than unity, say c. Eq. (3) then yields the following relation between the effective variables:

$$M_{0e} \sin \theta_{01e} = c \tag{4}$$

If the meridional angle ω between the normal to the cylinder $\boldsymbol{n}$ and the $\boldsymbol{y}$-axis (Fig. 4) is used as the parameter defining the location of point P on the intersection $\boldsymbol{i}$, it is shown in the Appendix that the "effective" wave angle is given by the simple relation

$$\cos \theta_{01e} = \cos \omega \cos \theta_{01} \tag{5}$$

Eqs. (4) and (5) completely determine the "effective" variables M_{0e} and θ_{01e}. For later purposes, it is desirable to derive from Eq. (5) the expression for $\csc \theta_{01e}$

$$\csc \theta_{01e} = \csc \theta_{01} / \sqrt{1 + \sin^2 \omega \cot^2 \theta_{01}} \tag{6}$$

It is shown in the Appendix that Eqs. (4), (5), and (6) remain valid for the case of a conical shock, with axis parallel to the uniform stream, impinging upon a plane wall, also parallel to the free stream (Fig. 6). The reasons for this duality between the reflection of a

plane shock from a cylinder and the reflection of a conical shock from a plane are also discussed in the Appendix.

(4) Discussion of Results

In Section (2) it was shown that the principles of two-dimensional shock reflection can be extended to three-dimensional reflection if the "effective" variables M_{0e} and θ_{01e} in the plane normal to the intersection line i are used rather than the true free-stream Mach Number M_0 and true shock angle θ_{01}. In particular, the boundary of the "forbidden" range, where regular shock reflection becomes impossible, is again the curve A of Fig. 7 if M_{0e} and csc θ_{01e} are the coordinates. Similarly, the curve B of Fig. 7 bounds the region of the M_{0e} and csc θ_{01e} variables for which the normal component of the velocity behind the oncoming shock wave is subsonic. In Section (3) and in the Appendix, the particular dependence of these basic variables on the parameter ω, specifying the position on the intersection curve i, is developed in the two special cases considered. For these cases, it is now possible to examine what type of reflection is to be expected at any point on the body.

The criterion for the existence of the regular reflection is that the geometry of the oncoming plane shock wave and of the body produces a combination of the effective variables M_{0e} and csc θ_{01e} which would fall above the curve A in Fig. 7. For values of M_{0e} and csc θ_{01e} falling between curves A and B, a Mach type reflection is indicated; for the values of M_{0e} and csc θ_{01e} below curve B, no reflection would be possible if oncoming shock were to remain plane. In the case of shocks with constant strength, it was seen that the possible combinations of M_{0e} and θ_{01e} are governed by Eq. (4), which can be put into the more useful form of

$$\csc \theta_{01e} = (1/c)\ M_{0e} \tag{7}$$

The advantage of using csc θ_{01e} and M_{0e} for the coordinates in Fig. 7 is seen from the fact that, for a given shock strength characterized by c, the possible combinations of these "effective" variables lie along a straight line. The intercept of this line on the ordinate csc $\theta_{01e} = 1$ is equal to c, the component of the free-stream Mach vector normal to the shock wave, which is therefore larger than unity. If the oncoming shock strength is increased monotonically from that of a Mach wave ($c = 1$), the straight-line locus of the possible combination of the "effective" variables shifts to the right and becomes increasingly flatter.* In all cases of shocks with finite strength, therefore, these loci pass through both the zones of "no reflection" and "Mach-type reflection."

In order to verify that the points on the loci in these two zones correspond to actual points on the reflecting

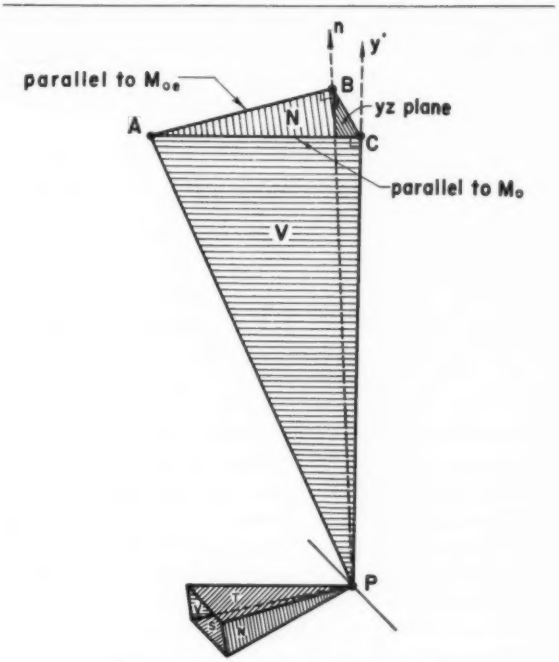

Fig. 5. Geometry leading to Eq. (5).

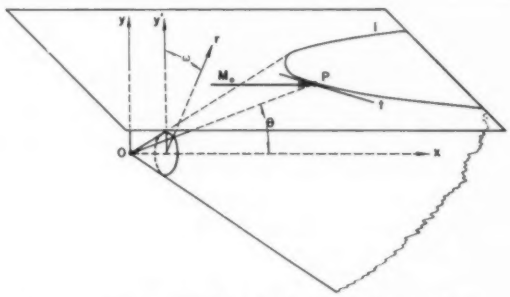

Fig. 6. Conical shock impinging on a plane surface.

body, consider Eq. (5), which relates the effective wave angle θ_{01e} with the position of the point P on the curve of intersection i. In both of the special geometries considered, let the meridional angle ω vary continuously from 0° to 90°. Then, by Eq. (6), csc θ_{01e} will decrease continuously and monotonically from csc θ_{01} to unity, the value corresponding to the intercept c. From Fig. 7 it is therefore seen that, even if regular reflection is possible for $\omega = 0$, there always exists a set of points on the intersection curve i (corresponding to $\omega_A < \omega \leqq 90°$) for which regular reflection is not possible. Furthermore, there will also exist a region ($\omega_B \leqq \omega < 90°$) in which no reflection would be possible if the shock remained plane.

As an example, consider the following configuration: $M_0 = 1.90$ and $\theta_{01} = 40°$ ($c = 1.222$). For this case, the variation of M_{0e} and θ_{01e} with ω is plotted in Fig. 8 (solid curves). The critical value ω_A is 23.8° here. If

* The loci form a one-parameter family of straight lines through (0, 0). The significance of the single parameter was pointed out in comments under Eq. (3).

the free-stream Mach Number is increased to 2.5 and θ_{01} is taken to be 29.2° (in order to keep the strength of the shock and c constant), the critical angle ω_A is increased to 36.2°; however, the region of nonregular reflection still exists.

Whereas the local shock reflection phenomena for $0° < \omega < 90°$ are identical for the two special geometries considered, there does exist a region in the case of the plane shock reflecting from the cylinder which has no counterpart in the conical shock reflecting from the plane wall. This is the region on the lee side of the cylinder ($90° < \omega < 270°$). In this region, the boundary condition at the (here fictitious) line of intersection ***i***, which requires the flow to be tangent to the body, is of opposite sense to that of the regions $0° < \omega < 90°$ and $270° < \omega < 360°$. Thus, instead of a reflected shock, an expansion wave is required to turn the flow back toward the cylinder.* If one visualized the expansion wave as originating immediately downstream from the intersection line ***i***, the Mach lines of this wave, corresponding to a reduced Mach Number, would intersect the original shock from behind and thus reduce its strength in the vicinity of the body. In fact, the strength of the expansion wave at the point corresponding to $\omega = 180°$ is sufficient to reduce the shock to zero strength. As a result, there is, on the lee side of the body, a "shadow" that weakens the shock.

In the region $0 \leqq \omega < \omega_A$ where regular reflection occurs, the analysis of the shock reflection in the normal plane N leads to the initial direction of the reflected wave at the line of intersection. However, it is impossible to predict the shape of the reflected shock away from the body without a rather difficult analysis of the complete three-dimensional flow. Still, an interesting application of the information on the initial direction of the reflected shock can be made in supersonic wind-tunnel calibration. Plane shock waves originating at the sidewalls of a tunnel are not visible with a schlieren beam passing through the side windows, but the introduction of a cylindrical body into the channel renders the reflections off the cylinder visible and thereby makes detection of sidewall shocks possible.

These considerations have assumed the fluid to be nonviscous. Actually, a boundary layer will always cover the reflecting surface. One effect of the presence of the boundary layer has been observed on schlieren pictures of bodies of revolution supported by a vertical wedge from the floor of supersonic tunnels. As the shock wave generated by the support cuts across the cylindrical body, the expansion wave on the lee side does not seem to build up to its theoretical strength,

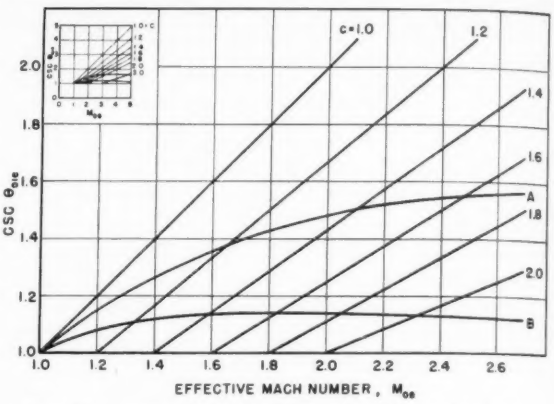

FIG. 7. Representation of the possible shock reflections.

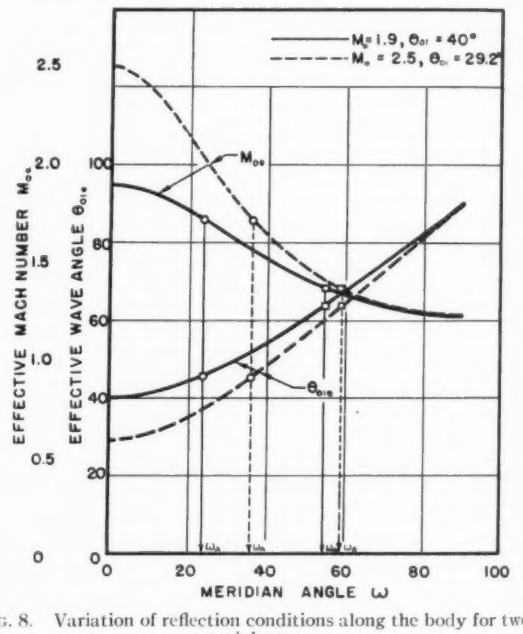

FIG. 8. Variation of reflection conditions along the body for two special cases.

and a sharp thickening of the boundary layer occurs. In some cases a deflection of 2° to 3° is thus accommodated by the boundary layer. Transition or separation of the boundary layer on bodies of revolution tested in tunnels has sometimes been ascribed to the impingement upon the body of the nose shock reflected from the walls. The preceding discussion indicates that the region on the lee side of the body is critical in this respect, perhaps more so than the region where the shock strikes the body. The implications of this tendency toward separation for wing-body configurations are clear.

In the region where Mach-type reflection is indicated, the boundary layer may thicken and even separate. This is the region where strongest anomalies are expected because the reflected shock should be relatively

* Here, it is useful to visualize an existing plane shock pierced by the cylinder and call "reflection" the complete field, which would account for the distortion of the shock from its plane form and constant strength. The point of view of refraction of a shock wave around the cylinder would probably be more fruitful if linearized methods of analysis were used.

strong. It is difficult to visualize a discontinuous change in the vicinity of ω_A.

Clearly, the location of the critical regions on the body, $\omega_A < \omega < 90°$, makes it difficult to observe the actual phenomenon by optical methods. This undoubtedly explains why no similar anomalies have been seen thus far. Experiments designed to clarify the behavior of the shock and boundary layer in some of these regions are scheduled in the 8- by 13-in. supersonic tunnel at the University of Michigan.

It is paradoxical that investigations of any shock, and in particular of the shock reflected from a body, by probing with a thin static pressure "needle" from behind are likely to be inaccurate because of the same phenomenon; the shock is impinging on the cylindrical body of the probe. It would seem desirable to place the orifices at meridional positions 90° from that at which the shock first intersects the probe; at these points the pressure is least likely to be disturbed.

(5) Concluding Remarks

The sweepback principle applied locally at points along the line of intersection of a shock-wave surface and a three-dimensional body makes it possible to analyze what type of reflection should take place in absence of the boundary layer. For the important special cases of a plane shock impinging on a cylindrical body and a conical shock impinging on a plane wall, the mathematical analyses are identical because of the underlying similarity of local geometries. In both cases it is concluded that, even if regular reflection is possible at the points on the zero meridian $\omega = 0$ where the shock first impinges upon the body, there will always be a region $\omega_A < \omega < \omega_B$ where regular reflection must be replaced by some type of a Mach reflection and a region $\omega_B < \omega < 90°$ where no reflection would be possible if the shock remained plane. Furthermore, the existence of an expansion wave originating along the line of shock intersection on the lee side of the circular cylinder is indicated. These phenomena, whether appreciably modified by the presence of the boundary layer or not, may have practical implications for wing-body interactions, testing of three-dimensional models in rectangular supersonic tunnels, pressure probing near shock waves, etc.

References

[1] Courant, R., and Friedrichs, K. O., *Supersonic Flow and Shock Waves*, pp. 318–350; Interscience Publishers, New York, 1948.

[2] Lees, L., *Interaction Between the Laminar Boundary Layer Over a Plane Surface and an Incident Oblique Shock Wave*, Princeton University, Aero. Engin. Lab., Report No. 143, January, 1949.

[3] Ashkenas, H., Dhawan, S., Liepmann, H. W., Marble, F., and Roshko, A., *Problems in Shock Reflection*, GALCIT Report to A.A.F., 1948.

[4] Fage, A., and Sargent, R. F., *Shock Wave and Boundary Layer Phenomena Near a Flat Surface*, Proceedings, Royal Society A, Vol. 190, 1947.

[5] Geiger, F., and Kajencki, S., *Two-Dimensional Simulation of Boundary Layer Shock Wave Interaction in Ostwatitch Diffusors*, Cornell Aero. Lab., G. E. Report No. 55237, November, 1947.

[6] Liepmann, H. W., and Puckett, A. E., *Aerodynamics of a Compressible Fluid*, p. 61; John Wiley & Sons, Inc., New York, 1947.

[7] Shapiro, A. H., Neumann, E. P., and Barry, F. W., *Some Experiments on the Interaction of Shock Waves with Boundary Layers on a Flat Plate*, M.I.T. Gas Turbine Lab., Meteor Report No. 29, October, 1948.

[8] Liepmann, H. W., *Boundary Layer Shock Wave Interaction*, pp. 39–66, Symposium on Experimental Compressible Flow, U.S. NOL, Memorandum No. 1133, June, 1949.

Appendix

In general, relations of the type of Eq. (5) can be derived most easily with the aid of vector analysis; in the present case it is obtained from the following geometrical construction shown in Fig. 5: The vertical plane V and the normal plane N through the point P as seen in Fig. 3 are extended beyond P into the body of the cylinder if necessary. The $\boldsymbol{yz}$ plane is also made to pass through P. Finally, a plane T' parallel to the tangent plane T is constructed so that it forms a tetrahedron $PABC$ with the three planes V, N, and $\boldsymbol{yz}$. The edge AC between T' and V is parallel to the free-stream Mach vector and the generators of the cylinder; AC makes, therefore, a right angle with all the lines in the $\boldsymbol{yz}$ plane, in particular with CB and CP (which is parallel to the $\boldsymbol{y}$ axis). The edge PB is identified with $\boldsymbol{n}$, the normal to the cylinder at P—as a line in the normal plane N, it is perpendicular to the tangent line $\boldsymbol{t}$; as a line in $\boldsymbol{yz}$ plane, it is perpendicular to the generators of the cylinder. Hence, $\boldsymbol{n}$ (PB) makes a right angle with the edges BA and BC located in the T' plane. Furthermore, the angle between $\boldsymbol{n}$ and PC in the $\boldsymbol{yz}$ plane is equal to ω by definition. As an intersection between the vertical plane V and the normal plane N, the edge AP is normal to the shock plane S and to the lines DP and EP of Fig. 3 used in defining the shock angles* θ and θ_c. Hence, by plane geometry, the angle between AP and CP in the vertical plane V is equal to θ, and the angle between AP and BP in the normal plane N is equal to θ_c.

Having identified the three angles at P of the tetrahedron as ω, θ, and θ_c, one obtains the required relation (5) from the identity of ratios

$$\overline{BP}/\overline{AP} \equiv (\overline{BP}/\overline{CP})\ (\overline{CP}/\overline{AP})$$
$$\cos\theta_c = \cos\omega \cos\theta$$

The case of a conical shock, with axis parallel to the uniform supersonic stream, impinging upon a plane

* Since the Appendix is concerned with the oncoming shock wave only, the subscript 01, which differentiates between it and the reflected shock, is dropped everywhere.

(*Continued on page 504*)

The Laminar-Turbulent Transition in a Boundary Layer*—Part I†

H. W. EMMONS‡
Harvard University

SUMMARY

A theory of transition from laminar to turbulent flow is developed from some new observations of the transition phenomena. Every point of a body is turbulent a fraction of the time, and a formula is derived for this fraction in a phenomenological manner. Application of the theory to available flat plate data gives some insight into observed effects and shows the way to additional experimental results required.

INTRODUCTION

THE BOUNDARY LAYER that grows on the surface of any body is at first laminar. Any fluctuations with time which are carried in from the free-stream turbulence, which are carried in by the passage of sound waves, or which are produced by roughness on the body or by vibrations of the body are generally damped rapidly near the leading edge.

As one proceeds downstream from the leading edge, confused time-dependent velocities arise which consume the laminar boundary layer and replace it by a more rapidly growing and thicker turbulent one. Data on the overall drag of bodies clearly show the characteristic values of laminar drag at low Reynolds Numbers and the characteristic values of turbulent drag at high Reynolds Numbers. In between there is a more or less extensive region of transition from one to the other.

The laminar-flow drag and heat-transfer coefficients agree well with theoretical results where the calculations have been carried out. The turbulent flow, while too complex to permit a basic theory as yet, gives experimental drag and heat-transfer coefficients that correlate well against the appropriate dimensionless variables, Reynolds Number and Prandtl Number. Transition data have not been treatable in either way, so that at present no precision of prediction is possible if transition conditions are encountered.

It has appeared empirically that there is a critical value of Reynolds Number at which transition starts. Fig. 1 shows the data of Schubauer and Skramstad[1] and of Hall and Hislop[2] for a flat plate lined up carefully with the air in a zero pressure gradient wind tunnel. The apparent agreement is belied by the authors' statements that the Reynolds Numbers given were the "approximate beginning and end of transition" and "the mean transition position" in the two references, respectively. The unsteady nature of transition prevents more precise work on critical Reynolds Numbers.

It has long been known that the theoretically derived laminar-flow formulas are correct solutions for all Reynolds Numbers. Thus, turbulent flow appears as a more stable, though nonsteady, type of flow which replaces the laminar flow. Considerations of stability of the laminar boundary layer by many authors (see, for example, Lees[3]) show that the damping of infinitesimal disturbances in the laminar boundary layer depends upon the Reynolds Number, the disturbance frequency, and the rate of heat transfer. A typical curve is given as Fig. 2. The amplified frequencies appear as measurable Tollmein-Schlichting waves in the boundary layer as shown by Schubauer and Skramstad.[1] The agreement between computed and experimentally determined neutral curves is fair. The differences may well be caused by the fact that the experimental disturbances were finite.

No theory has yet been attempted on the effects of finite disturbances on a boundary layer. The nonlinear nature of this problem has, and will for some time, continue to block further progress in this direc-

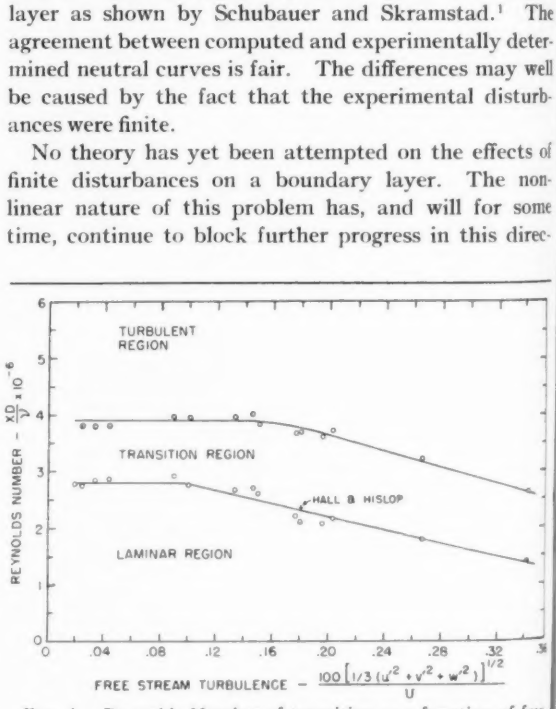

FIG. 1. Reynolds Number of transition as a function of free-stream turbulence for a flat plate in a flow without pressure gradient.[2]

Received November 18, 1950.

* The author is indebted to A. E. Bryson for extensive discussions and assistance with the numerical work, to Dr. Edwards for some useful suggestions leading to the solution of the basic integral equation, and to the Hughes Aircraft Company for providing the stimulating atmosphere in which this fundamental investigation was carried out.

† Part II will be published in the *Proceedings of the First U.S. National Congress of Theoretical and Applied Mechanics.*

‡ Gordon McKay Professor of Engineering Science.

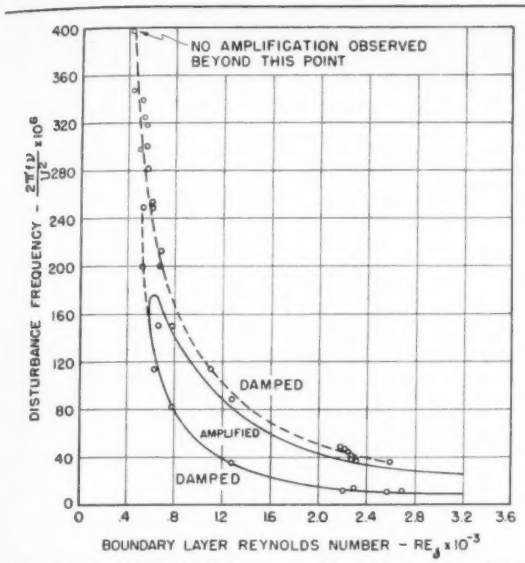

FIG. 2. Schlichting's laminar boundary-layer curve (*solid*). Frequency of disturbances vs. Reynolds Number. Experimental points (*dashed*) by Schubauer and Skramstad.

tion. On the other hand, correlation of transition data has not been successful, as Fig. 3 (taken from Schoenherr[4]) shows. von Kármán[5] has stated in this connection: "However, in view of the Schoenherr curves, it must be remarked that the transition phenomenon is probably too unstable to be represented by a simple equation."

A New Observation

During the past year, a simple water-table analogy to supersonic flow was completed at Harvard as a student demonstration. On this table, water flows in a $^1/_8$- to $^1/_4$-in. deep layer over a nearly horizontal piece of plate glass about 3 by 6 ft. The velocity and volume flow of the water are controlled by the adjustment of the tilt of the glass plate and the adjustment of a by-pass to the pump. It was observed that, in addition to the anticipated "supersonic" phenomena, laminar to turbulent transition was obtained.

The mechanics of transition could be clearly observed, since the turbulent motion of the thin layer of water disturbed the water surface and, hence, altered the appearance of the surface in both reflected and transmitted light. Fig. 4 shows a plane view of the glass plate with water flowing over it. At some instant and at some point (both random), a tiny spot of turbulence appeared as at *S*. The spot was small and of irregular shape. This spot grew as it was washed along with the boundary-layer fluid. The approximate shape and size of the spot after a period of growth is shown at *A* in Fig. 4, as is also the locus of successive spot positions. Each turbulent spot was washed off the end of the plate. At random times, spots appeared at random locations over the plate surface. These tiny turbulent origins will be called "turbulent sources" (more briefly "sources"). Sources could be increased in density and frequency at a given location on the plate either by increasing the water velocity or adding disturbances by placing an object (finger) in the deep (low-velocity) water well ahead of the plate. A disturbance (as a vertical wire) placed directly into the water on the plate acted as a continuous source, as at *B* of Fig. 4, and thus filled a sector of the plate surface with turbulent water.

The growing spot approximately preserved its shape as it grew, and the locus of successive spot positions appeared straight and at the same angle as the continuous turbulence from a wake. These facts suggest that the oriented vorticity of the laminar boundary layer is confused at the edge of the spot by the velocities induced (in the oriented flow) by the already confused vorticity of the turbulent region. Thus, the spot grows at each point normal to its surface by consuming the laminar region. The velocity of turbulence propagation would be expected to be a function of the angle between the spot normal and the local direction and strength of the oriented vorticity. (The noncircular spot shape shows the direction of the normal to be important.) The initial vorticity is important because a turbulent region spreads through a boundary layer much faster than into the potential flow region outside of the boundary layer.

The turbulence in transition is thus seen to be essentially intermittent. Each point of the plate is covered by a laminar boundary layer, except during those periods of time during which a turbulent spot moves over it. Since spots grow as they move, the downstream points of the plate are covered for greater fractions of the time by a turbulent layer. In fact, the spots soon overlap and cover downstream portions continuously.

No quantitative measurements have yet been made on the water table, so that other evidence must be used at present for evaluating the spot characteristics. Although the above-detailed process has not been described before, there is abundant evidence that the same process occurs generally.

Charters[6] discovered that turbulence in a boundary layer on a flat plate in a wind tunnel grew over the plate from the edges where the plate was supported at the tunnel walls. The boundary between the laminar and turbulent region was mapped out by hot-wire exploration and was found to be a straight line making an angle with the free stream of about 9.6°. Such straight-sided turbulent areas could also be produced by allowing the (eddying) wake from a body to strike the plate boundary layer. These effects describe precisely the continuous sources mentioned above.

Schubauer and Skramstad,[1] while studying the growth of the Tollmien-Schlicting waves in the laminar boundary layer, observed that, at a sufficient distance from the

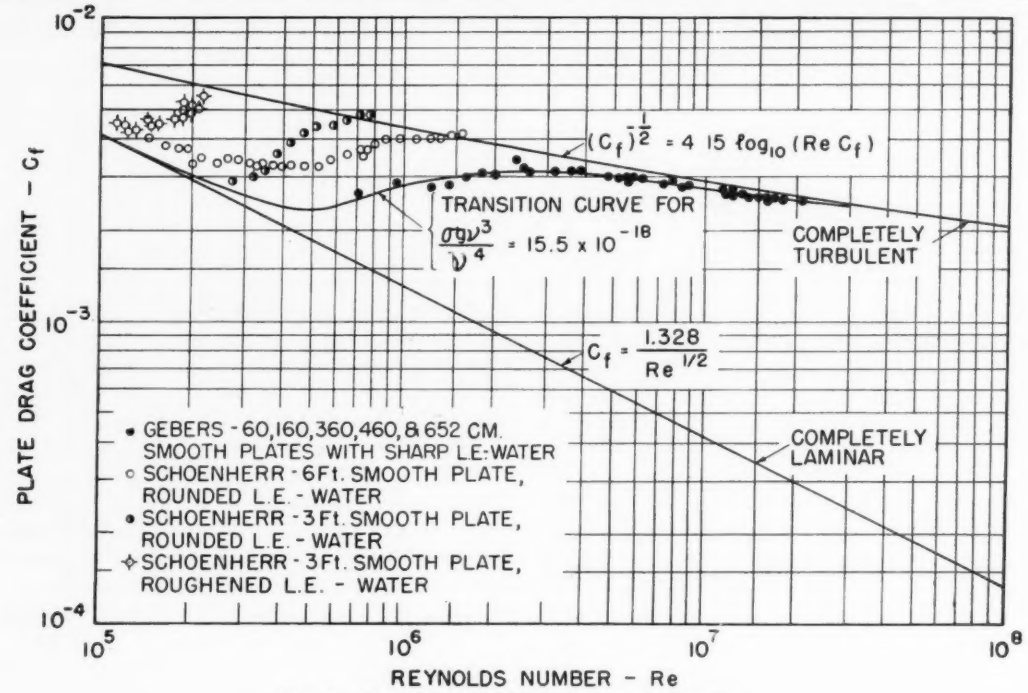
10^{-2}
10^{-3}
10^{-4}
PLATE DRAG COEFFICIENT - C_f
$(C_f)^{-\frac{1}{2}} = 4.15 \log_{10}(Re\, C_f)$
TRANSITION CURVE FOR
$\frac{\sigma g \nu^3}{\nu^4} = 15.5 \times 10^{-18}$
COMPLETELY TURBULENT
$C_f = \frac{1.328}{Re^{1/2}}$
COMPLETELY LAMINAR
• GEBERS - 60,160,360,460,& 652 CM. SMOOTH PLATES WITH SHARP LE-WATER
○ SCHOENHERR - 6Ft. SMOOTH PLATE, ROUNDED L.E. - WATER
• SCHOENHERR - 3Ft. SMOOTH PLATE, ROUNDED L.E. - WATER
✧ SCHOENHERR - 3Ft. SMOOTH PLATE, ROUGHENED L.E. - WATER
10^5
10^6
10^7
10^8
REYNOLDS NUMBER - Re

FIG. 3. Plate drag coefficient vs. Reynolds Number.[4]

plate leading edge, the hot-wire record showed more or less frequent bursts of turbulence interrupting the otherwise relatively low-frequency smooth wave pattern. These bursts would, by present theory, be interpreted as the passage of turbulent spots over the wire.

Charters (personal communication) has recently obtained some spark photographs of a projectile in flight on a range at Aberdeen Proving Ground which show a boundary layer partly turbulent and partly laminar (see Fig. 5). The turbulent spots were different at each spark station along the flight path. This appears to be good evidence that the above-described transition process occurs in a boundary layer in air at supersonic speed. The fact that the boundary layer on some projectiles is wholly turbulent can probably be ascribed to fixed disturbances in the projectile geometry.

The transition from laminar to turbulent flow is therefore to be visualized as follows: Viscosity builds a laminar boundary layer completely covering the given body (this may include regions of separation). This boundary layer is disturbed (in space, time, frequency, and amplitude) by random motions carried in by the fluid from the free stream, carried in through the fluid as sound waves, produced in the boundary layer by surface irregularities, or produced by the vibrations of the plate. Each of these disturbances amplifies or damps as it moves along the surface. The sum total of these disturbances is to be visualized as disturbing the calm of the laminar boundary layer in the same way as random waves disturb the calm of the sea.

At each point of the laminar boundary layer there is assumed to be a certain critical (finite) amplitude (and perhaps critical frequency range) which, when exceeded by a disturbance, is capable of causing the oriented vorticity of the laminar flow to be replaced by the confused motion of turbulence, just as the waves of the ocean may break into white caps. As the ocean waves approach the shore, their amplitudes (and frequency) change, so that at random points the wave tips break. Similarly, in the laminar boundary layer the amplitude and frequency of disturbances and the critical conditions change with the distance from the leading edge. Every now and then at various points, the boundary-layer disturbances "break" (whatever this may mean), and the flow becomes locally turbulent

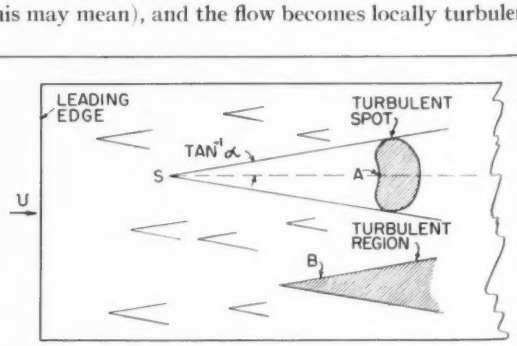

FIG. 4. Transition on a flat plate.

—a turbulent spot has been born. From this spot, the confusion grows in all directions (relative to the fluid), carrying all before it. Thus, the flow at any point on the body will be laminar part of the time and completely turbulent for the remainder. Transition is thus a random phenomenon, which can be described by a probability function specifying the fraction of the time that the flow at each point is turbulent.

Probability Transition Theory

In order to develop a quantitative formulation of the transition process, we assume the existence of a function $g(x, y, t)$ of position (on the surface) and time which specifies the rate of spot production per unit area. Each spot so produced must be followed in its subsequent history. These spots grow and overlap as described before. Thus, if the fraction of the time $f(x, y)$ that a given point $P(x, y)$ is turbulent is to be computed, we must add up the times that it is covered by spots (originating upstream somewhere). In this summation, however, we must not count twice those portions of spots which overlap.

To do this, consider an x, y, t space, Fig. 6, where x, y are coordinates on the body surface and t is the time—the coordinate x to be taken along spot transport stream lines. A source at P_0 produces a spot that, on the body surface (projection in the x, y plane), moves and grows as described above. In the x, y, t space, the spot sweeps out a volume of a shape dependent upon the manner and rate of spot movement and growth. Since the spot is swept away by the stream (does not propagate ahead of its source—if it did, the spot would be self-sustaining and the body would be permanently covered by turbulence) and grows relative to the fluid, the volume will always diverge from P_0 in a conelike manner. We shall call this the "propagation cone" for a source at $P_0(x_0, y_0, t_0)$—its surface elements are propagation rays of the spot (the rays may or may not be straight).

We are interested in finding the fraction of the time that a given point $P(x, y, t)$ is turbulent. P will be turbulent if a source has occurred upstream ($x_0 < x$) at such a time that P lies in the propagation cone from P_0. The locus of all points P_0 which can influence the state of turbulence at point P is a volume upstream of P as shown in Fig. 7. This volume is also conelike and has generators that are propagation rays drawn *upstream* from P. This will be called "the dependence volume"—R for P. If there is only one source, then P is turbulent if that source is in R; otherwise, P is laminar. Thus, the probability of turbulence at P due to a source at P_0 is

$$\varphi(P, P_0) = \begin{cases} 1 \text{ if } P_0 \text{ is in } R \\ 0 \text{ if } P_0 \text{ is not in } R \end{cases} \qquad (1)$$

In a volume element dV_0 ($= dx_0\, dy_0\, dt_0$) at point P_0, there will be $g(P_0)\, dV_0$ sources, each of which will cause

FIG. 5. Spark photograph of projectile showing turbulent boundary-layer spot (by A. C. Charters, Aberdeen Proving Ground).

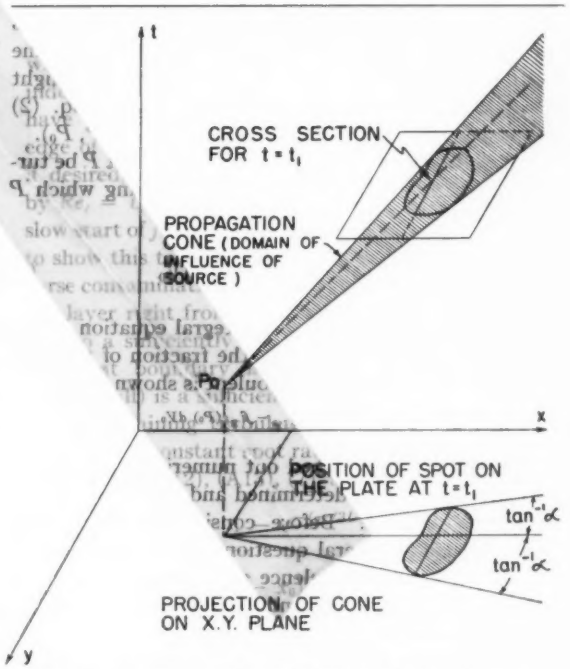

FIG. 6. Propagation of a turbulent spot in x, y, t space.

P to be turbulent with probability $\varphi(P, P_0)$. We cannot find the fraction $f(P)$ of the time that P is turbulent by integrating $\varphi(P, P_0)g(P_0)\, dV_0$ however, since there may be more than one source in R and the resultant turbulence at P would thus be counted twice. To avoid these overlaps, we shall assume that the turbulence produced nearest the leading edge of the body will be counted as causing the turbulence in the spot overlap regions. There is some physical justification for

this assumption in that the turbulent boundary layer grows faster than the laminar one and, hence, the spot that has traveled furthest will generally be thicker. Until many of the physical parameters are better known, this assumption makes little (sometimes no) difference as compared with other plausible assumptions.

Let $\psi(P, P_0)\, dV_0$ be the probability that the flow at P be turbulent because of sources in dV_0 at P_0 but not because of any source at $P_0{}^1(x_0{}^1, y_0{}^1, t_0{}^1)$ with $x_0{}^1 < x_0$—i.e., the source at P_0 is to be counted only if it is the point nearest the leading edge that is affecting P. The probability $\psi(P, P_0)\, dV_0$ is connected with $g(P_0)$ by

$$\psi(P, P_0)\, dV_0 = \varphi(P, P_0)\, g(P_0)\, dV_0 \times \left[1 - \int_{R^1} \psi(P, P_0{}^1)\, dV_0{}^1\right] \quad (2)$$

where R^1 is the portion of the influence volume R for P which lies between the leading-edge plane $x = 0$ and the plane through $x = x_0$. The factor

$$\left[1 - \int_{R^1} \psi(P, P_0{}^1)\, dV_0{}^1\right]$$

is the fraction of the time that P is laminar so far as sources ahead of x_0 are concerned and, hence, is the fraction of the time during which a source in dV_0 might be effective in producing turbulence at P. Eq. (2) is to be regarded as an integral equation for $\psi(P, P_0)$.

After $\psi(P, P_0)$ is found, the probability that P be turbulent—the fraction $f(P)$ of the time during which P is turbulent—is

$$f(P) = \int_R \psi(P, P_0)\, dV_0 \quad (3)$$

The general solution of the integral equation is carried out in Appendix (I), and the fraction of the time during which a point P is turbulent is shown to be

$$f(P) = 1 - e^{-\int_R g(P_0)\, dV_0} \quad (4)$$

This can now be worked out numerically as soon as the function $g(P_0)$ is determined and the influence volume R is defined. Before considering these questions, one other general question should be examined. The record of the turbulence at a given point on the body would show turbulent and laminar periods following one another. The frequency and size of the turbulent bursts can be computed. Spots from various sources pass over P, without necessarily being separated by laminar regions. We shall call the number of sources that contribute to the turbulence at P "the spot frequency $N(P)$," whether or not the spots are separated by laminar flow. The number of distinct spots would be somewhat less than this.

To find the spot frequency $N(P)$, observe that during a time τ, point P will be turbulent for $\tau\psi(P, P_0)\, dV_0$ sec. because of sources in dV_0. Each spot from a source at P_0 will cause P to be turbulent for $\Delta t(P, P_0)$ sec., where Δt is the y_0 = constant chord of the $S(P, x_0)$ cross section of R as shown in Fig. 7. Hence, the number of spots passing P from sources in dV_0 as P_0 in τ sec. is

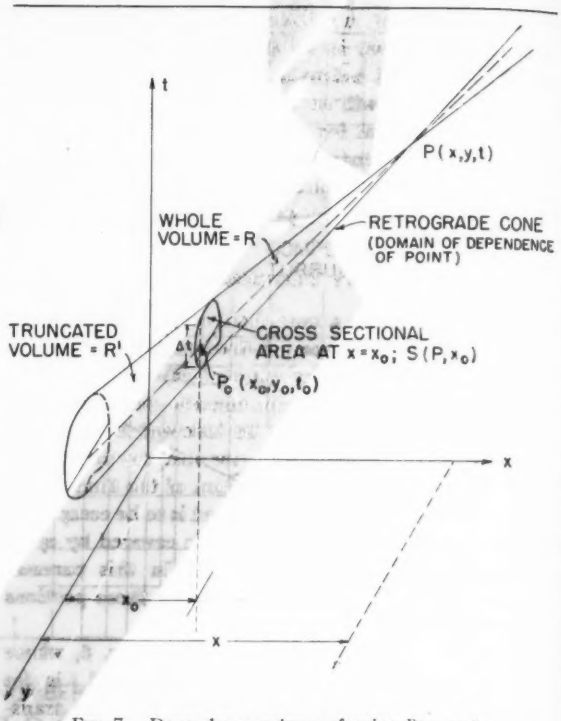

FIG. 7. Dependence volume of point $P(x, y, t)$.

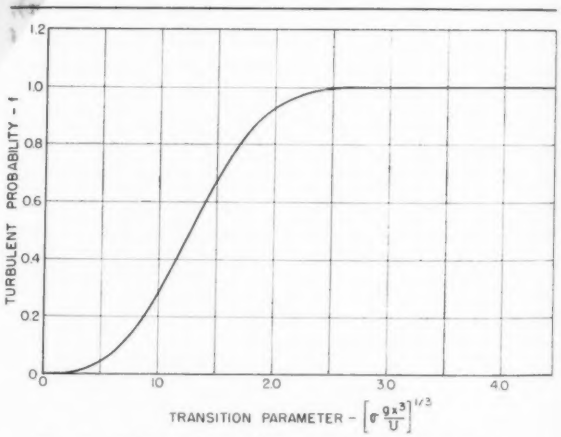

FIG. 8. Turbulent probability vs. transition parameter.

$$\tau\psi(P, P_0)\, dV_0/\Delta t \quad (5)$$

The spots per second passing P from dV_0 at P_0 is

$$dN = \psi(P, P_0)\, dV_0/\Delta t \quad (6)$$

and the total number of spots per second passing P is

$$N(P) = \int_R \frac{\psi(P, P_0)\, dV_0}{\Delta t} = \int_R \frac{g(P_0) e^{-\int_R g(P_0)\, dV_0}}{\Delta t}\, dV_0 \quad (7)$$

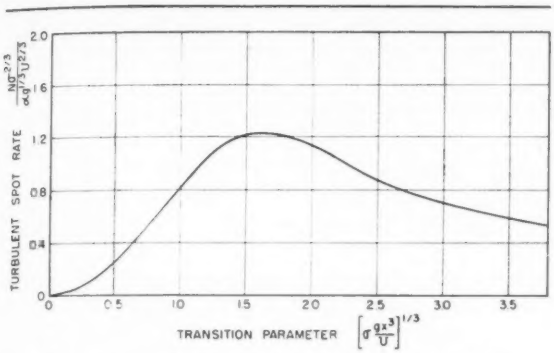

FIG. 9. Dimensionless turbulent spot rate vs. transition parameter.

The average duration of a turbulent spot is then

$$T = f/N \tag{8}$$

TRANSITION THEORY FOR A FLAT PLATE

To make application of the preceding theory to transition on a flat plate, it is necessary to know the source rate density $g(x, y, t)$ and the propagation constants for the resultant turbulent spot. Until further experimental work has been done (a theoretical approach to source production appears difficult), no definite information on g is available. As a first and simplest assumption, g will be taken as independent of position on the plate. For a steady mean flow, g will be independent of the time.

Again, for the spot propagation constants more experimental work is needed before precise values can be known. (A theoretical approach is probably feasible, although it has not yet been attempted.) We shall assume that each point of the spot boundary propagates at a constant rate away from the source. Thus, the propagation cone of Fig. 6 is a true cone with straight generators. (It is not a circular cone, however.) The dependence volume R is also a true (noncircular) cone.

Therefore, the integral of importance is

$$\int_R g \, dV = gV \tag{9}$$

where V is the volume of the dependence region of x. The volume of a cone is one-third the area of the base A_b times the altitude

$$V = A_b x/3 = A_1 x^3/3 \tag{10}$$

where A_1 = cone cross section at unit distance from the apex = area of $S(x, x_1)$ at $x - x_1 = 1$. Therefore,

$$A_1 = \frac{1}{(x - x_1)^2} \int_{x \text{ constant section of cone}} dy_1 \, dt_1 = \frac{\sigma}{U} \tag{11}$$

The x = constant cross section of the dependence cone may be considered the "time-width shape" of a spot. It could be measured by noting the time history of a spot as it passes over a line at a fixed distance x from the leading edge of the plate. Thus, the parameter σ is a dimensionless propagation parameter of the spot.

The area of the x = constant cross section of the cone can be obtained from the t = constant cross section (spot) as shown in Appendix (II). Thus, the dimensionless x = constant cross-section area of the propagation cone is given in terms of the turbulent spot dimensions by

$$\sigma = \alpha^2 \lambda / \beta \tag{12}$$

where

α = tan (one-half propagation angle) = 0.17 [see Fig. 4 and Eq. (19)]

$$\beta = \frac{\text{velocity of center of spot}}{\text{free-stream velocity } U}$$

$$\lambda = \frac{\text{area of spot}}{\text{square of half width}}$$

The fraction of time that x is turbulent thus becomes

$$f(x) = 1 - e^{-\sigma g x^3/3U} \tag{13}$$

which is plotted as Fig. 8. Although g was assumed independent of x in the above derivation, it does not have to be considered as starting from the leading edge of the plate—i.e., x in the above formulas could, if desired, be measured from a critical value x_c given by $Re_c = Ux_c/\nu$ = constant. However, in view of the slow start of $f(x)$, there is insufficient data now available to show this to be necessary. Furthermore, the transverse contamination of Charters[6] shows that the boundary layer right from the leading edge is unstable relative to a sufficiently violent disturbance of which the turbulent boundary layer along another body (the tunnel wall) is a sufficient sample.

The remaining turbulence characteristics for a flat plate with a constant spot rate density now follow from Eqs. (A10), (A12), (A13), (7), and (8).

$$F(x, x_0) = 1 - e^{-(\sigma g/3U)\,[X^3 - (x - x_0)^3]} \tag{14}$$

$$\phi(x, x_0) = \frac{\sigma g}{U} (x - x_0)^2 e^{-(\sigma g/3U)\,[x^3 - (x - x_0)^3]} \tag{15}$$

$$\psi(x, x_0) = \varphi(x, x_0) g e^{-(\sigma g/3U)\,[x^3 - (x - x_0)^3]} \tag{16}$$

$$N(x) = 2\alpha g e^{-\sigma g x^3/3U} \int_0^x \zeta e^{-\sigma g \zeta^3/3U} \, d\zeta \tag{17}$$

$$T(x) = \frac{e^{\sigma g x^3/3U} - 1}{2\alpha g \int_0^x \zeta e^{-\sigma g x^3/3U} \, d\zeta} \tag{18}$$

Of these, the number of turbulent spots passing a point x is plotted as in Fig. 9.

The values of the "constants" σ and g can only be crudely estimated from currently available data. The most important constant g can best be estimated

by fitting the present theory to the small amount of transition data available.

The spot characteristic σ can, at present, be estimated as follows: The spread of the permanent turbulence of transverse contamination was measured by Charters.[6] The angle was about 9.6°. Thus, for present purposes,

$$\alpha = \tan^{-1} 9.6 = 0.17 \tag{19}$$

The value of β can be estimated from the recent spark photograph, Fig. 5. A small shock wave is visible at the edge of the turbulent spot and is at an angle different from the Mach waves in this region. Since a spot is a (supersonically) small disturbance, the shock angle is evidence of the spot velocity relative to the projectile. From this photo,

$$\beta = 0.43 \tag{20}$$

that is, the spot travels at about one-half of the free-stream velocity.

The value of λ which depends approximately upon the spot area can be estimated at present only by the spot appearance as visually observed. The spot looks about as shown in Fig. 4 and, hence,

$$\lambda \approx 2 \tag{21}$$

Thus,

$$\sigma = \alpha^2\lambda/\beta \approx 0.134 \approx 0.1 \tag{22}$$

In view of the crudeness of the approximations, σ will be taken as 0.1.

We note that σ above was evaluated from some low subsonic boundary-layer tests, some supersonic tests, and water flow in a sheet (not a real boundary layer). It is an assumption that must be eliminated by further tests or theory that the spot propagation constants are the same for such diverse conditions.

Transition Drag on a Flat Plate

The drag on a flat plate arising from the laminar boundary layer near the leading edge is given by the theoretical formula

$$C_{fl} = \tau/(1/2)\rho U^2 = 0.664/Re^{1/2} \tag{23}$$

The corresponding mean friction coefficient is

$$C_{Dl} = D/(1/2)A\rho U^2 = 1.328/Re^{1/2} \tag{24}$$

If the boundary layer is turbulent, the local friction coefficient is given by the semiempirical formula

$$1/\sqrt{C_{ft}} = 1.7 + 4.15 \log_{10} (ReC_{ft}) \tag{25}$$

The corresponding mean friction coefficient is given by

$$1/\sqrt{C_{Dt}} = 4.15 \log_{10} (ReC_{Dt}) \tag{26}$$

Using a C_{ft} based upon the distance from the leading edge, the mean local coefficient is

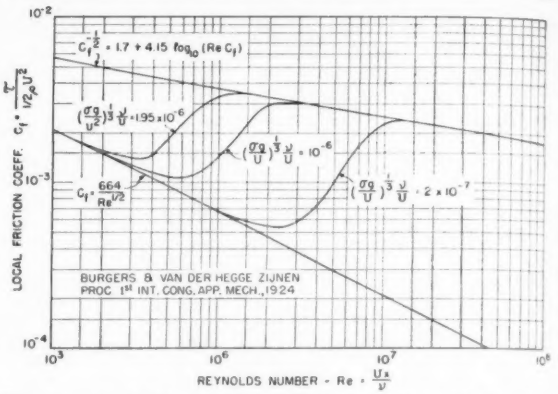

FIG. 10. Local skin friction coefficient vs. Reynolds Number (transition curves varying x).

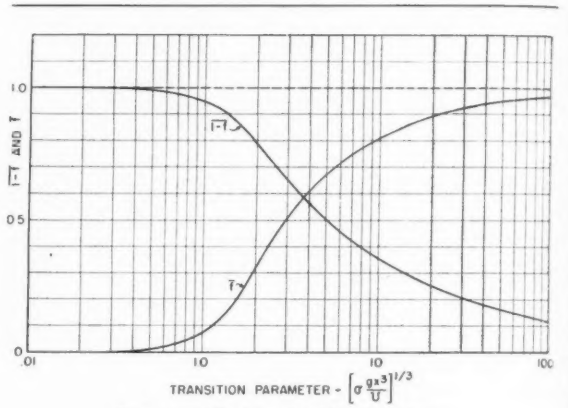

FIG. 11. Mean probability functions.

$$C_f = C_{ft}(1 - f) + C_{ft}f \tag{27}$$

Fig. 10 shows these coefficients for several values of the transition parameter $\sigma g\nu^3/U^4$. Measurements of the surface velocity gradient at various points along a glass plate by Burgers and van der Hegge Zijnen[7] have been converted to local friction coefficients and are compared with the theoretical curves. The reason for the poor agreement in both laminar and turbulent regions has not been investigated. More local coefficient data are badly needed.

In Fig. 10 we note that, although no critical Reynolds Number has been assumed, the different values of $\sigma g\nu^3/U^4$ lead to different curves, which could well have been interpreted as implying a critical Reynolds Number. We further note that, as the spot rate density g is increased, the transition region moves forward on the plate and becomes narrower.

If we define "the transition point" x_t as the point on the plate which is turbulent just half of the time, then

$$\sigma g x_t^3/U = 2.077 \tag{28}$$

or

$$x_t = 1.278\,(U/\sigma g)^{1/3} \tag{29}$$

This relation, while a basic one, will not become useful until further study (much of it experimental) permits the prediction of σ and g.

The transition curves of Fig. 10 are to be considered as those appearing at various points along a plate—not those at a fixed point of a plate as the velocity or viscosity varies the Reynolds Number. The source rate density g has not been assumed independent of U and ν, and, in fact, it seems unlikely that this is so. Therefore, it is not correct to attempt to deduce a critical Reynolds Number from the present theory. In fact, such a Reynolds Number probably does not exist with any great precision.

The mean values of the coefficients for the whole plate can be derived by integrating the local values

$$C_D = \frac{1}{L}\int_0^L C_f\,dx = \frac{1}{L}\int_0^L (1-f)\,C_{fl}\,dx + \frac{1}{L}\int_0^L f\,C_{ft}dx \quad (30)$$

This may be expressed in the form (by assuming $C_f = A/Re^n$)

$$C_D = C_{Dl}\overline{(1-f)} + C_{Dt}\bar{f} \quad (31)$$

where C_{Dl} is the mean coefficient for the plate if the whole boundary layer were laminar, where C_{Dt} is the mean coefficient for the plate if the whole boundary layer were turbulent, and where

$$\overline{1-f} = \frac{1}{2z^{1/2}}\int_0^z \frac{1-f}{z^{1/2}}\,dz$$

$$\bar{f} = \frac{1-n}{z^{1-n}}\int_0^z \frac{f}{z^n}\,dz$$

$$z^3 = \sigma g x^3/U$$

The mean coefficient functions $\bar{f}$ and $\overline{1-f}$ are plotted in Fig. 11. The resultant mean transition coefficients are compared with the data of Gebers on Fig. 3. Gebers' data were obtained on six different length plates and, hence, might be expected to agree better with the present theory (in which Reynolds Number is varied by varying the plate length) than Schoenherr's data obtained by varying the velocity.

A curve (not shown) can be fitted fairly well to Schoenherr's 6-ft. plate results, but the 3-ft. plate cannot be fitted unless g increases sufficiently rapidly with the velocity U.

The measurements of transition on a flat plate made by Schubauer and Skramstad[1] included hot-wire records showing the turbulent bursts. A few $^1/_5$-sec. strips of these records were published. Fig. 12 of their N.A.C.A. report showed bursts, as in Table 1. The corresponding maximum burst frequency computed from

$$N_{\max.}\,\sigma^{2/3}/\alpha g^{1/3}U^{2/3} = 1.228$$

from Fig. 9 are also shown for comparison.

TABLE 1

U, Ft. per Sec.	$\sqrt{\bar{u}^2}/U$	$N_{expt.}$ (Bursts per Sec.)	$g\left(\frac{\text{Sources}}{\text{Ft.}^2\,\text{Sec.}}\right)$	$N_{calc.}$
50	0.0033	~10	3.1	19.2
105	0.0034	~20	63.3	86.3

Considering that the range of g values computed from various data sources is from 10^{-3} to 10^4 and the crudeness of the values of several of the constants, the agreement of Table 1 is fair.

A second paper, already submitted for publication in the *Proceedings of the First U.S. National Congress of Theoretical and Applied Mechanics*, discusses further developments of this transition theory and makes application to plates and cones.

Appendix (I)

In order to solve Eq. (2), it is convenient to introduce several other probabilities. Let $\phi(P, x_0)\,dx_0$ be the probability that P be turbulent because of a source between the planes $x = x_0$ and $x = x_0 + dx_0$ but not because of a source closer to the leading edge.

$$\phi(P, x_0) = \int_{S(P, x_0)} \psi(P, P_0)\,dy_0\,dt_0 \quad (A1)$$

where $S(P, x_0)$ is the cross section of R produced by the $x = x_0$ plane. Further, let $F(P, x_0)$ be the probability that P be turbulent because of a source between the leading edge and x_0.

$$F(P, x_0) = \int_0^{x_0} \phi(P, x_0^1)\,dx_0^1 = \int_{R^1} \psi(P, P_0)\,dV_0 \quad (A2)$$

The probability of turbulence at P is then

$$f(P) = F(P, x) \quad (A3)$$

Using the definition of Eq. (A2) in Eq. (2)

$$\psi(P, P_0) = \varphi(P, P_0)\,g\,(P_0)\,[1 - F(P, x_0)] \quad (A4)$$

By integration over $S(P, x_0)$, the $x = x_0$ cross section of R, we find

$$\phi(P, x_0) = \int_{S(P, x_0)} g(P_0)\,[1 - F(P, x_0)]\,dy_0\,dt_0 \quad (A5)$$

where $\varphi(P, P_0)$ is dropped, since it is equal to 1 in the area of integration.

By differentiating Eq. (A2) partially with respect to x_0, we find that

$$\phi(P, x_0) = \partial F(P, x_0)/\partial x_0 \quad (A6)$$

Therefore,

$$\frac{\partial F(P, x_0)}{\partial x_0} = [1 - F(P, x_0)] \int_{S(P, x_0)} g(P_0)\,dy_0\,dt_0 \quad (A7)$$

Now, Eq. (A7) may be integrated in x_0 directly, using the boundary condition [from the definition Eq. (A2)],

$$F(P, 0) = 0 \quad (A8)$$

$$\ln[1 - F(P, x_0)] = -\int_{R'} g(P_0)\, dV_0 \qquad \text{(A9)}$$

Thus, the probability that P be turbulent because of a source between 0 and x_0 is

$$F(P, x_0) = 1 - e^{-\int_{R'} g(P_0)\, dV_0} \qquad \text{(A10)}$$

and, by Eq. (A3), the probability that P be turbulent is

$$f(P) = 1 - e^{-\int_R g(P_0)\, dV_0} \qquad \text{(A11)}$$

The other probability functions of interest now follow from various of the preceding equations.

The probability density that P be turbulent because of sources between the planes $x = x_0$ and $x = x_0 + dx_0$ but not from some more distant source $x_0^1 < x_0$ is

$$\phi(P, x_0) = -\frac{\partial}{\partial x_0}\left[e^{-\int_{R'} g(P_0)\, dV_0}\right] = e^{-\int_{R'} g(P_0)\, dV_0} \int_{S(P, x_0)} g(P_0)\, dx_0\, dl_0 \qquad \text{(A12)}$$

and the probability density that P be turbulent because of sources in dV_0 at P_0 but not any more distant point is [by Eqs. (A4) and (A10)]

$$\psi(P, P_0) = \varphi(P, P_0) g(P_0) e^{-\int_{R'} g(P_0)\, dV_0} \qquad \text{(A13)}$$

Appendix (II)—Relation Between Perpendicular Cross Sections of a Cone

The cross-section area formed by a horizontal plane from a cone with an oblique axis is known, and it is desired to find the dimensionless cross section formed by a vertical plane normal to the vertical plane containing the axis. Consider a cone in the ξ, η, y space symmetrical with respect to the $y = 0$ plane. The relation between elements of area on a horizontal cross section at

$$\eta = \eta_2 \qquad (dA_2 = dy_2\, d\xi_2)$$

and a vertical cross section at

$$\xi = \xi_1 \qquad (dA_1 = dy_1\, d\eta_1)$$

is

$$dy_1 = \frac{\xi_1}{\xi_2}\, dy_2, \qquad d\eta_2 = \frac{\xi_1}{\xi_2}\left(\frac{\eta_2}{\xi_2}\, d\xi_2\right) \qquad \text{(A14)}$$

Thus, the desired dimensionless area is given by

$$A_1 = \frac{1}{{\xi_1}^2}\int dy_1\, d\eta_1 = \eta_2 \int \frac{d\eta_2\, d\xi_2}{{\xi_2}^3} \qquad \text{(A15)}$$

Since η_2 is arbitrary, we can choose it as we please. There does not seem to be any good reason for selection between several possibilities. Arbitrarily then, the center of area of the x, y spot will be used. Thus, set

$$\eta_2 = \bar{\xi}/\beta U \qquad \text{(A16)}$$

where $\bar{\xi}$ is the distance from the cone apex to the center of area of the spot and βU is the rate of propagation of the center of area of the spot—i.e., the cotangent of the angle between the ξ axis and cone axis defined by the center of area of the $\eta = \eta_2$ spot.

Finally, introduce the lateral dimension of a spot by using $\alpha\xi$ in place of ξ, where $\tan^{-1}\alpha$ is the half angle between the two loci of successive spot positions as in Fig. 4. Then,

$$A_1 = \frac{\alpha^2}{\beta U}\left[\alpha\bar{\xi}\int \frac{dy\, d\xi}{(\alpha\xi)^3}\right] = \frac{\alpha^2\lambda}{\beta U} \qquad \text{(A17)}$$

where

$$\lambda = \alpha\bar{\xi}\int dy\, d\xi/(\alpha\xi)^3$$

Thus, σ the dimensionless vertical propagation cone cross section is given in terms of the turbulent spot dimensions by

$$\sigma = \alpha^2\lambda/\beta \qquad \text{(A18)}$$

The integral λ can be simplified by an approximation by supposing the spot to be small compared to its distance from its source. In this case, $\xi \approx \bar{\xi}$ and λ reduces to

$$\lambda = A/(\alpha\xi)^2 \qquad \text{(A19)}$$

Thus, λ is approximately a dimensionless area of a spot—the area A of the spot divided by the square of the half width.

References

[1] Schubauer, G. B., and Skramstad, H. K., *Laminar Boundary Layer Oscillations and Stability of Laminar Flow*, Journal of the Aeronautical Sciences, Vol. 14, No. 2, 1947. (Also, *Laminar Boundary Layer Oscillation and Transition on a Flat Plate*, N.A.C.A. T.R. No. 909.)

[2] Hall, A. A., and Hislop, G. S., *Experiments on the Transition of the Laminar Boundary Layer on a Flat Plate*, Aeronautical Res. Comm. R. & M. No. 1843.

[3] Lees, Lester, *The Stability of the Laminar Boundary Layer in a Compressible Fluid*, N.A.C.A. T.N. No. 1360, July, 1947.

[4] Schoenherr, K. E., *Resistance of Flat Surfaces Moving Through a Fluid*, Trans. Soc. Nav. Arch. & Marine Engineering, Vol. 40, pp. 279–313, 1932.

[5] von Kármán, Th., *Turbulence and Skin Friction*, Journal of the Aeronautical Sciences, Vol. 1, No. 1, p. 14, 1934.

[6] Charters, A. C., *Transition Between Laminar and Turbulent Flow by Transverse Contamination*, N.A.C.A. T.N. No. 891, March, 1943.

[7] Burgers and van der Hegge Zijnen, Proc. 1st Int. Congress for Applied Mechanics, Delft, p. 113, 1924.

Readers' Forum

BRIEF REPORTS of investigations in the aeronautical sciences and discussions of papers published in the JOURNAL are presented in this special department. Publication will be completed approximately 8 to 10 weeks after receipt of the material. The Editorial Committee does not hold itself responsible for the opinions expressed by the correspondents. Contributions should not exceed 800 words in length.

A Possible Relation Between Cellular Flame Structure and Quenching

Raymond Friedman
Thermodynamics Section, Westinghouse Research Laboratories, East Pittsburgh, Pa.
April 9, 1951

IN THE PAPER "Experimental and Theoretical Studies of Flame-Front Stability" (JOURNAL OF THE AERONAUTICAL SCIENCES, Vol. 18, No. 3, pp. 199–209, March, 1951), G. H. Markstein describes observations of cellular structure in rich laminar hydrocarbon flames and presents a theory that predicts the following relationship:

$$\lambda_{max.}\,(c_p\rho_u S_u/k) \simeq 10\pi$$

where $\lambda_{max.}$ is the wave length for maximum instability of the flame front and is identified with the mean flame cell size and where c_p, ρ_u, k, and S_u are the specific heat, density, thermal conductivity, and normal burning velocity, respectively.

It is interesting to note that $\lambda_{max.}$ is of the same order of magnitude as the quenching distance of these flames. Unfortunately, it is difficult to make a direct comparison, since Markstein's experiments were made with air containing 30 per cent added nitrogen and since quenching data are not available for such mixtures. However, the present writer[1] has shown that the dimensionless group

$$X(c_p\rho_u S_u/k)$$

does not change greatly from one set of conditions to another. X is the distance between plane parallel plates which will just quench a laminar flame. Data are available for all the quantities in this dimensionless quenching group for various mixtures of propane-air, of methane-oxygen, and of hydrogen-air; the numerical value of the group is found to range from 14 to 33 (when k is calculated at 1,800°R.). This range of values is in good agreement with 10π.

In addition to this order-of-magnitude agreement, there are several other aspects of cellular flames which closely parallel quenching phenomena. These are:

(A) The present writer[2] has found that the quenching distance of moderately rich propane-air flames varies with the inverse 0.9 power of pressure, whereas Markstein's Fig. 5 shows that cell size varies as an inverse power of pressure near 0.75. In view of the nature of the observations, great precision is not possible, and this agreement appears satisfactory.

(B) Markstein finds that replacement of nitrogen by carbon dioxide slightly decreases cell size, while replacement by helium increases cell size considerably. The effects of these diluents upon quenching distance are found[1] to be similar.

(C) Markstein reports that cell size is constant for fuel concentrations between 1.2 and 1.4 times stoichiometric and increases gradually for richer compositions. Quenching distance behaves similarly, the minimum distance occurring on the rich side.

(D) Cell size was found to decrease markedly with increasing molecular weight at fuel concentration near 1.3 times stoichiometric. Since no quenching data are available for heavier hydrocarbons, it is necessary to consider minimum spark-ignition energy measurements;[3] this energy is roughly proportional to the square of quenching distance.[4] Fig. 4 of reference 3 shows that the minimum value of the minimum energy vs. composition plot shifts progressively toward richer mixtures for six hydrocarbons ranging from methane to heptane, even though the minimum value of the minimum energy is nearly the same for all of the hydrocarbons except methane. If such a shift were also to take place in cell size vs. composition plots, it could conceivably "explain" the effect observed by Markstein, although the reason for this shift is still obscure. Experiments are in order to determine how quenching distance vs. composition curves depend upon molecular weight of fuel.

The foregoing arguments [with the possible exception of (D)] show rather convincingly that both flame quenching and cellular instability are related in similar ways to the same basic parameters, particularly to the reaction zone thickness.

REFERENCES

[1] Friedman, R., *Third Symposium on Combustion, Flame, and Explosion Phenomena*, pp. 110–120; Williams & Wilkins, Baltimore, 1949.
[2] Friedman, R., and Johnston, W. C., Jour. Appl. Physics, Vol. 21, pp. 791–795, 1950.
[3] Blanc, M. V., Guest, P. G., von Elbe, G., and Lewis, B., *ibid.*, pp. 363–367.
[4] Friedman, R., and Burke, E., Jour. Chem. Physics, Vol. 17, p. 667, 1949.

The Combined Supersonic-Hypersonic Similarity Rule

Milton D. Van Dyke
Ames Aeronautical Laboratory, N.A.C.A., Moffett Field, Calif.
April 18, 1951

THE HYPERSONIC SIMILARITY RULE of Tsien[1] and Hayes[2] can be combined with the similarity rule for linearized supersonic flow. There results a single rule valid throughout the range of supersonic speeds from just above the transonic range up to infinite Mach Number and for general three-dimensional slender bodies. Thus, the value of the rule for correlating experimental results is considerably increased.

Similarity rules of the sort considered here correlate compressible flows past slender bodies that differ from one another only by a uniform expansion or contraction of all dimensions normal to the free-stream direction. For example, the second body in Fig. 1 is derived from the first by reducing its thickness, angle of attack, and aspect ratio by the factor τ_2/τ_1, where τ is some representative thickness parameter. (In practice, it seems best to take τ to be the maximum streamwise slope of the body surface.)

At hypersonic speeds, as the thickness is reduced, flow similarity is maintained if the free-stream Mach Number M is simultaneously increased so that the product τM remains constant. Then, at corresponding points Q (Fig. 1), the ratio of local pressure coefficient C_p to τ^2 remains constant. Hence, the hypersonic similarity rule may be written

$$C_p = \tau^2 P_1(\tau M) \qquad (1)$$

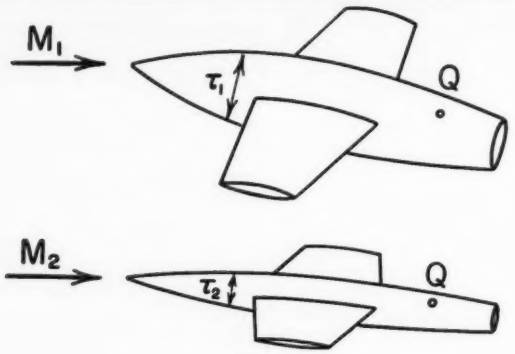

FIG. 1.

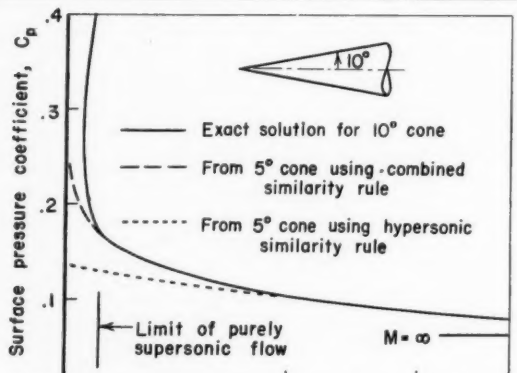

FIG. 2.

where P_1 is some function of the hypersonic similarity parameter τM. The range of validity of this rule has recently been investigated both analytically[3] and experimentally.[4]

At moderate supersonic speeds, linearized theory yields a different rule. The similarity parameter is $\tau\sqrt{M^2-1}$, and corresponding to Eq. (1) the supersonic similarity rule may be written

$$C_p = \tau^2 P(\tau\sqrt{M^2-1}) \tag{2}$$

These two separate rules can be combined by adopting the latter form, because the difference between M and $\sqrt{M^2-1}$ is negligible in hypersonic flow. (This can be justified rigorously by re-examining the derivation of the rule.) Therefore, Eq. (2) expresses a combined supersonic-hypersonic similarity rule valid at all speeds above the transonic range.

To illustrate the superiority of the combined rule, suppose that the pressures on a cone of 5° semivertex angle are known (from the M.I.T. Tables[5]) and that approximate values for a 10° cone are derived therefrom using the similarity rule. Fig. 2 shows that the results of applying the combined rule almost coincide with the exact values down to the Mach Number at which sonic velocity is attained at the surface, while the hypersonic rule becomes inaccurate at considerably higher speeds.

The combined similarity rule is obtained at the expense of some loss of generality in the supersonic rule. Supersonic similarity is independent of the adiabatic exponent γ, while for the combined rule γ must remain fixed. Another penalty attached to the combined rule is that an alternative form of the hypersonic rule, which relates local to free-stream pressure,

$$p/p_0 = F(\tau M) \tag{3}$$

loses its simplicity, becoming

$$p/p_0 = 1 + \tau^2 M^2 G(\tau\sqrt{M^2-1}) \tag{4}$$

Recently, Smelt[6] has proposed an alternative similarity parameter valid at both supersonic and hypersonic speeds. His rule, analogous to Eq. (4), is

$$p/p_0 = F(\tau M^2/\sqrt{M^2-1}) \tag{5}$$

However, it can be shown that this rule is restricted to two-dimensional flow or flow past planar systems such as flat wings (for which the similarity parameter is not uniquely determined), whereas the rule expressed by Eq. (2) applies to general three-dimensional flow.

The combined similarity rule may be expressed in other forms, such as

$$C_p = [1/(M^2-1)]P_2(\tau\sqrt{M^2-1}) \tag{6}$$

but the first form [Eq. (2)] seems preferable because only in this case does the function P remain finite at infinite Mach Number.

The corresponding rules for drag coefficient C_D and lift coefficient C_L are

$$C_D = \tau^{2+k} D(\tau\sqrt{M^2-1}) \tag{7a}$$

$$C_L = \tau^{1+k} L(\tau\sqrt{M^2-1}) \tag{7b}$$

where D and L are functions of the similarity parameter $\tau\sqrt{M^2-1}$, $k = 1$ if some plan-form area is taken for reference and $k = 0$ if some cross-sectional area is used. The center of pressure position is a function only of the similarity parameter.

At high Mach Numbers, the hypersonic (or combined) similarity rule applies to rather thick bodies in some cases if τ is taken to be the sine of the maximum angle of inclination of the body surface. The reason for this is that, for bodies of any thickness at $M = \infty$ (and $\gamma = 1$), Newtonian theory predicts pressure coefficients proportional to the square of the sine of the angle of inclination.

Just as the supersonic and hypersonic similarity rules are combined here, Spreiter[7] has shown that for two-dimensional or planar bodies the subsonic, transonic, and supersonic similarity rules can be combined. However, it does not seem possible, even for planar bodies, to combine all four régimes.

REFERENCES

[1] Tsien, H. S., *Similarity Laws of Hypersonic Flows*, Jour. Math. Physics, Vol. 25, No. 3, pp. 247–251, October, 1946.

[2] Hayes, Wallace D., *On Hypersonic Similitude*, Quart. Appl. Math., Vol. 5, No. 1, pp. 105–106, April, 1947.

[3] Ehret, Dorris M., Rossow, Vernon J., and Stevens, Victor I., *An Analysis of the Applicability of the Hypersonic Similarity Law to the Study of Flow About Bodies of Revolution at Zero Angle of Attack*, N.A.C.A. T.N. No. 2250, 1950.

[4] Neice, Stanford E., and Ehret, Dorris M., *Similarity Laws for Slender Bodies of Revolution in Hypersonic Flows*, Preprint No. 321, Institute of the Aeronautical Sciences, January, 1950. (To be published in a forthcoming issue of the JOURNAL OF THE AERONAUTICAL SCIENCES.)

[5] Kopal, Zdenek (Ed.), *Tables of Supersonic Flow Around Cones*, M.I.T. Tech. Report No. 1, Massachusetts Institute of Technology, Cambridge, 1947.

[6] Smelt, R., *Problems of Missiles at Extreme Speeds*, Symposium on Ordnance Ballistics, U.S. Naval Ordnance Laboratory, White Oak, Silver Spring, Md., pp. 51–68, June 28, 1949 (published March 1, 1950).

Spreiter, John R., *Similarity Laws for Transonic Flow About Wings of Finite Span*, N.A.C.A. T.N. No. 2273, 1951.

On the Velocity of Sound in Fluids

C. Truesdell
Professor of Mathematics, Graduate Institute for Applied Mathematics, Indiana University, Bloomington, Ind.
April 23, 1951

NOT LONG AGO there was a protracted discussion of the velocity of sound, begun by Professor Morduchow's[1] objection to the "lack of rigor" in the customary derivations and carried on by Professors Morkovin,[2] Morduchow,[3] and Millikan,[4] and by Dr. Munk.[5] None of these authors saw fit to define the velocity of sound before deriving its value; most of the discussion assumed the existence of a barotropic relation $p = f(\rho)$. The present communication makes no original contribution; its only purpose is to call attention to the basic known results on the subject, which were not mentioned by any of the four disputants.

For an inviscid fluid, the local velocity of sound c may be defined as the speed of advance, relative to the particles instantaneously situate upon it and in a direction normal to itself, of a surface (not necessarily plane) across which the velocity, pressure, and density are continuous, but at least one of the nine components of the velocity gradient suffers a discontinuity. In the terminology of Hadamard,[6] such a surface is called a "wave of second order"; Appell[7] calls such a wave a "sound wave." In the case when $p = f(\rho)$, it was shown by Hugoniot[8] in full generality that $c^2 = dp/d\rho$. Of the customary infinitesimal arguments he says: "[Treatments of] the theory of propagation of motion in a fluid..., have introduced into the equations of hydrodynamics hypotheses, disguised, it is true, under the name of approximations, but singularly altering the worth of the results which can be deduced from them." His analysis is reproduced (in two different forms) in the texts of Webster,[9] Appell,[7] and Lichtenstein,[10] and the matter is treated in detail by Hadamard in his great classical treatise on waves.[11]

A part of Professor Morkovin's note[2] and all of Dr. Munk's note[5] are devoted to the more interesting case when a barotropic relation $p = f(\rho)$ does *not* exist. According to Dr. Munk, "the necessity to give a Mach angle μ leading to physically significant Mach lines" indicates that $c^2 = \partial p/\partial\rho$, the derivative being taken "in the direction of the stream line of a steady flow." It is hard to take this proposal seriously, since, quite apart from the purely physical objection that no mention or use whatever is made of any property of sound waves, the classical result, $c^2 = dp/d\rho$ when $p = p(\rho)$, is not even included in all cases when it holds. The statement fails to have a meaning when the flow is three-dimensional or unsteady, and the adduced arguments do not hold if the flow is subsonic, there being then no real characteristics, physically significant or otherwise. Professor Morkovin's proposal is

$$c^2 = (\partial p/\partial\rho)_s$$

s being the entropy, but he presents no analysis and makes no attempt to discuss the propagation of motion.

Now in fact the second derivation of Hugoniot[12] remains valid even if the relation $p = p(\rho)$ has a form *varying from one fluid particle to another*. Such a relation would be of the form

$$p = f(\rho, X, Y, Z)$$

where X, Y, Z are "Lagrangian" coordinates. In a flow of an inviscid fluid when heat conduction is neglected, the entropy remains constant for each particle, and hence by Hugoniot's result there is indeed a definite velocity of sound, and it is given by Professor Morkovin's formula. However, in a flow where each fluid particle conserved, for example, its own temperature θ, the speed of sound would be given by

$$c^2 = (\partial p/\partial\rho)_\theta$$

If we really wish the term "speed of sound" to represent the speed of advance of a physical sound wave (not necessarily plane), we should recognize the fact that there is no physical reason *a priori* to expect that speed to be a function of the thermodynamic state only. Hugoniot's result yields a broad class of flows in which it *is* a function of state, but probably one could show that if there is no barotropic relation $p = f(\rho, X, Y, Z)$, then more information than simply the values of ρ, θ, X, Y, Z is required in order to determine the value of c.

A closer representation of the physical situation is the *quasi-wave* of Duhem,[13] which is a layer of small thickness, ϵ, across which the change in pressure, density, and velocity is of the order of ϵ, but at least one of the nine components of the velocity gradient suffers a large (though possibly continuous) change. In a remarkable analysis, which has apparently escaped the notice of all current writers on this subject, Duhem shows that in the case of a slightly conducting perfect fluid any approximately transversal quasi-wave is stationary, but there are two types of approximately longitudinal quasi-waves. One, of thickness small in comparison to the coefficient of conductivity, propagates approximately according to the Newtonian formula $c^2 = (\partial p/\partial\rho)_\theta$, while the other, of thickness of the same order as the coefficient of conductivity, propagates approximately according to the Laplacian formula $c^2 = (\partial p/\partial\rho)_s$. He concludes further that when the effect of viscosity is taken into account the foregoing conclusions are not modified, provided that the thickness of the quasi-wave be of the same order as the viscosity coefficients. Since these statements cannot be expressed in dimensionless terms, it is clear that they can be given a precise meaning only in terms of a limiting process $\epsilon \to 0$.

If, finally, we have no interest in sound waves but merely wish a local reference quantity, endowed with the dimensions of velocity, to be used in scaling laws (e.g., in definition of the Mach Number), then any sufficiently general definition is admissible, providing it be used consistently. Thus Bateman[14] regarded the term *local velocity of sound* as "merely a convenient name." Two different such "velocities of sound" occur in the work of Hicks.[15]

REFERENCES

[1] Morduchow, Morris, *A Note on the Velocity of Sound*, Readers' Forum, Journal of the Aeronautical Sciences, Vol. 16, No. 10, p. 635, October, 1949.

[2] Morkovin, M. V., *A Note on the Velocity of Sound*, Readers' Forum, Journal of the Aeronautical Sciences, Vol. 17, No. 3, p. 180, March, 1950.

[3] Morduchow, Morris, *Further Remarks on the Velocity of Sound*, Readers' Forum, Journal of the Aeronautical Sciences, Vol. 17, No. 3, pp. 180–181, March, 1950; Morduchow, M., and Morkovin, M., *Concluding Remarks on the Speed of Sound*, Readers' Forum, Journal of the Aeronautical Sciences, Vol. 18, No. 1, pp. 66–68, January, 1951.

[4] Millikan, C. B., *Another Note on the Velocity of Sound*, Readers' Forum, Journal of the Aeronautical Sciences, Vol. 17, No. 4, p. 252, April, 1950.

[5] Munk, Max M., *Remarks on the Velocity of Sound*, Readers' Forum, Journal of the Aeronautical Sciences, Vol. 17, No. 6, p. 376, June, 1950.

[6] Hadamard, J., *Leçons sur la Propagation des Ondes et les Équations de l'Hydrodynamique*; Paris, 1903, see Section 75.

[7] Appell, P., *Traité de Mécanique Rationnelle*, t. 3, 3rd. Ed.; Paris, 1920, see Section 732.

[8] Comptes Rendus Acad. Sci. Paris, Vol. 101, pp. 1118–1120, 1885.

[9] *Partial Differential Equations of Mathematical Physics;* New York and Leipzig, 1927, see Section 84.

[10] *Grundlagen der Hydromechanik;* Berlin, 1929, see Chap. 7, Section 5.

[11] See reference 6, Section 239.

[12] Comptes Rendus Acad. Sci. Paris, Vol. 101, pp. 1229–1232, 1885; J. Math. Pures Appl., (4), Vol. 3, pp. 477–492, 1887; Vol. 4, pp. 153–167, 1888. See also reference 6, Section 242.

[13] Ann. Fac. Sci. Toulouse, (2), Vol. 5, pp. 5–24, 1903.

[14] Proc. R. Soc. London, Series A, Vol. 125, pp. 598–618, 1929; see Section 1, footnote.

[15] Hicks, B. L., Q. Appl. Math., Vol. 6, pp. 221–237, 1948, see Section 4.

The Analogy Between Irrotational Gas Flow and Minimal Surfaces

C. Truesdell
Professor of Mathematics, Graduate Institute for Applied Mathematics, Indiana University, Bloomington, Ind.
April 23, 1951

IN A RECENT NOTE, Professor Szebehely[1] points out an analogy between an open soap bubble (minimal surface) and an irrotational flow of a perfect fluid. This analogy [exactly valid if and only if the pressure-density relation is of the Earnshaw-Chaplygin type $p = A - (B/\rho)$ was discovered by Chaplygin[2] and Bateman,[3] is mentioned in Sauer's textbook,[4] and has been made the subject of extensive study.[5]

REFERENCES

[1] Szebehely, V. G., *An Analogy Between Open Soap Bubble and Compressible Flow*, Readers' Forum, Journal of the Aeronautical Sciences, Vol. 17, No. 12, p. 809, December, 1950.

[2] *On Gas Jets* (1904). Trans. Brown Univ., Providence, 1944, see Supplementary Note 2.

[3] Proc. R. Soc. London (A), Vol. 125, pp. 598–618, 1929, see Section 3.

[4] *Theoretische Einführung in die Gasdynamik*, Berlin, 1943; see Section 17, Paragraph 1.

[5] A bibliography is given by Behrbohm and Pinl, Z.A.M.M., Vol. 21, pp. 193–203, 1941. (Cf. also Truesdell, Proc. Nat. Acad. Sci., Vol. 32, pp. 289–293, 1946.)

On Broszko's Theory of Turbulent Flow

William Squire
Aerodynamic Research Department, Cornell Aeronautical Laboratory, Inc., Buffalo, N.Y.
April 19, 1951

IN A LITTLE KNOWN PAPER, Broszko[1] attempted to formulate a rational theory of turbulent flow by deriving additional relations between the mean motion and the turbulent fluctuations. No discussion of the theory seems to have been published; therefore, it is believed that some critical comments on the derivation and consequences of the additional equations may be of interest.

Broszko employs Reynolds' equations

$$\frac{\partial \bar{u}_i}{\partial t} + \frac{\partial \bar{u}_i \bar{u}_j}{\partial x^j} + \frac{1}{\rho}\frac{\partial \bar{p}}{\partial x_i} = \epsilon \frac{\partial^2 \bar{u}_i}{\partial x_j \partial x^j} - \frac{\partial \overline{u_i' u_j'}}{\partial x^j} \tag{1}$$

with ϵ independent of position but much larger than the ordinary kinematic viscosity. In order for the results of the theory to agree with experiment, ϵ must vary with Reynolds Number. The averaging process is defined in Reynolds' manner as

$$\bar{g} = \int g dV / \int dV \tag{2}$$

where V is a small fixed volume around the point considered. Aside from such obvious properties as linearity and commutation with partial differentiation, the characteristic property of averaging is

$$\overline{(U_i + C_i)\, u_j'} = \overline{u_i' u_j'} \tag{3}$$

where $U_i = \bar{u}_i + u_i'$ and C_i is a constant velocity. This implies that both

$$\bar{u}_j' = 0, \qquad \overline{\bar{u}_i u_j'} = 0 \tag{4}$$

Broszko attempts to derive the additional equations from Eq. (3) rather than from a physical principle. Differentiating both sides of Eq. (3) with respect to time gives

$$\frac{1}{V}\int \frac{d}{dt}(U_i + C_i)\, u_j' dV = \frac{1}{V}\int \frac{d}{dt}\, u_i' u_j'\, dV \tag{5}$$

Using the continuity equation,

$$\frac{dg}{dt} = \frac{\partial g}{\partial t} + \frac{\partial}{\partial x^k}(\bar{u}_k + u_k')g \tag{6}$$

and setting the average of terms containing only one fluctuating quantity equal to zero, leads to the set of nine equations.

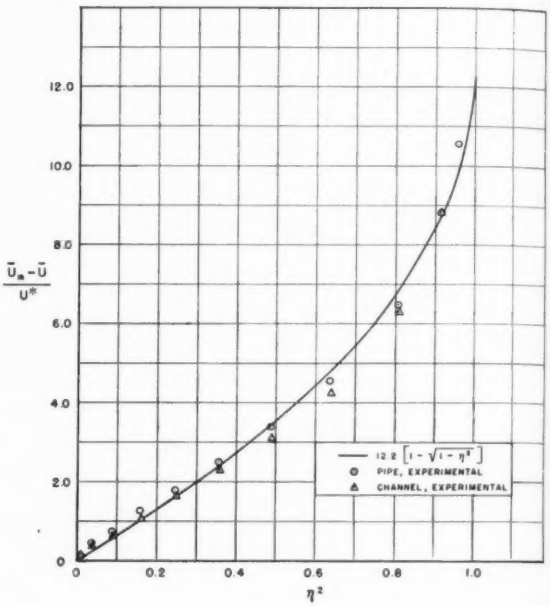

FIG. 1

$$[\partial(\bar{u}_i + C_i)\,\overline{u_j' u_k'}]/\partial x^k = 0 \tag{7}$$

There are two principal difficulties in the derivation. First, the differentiation of the integrals in Eq. (5) is derived[2] for material volumes, not the fixed volumes of Eq. (3). Second, it seems equally plausible to start with

$$\overline{Mf'} = 0 \tag{8}$$

where M is any mean quantity and f' is any fluctuating quantity and to derive

$$\partial \overline{Mf' u_k'}/\partial x^k = 0 \tag{9}$$

For example, if M is a constant and $f' = u_j'$, the result is

$$\partial \overline{u_j' u_k'}/\partial x^k = 0 \tag{10}$$

which, in conjunction with Eq. (1), leads to Boussinesq's early theory of turbulent flow.

By considering flow through a long pipe of constant cross section, the equations are greatly simplified, since there is only one mean velocity component and no variation in the direction of flow. The simplified set corresponding to Eq. (7) is satisfied by

$$\overline{v'^2} \propto \overline{w'^2} \propto \overline{u'v'} \propto [1/(\bar{U} + C)] \tag{11}$$

However, $\overline{u'^2}$ is arbitrary, and, therefore,

$$K = \overline{u'v'}/\sqrt{\overline{u'^2}\,\overline{v'^2}}$$

is also undetermined. Following Broszko, $-C$ is equal to the apparent wall velocity, but infinite values do not appear because of transition to the laminar sublayer. The theoretical $\overline{v'^2}$ and $\overline{w'^2}$ distribution agrees qualitatively with experiment, but $\overline{u'v'}$ does not vanish at the center as required by current theory. To clarify the problem, consider the equation of motion for a channel:

$$\rho \frac{\partial \overline{u'v'}}{\partial y} - \rho\epsilon \frac{\partial^2 U}{\partial y^2} = -\frac{\partial P}{\partial x} = \frac{\tau_0}{d} \tag{12}$$

Integrating from 0 to y gives

$$(\rho\overline{u'v'} - \rho\overline{u'v'}_{y=0}) - \left(\rho\epsilon \frac{\partial U}{\partial y} - \rho\epsilon \frac{\partial U}{\partial y_{y=0}}\right) = \frac{\tau_0 y}{d} = \tau \tag{13}$$

At the center $\partial u/\partial y = 0$, and it has been assumed that $\overline{u'v'}$ is zero also so that

$$\tau = \tau_0 \frac{y}{d} = \rho\overline{u'v'} - \rho\epsilon \frac{\partial U}{\partial y} \cong \rho\overline{u'v'} \tag{14}$$

since the $\partial u/\partial y$ term is negligible if ϵ is the usual kinematic viscosity. This was not confirmed by experimental results until the recent work of Laufer.[3a, 3b] The earlier results of Wattendorf[4] and Reichardt[5] assumed Eq. (14). While Laufer's results show discrepancies up to 20 per cent from Eq. (13), the deviation from Eq. (11) is even greater, especially at the center.

In spite of its deficiencies as a complete rational theory of turbulent flow, Broszko's theory gives satisfactory results for the mean velocity distribution. The writer has obtained the following approximate solutions:

$$(\bar{U}_m - \bar{U})/U^* = 12.2\,(1 - \sqrt{1 - \eta^2}) \tag{15a}$$

$$(\bar{U}_m - \bar{U})/U^* = 3.2\eta^2 - 2.5 \ln (1 - \eta^2) \tag{15b}$$

$$(\bar{U}_m - \bar{U})/U^* = 4.9\eta^2 - 2.5\left[\ln\left(\frac{1-\eta}{1+\eta}\right) + 2\eta\right] \tag{15c}$$

where η is r/radius for a circular pipe and y/half width for a channel. Eq. (15a) is derived for either case, Eq. (15b) is derived for a circular pipe, and Eq. (15c) is derived for a channel. However, the three expressions give almost identical distributions. Fig. 1 compares Eq. (15a) with averaged experimental results.

References

[1] Broszko, M., *On the Problem of Turbulence and on the Foundations of Hydromechanics*, Annales de l'Academie Polonaise des Sciences Techniques, Vol. 7, pp. 75–98, 1939–1946.

[2] Frank and von Mises, *Die Differential und Integralgleichungen der Mechanik und Physik*, 2nd Ed., Vol. II, p. 374; Brunswick, 1935.

[3a] Laufer, J., *Investigation of Turbulent Flow in a Two-Dimensional Channel*, N.A.C.A. T.N. No. 2123, July, 1950.

[3b] Laufer, J., *Some Recent Measurements in a Two-Dimensional Turbulent Channel*, Journal of the Aeronautical Sciences, Vol. 17, No. 5, pp. 277–287, May, 1950.

[4] Wattendorf, F. L., *Investigation of Velocity Fluctuations in a Turbulent Flow*, Journal of the Aeronautical Sciences, Vol. 3, No. 6, pp. 200–202, April, 1936.

[5] Reichardt, H., *Messungen Turbulenter Schwankungen*, Die Naturwissenschaften, Jahrg 26, Heft 24/25, pp. 404–408, June 17, 1938.

Equivalence of the Spanwise Lift Distribution to the Spanwise Lift-Influence Function for Slender Wings and Wing Bodies

G. K. Morikawa and A. E. Puckett
Research and Development Laboratories, Hughes Aircraft Company

April 23, 1951

THE USEFULNESS of the concept of the spanwise lift-influence function* is apparent in the calculation of lift and rolling moment of lifting surfaces with twist (real or apparent). A particularly simple result has been obtained by Lagerstrom and Van Dyke[1] (also independently by Ward[2]), as expressed by their theorem on preservation of lift for wings with supersonic leading edges and straight supersonic trailing edges. The only comparable result available for plan forms with subsonic leading edges is given by the modified strip method of Graham,[3] applicable to cases where there is no interaction between edges.

Within the realm of slender-body theory, expressions for the spanwise lift-influence function are readily available for both wings and wing bodies. The analysis for this limiting case is reduced to a two-dimensional potential problem in the cross-flow plane,[4] and the problem of finding the lift-influence function is analogous to that of obtaining the Green's function. The solution for the velocity potential is simply obtained by considering symmetrical wings with respect to the y-axis (Fig. 1) and transforming the wing-body cross section into the unit circle.

The complex velocity potential is

$$w = \varphi + i\psi = \frac{Q}{2\pi} \ln \left\{ \frac{\sqrt{1 - (4/A^2)\,(z + a^2/z)^2} + \sqrt{1 - (4/A^2)\,(x_0 + a^2/x_0)^2}}{\sqrt{1 - (4/A^2)\,(z + a^2/z)^2} - \sqrt{1 - (4/A^2)\,(x_0 + a^2/x_0)^2}} \right\} \tag{1}$$

where

$Q = V\alpha\,\Delta x$, source strength
a = body radius
x_0 = position of deflected strip of width Δx
$A = (1/2)\,(s + a^2/s)$
s = semispan of wing

The portion of the lift acting on the wing is

$$\frac{\Delta L^{(W)}}{q} = \frac{8}{V} \int_a^s \varphi\, dx \tag{2a}$$

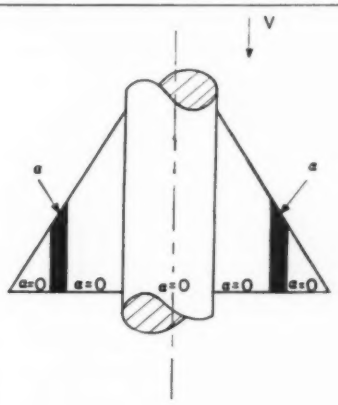

a) PLANFORM

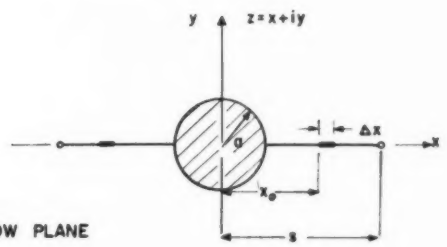

b) CROSSFLOW PLANE

FIGURE 1.
WING-BODY CONFIGURATION WITH SYMMETRICAL CHORDWISE LIFTING STRIPS

* Defined as the total lift due to a chordwise strip of unit width deflected at unit angle of attack (see Fig. 1).

where φ is obtained from Eq. (1) by setting $z = x$, and the portion of the lift acting on the body is

$$\frac{\Delta L^{(B)}}{q} = \frac{8}{V}\int_0^a \varphi\, dx \tag{2b}$$

where φ is obtained from Eq. (1) by setting $z = ae^{i\theta}$ and $a \cos \theta = x$.

Integrating Eqs. (2a) and (2b) gives

$$\frac{\Delta L^{(W)}}{q\alpha\,\Delta x} = \frac{4}{\pi}\left[\pi AB - 2AB\left(\cos^{-1}\sqrt{1-\frac{1}{A^2}} - \frac{\pi}{2}\right) - \ln\left|\frac{\sqrt{A^2-1}+AB}{\sqrt{A^2-1}-AB}\right| + A\sqrt{1-B^2}\times \ln\left|\frac{B+\sqrt{(A^2-1)(1-B^2)}}{B-\sqrt{(A^2-1)(1-B^2)}}\right|\right] \tag{3a}$$

and

$$\frac{\Delta L^{(B)}}{q\alpha\,\Delta x} = \frac{4}{\pi}\left[2AB\cos^{-1}\sqrt{1-\frac{1}{A^2}} + \ln\left|\frac{\sqrt{A^2-1}+AB}{\sqrt{A^2-1}-AB}\right| - A\sqrt{1-B^2}\times \ln\left|\frac{B+\sqrt{(A^2-1)(1-B^2)}}{B-\sqrt{(A^2-1)(1-B^2)}}\right|\right] \tag{3b}$$

where

$$B = \sqrt{1-\left[\frac{(x_0+a^2/x_0)}{(s+a^2/s)}\right]^2}$$

Then the spanwise lift-influence function is

$$\frac{\Delta L}{q\alpha\,\Delta x} = \frac{\Delta L^{(W)}+\Delta L^{(B)}}{q\alpha\,\Delta x} = 4\sqrt{(s+a^2/s)^2-(x_0+a^2/x_0)^2} \tag{4}$$

which is exactly the spanwise lift distribution. This is a verification of a result that is directly obtainable from the general reverse-flow theorem given by Ward[5] (also independently by W. D. Hayes* whose proof follows that of Munk[6] and Brown[7] for less general reverse-flow theorems) or an equivalent statement given by Jones[8] and some intuitive arguments (on slender-body configurations) such as those presented by Lagerstrom and Graham.[9]

References

[1] Lagerstrom, P. A., and Van Dyke, M. D., *General Consideration About Planar and Non-Planar Lifting Surfaces*, Douglas Report No. SM-13432, Santa Monica, June, 1949.

[2] Ward, G. N., *Supersonic Flow Past Slender Pointed Bodies*, Quarterly Journal of Mechanics and Applied Mathematics, Vol. II, Pt. 1, 1949.

[3] Graham, M. E., *Some Linearized Computations of Supersonic Wing-Tail Interference*, Douglas Report No. SM-13430, Santa Monica, December 23, 1948.

[4] Spreiter, J. R., *Aerodynamic Properties of Slender Wing-Body Combinations at Subsonic, Transonic, and Supersonic Speeds*, N.A.C.A. T.N. Report No. 1662, July, 1948.

[5] Ursell, F., and Ward, G. N., *On Some General Theorems in the Linearized Theory of Compressible Flow*, Quarterly Journal of Mechanics and Applied Mathematics, Vol. III, Pt. 3, 1950.

[6] Munk, M. M., *The Reversal Theorem of Linearized Supersonic Airfoil Theory*, Journal of Applied Physics, Vol. XXI, No. 2, February, 1950.

[7] Brown, C. E., *The Reversibility Theorem for Thin Airfoils in Subsonic and Supersonic Flow*, N.A.C.A. T.N. Report No. 1944, September, 1949.

[8] Jones, R. T., *The Minimum Drag of Thin Wings in Frictionless Flow*, Journal of the Aeronautical Sciences, Vol. 18, No. 2, p. 75, February, 1951.

[9] Lagerstrom, P. A., and Graham, M. E., *Remarks on Low-Aspect-Ratio Configurations in Supersonic Flow*, Journal of the Aeronautical Sciences, Vol. 18, No. 2, p. 91, February, 1951.

* Private communication.

Three-Dimensional Shock-Wave Reflections

(*Continued from page 489*)

wall, also parallel to the free stream (Fig. 6), turns out to be a complete dual of the preceding case of the plane shock impinging on a cylinder. One reason for this duality stems from the already mentioned fact that the reflection conditions, and therefore the geometry of various planes as in Figs. 3 and 5, have a purely local character; they are associated with the orientation of the tangent line $\boldsymbol{t}$ rather than with the shape of the impingement curve $\boldsymbol{i}$. The lack of similarity between the impingement hyperbola located in the wall plane here and the impingement ellipse located in the shock plane in the preceding case is immaterial. The other reason for the duality lies in the fact that the conical shock, like the plane one, has constant strength everywhere. Thus, the normal component of the Mach vector $M_0 \sin \theta$ again has a constant magnitude c and Eq. (4) remains valid.

Referring to Fig. 6, one identifies the wall plane which contains M_0 and $\boldsymbol{t}$ as the tangent T plane, and the plane through the cone generator $0P$ and $\boldsymbol{t}$ as the shock plane S. The shock angle is measured in the plane through M_0 and $0P$, which is therefore equivalent to the plane V. This plane is no longer vertical; on the other hand, the tangent plane T has become horizontal. As a matter of fact, one obtains the complete correspondence between the geometry of Fig. 5 and the present geometry by rotating the former configuration around the M_0 vector as axis until the plane T becomes horizontal. Inspection of Fig. 4 shows that the needed angle of rotation is exactly ω and that $\boldsymbol{n}$, the line normal to T, becomes coincident with the local vertical axis. Thus, the relations between the edges of the tetrahedron $PABC$ of Fig. 5 remain valid, and the Eq. (5) relating θ_e to the position parameter ω also holds.